# Computational Modeling Studies of Fundamental Aerosol-Cloud Interactions

Thesis by

Zachary J. Lebo

In Partial Fulfillment of the Requirements

for the Degree of

Doctor of Philosophy

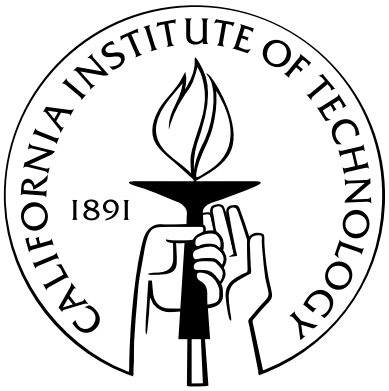


California Institute of Technology

Pasadena, California

2012

(Defended 19 March, 2012)

To Margaret C. Kohl

# Acknowledgements

Countless people have helped me throughout my five years at Caltech. Without their assistance and support, the contents presented in this thesis would not have been possible. I am forever indebted to my advisor, John Seinfeld, for his willingness to allow me to pursue my own ideas while a graduate student and for his trust and general support. I must also thank my committee members, Tapio Schneider, Andy Ingersoll, and Frank Li for their scientific feedback over the last few years.

Without the support of my advisor and good friend at Penn State, Jerry Harrington, I am certain that I would not be where I am today. Jerry trusted me from the very start and has been a great mentor and friend during the course of my years as a student. Our annual summer backpacking trips to places like Colorado, Oregon, and Wyoming gave me the break that I needed in order to keep pushing through until the end of my tenure at Caltech.

I must also thank Hugh Morrison, Rob Wood, Graham Feingold, and Adrian Hill for their scientific feedback at conferences and for ensuring that the work presented here is solid and robust. I must not forget to thank the computing staff, namely, Suresh Guptha, Naveed Near-Ansari, and John Lilley, for promptly answering all of my questions about the network and the GPS cluster. Without them, this research would have been far more challenging to conduct. Moreover, the support of both the chemical engineering and geological and planetary sciences staff has ensured that my experience at Caltech was as smooth as possible. It has been a pleasure working with the other modelers in the Seinfeld research group over the past few years, specifically, Havala Pye, Joey Ensburg, Andi Zuend, Jean Chen, and Anne Chen. I thoroughly enjoyed our Friday afternoon modelers' coffee hour and the fruitful conversations that we had regarding modeling techniques and algorithms. I would also like to thank the rest of the Seinfeld/Flagan research group, both present

and past — Scott Hersey, Christine Loza, Shane Murphy, Jason Suratt, Lindsay Yee, ManNin Chan, Jill Craven, Andy Downard, Andrew Metcalf, Andy Downard, Jason Gamba, Mandy Grantz, Xerxes Lopez-Yglesias, and Matt Coggan — for their scientific feedback, general conversations, and for making Caltech a pleasurable place to study.

The support from my academic and scientific colleagues, staff members at Caltech, and advisors and mentors enabled me to develop my own thoughts and present new ideas within quite a short amount of time. However, the support goes beyond just simply the years spent as a graduate student at Caltech. I owe many thanks to the teachers who believed in me when I was still too young to fully comprehend my full potential. For example, Susan Langkammer trusted me and supported through my years as a high school student in somewhat-rural Pennsylvania. She believed me and helped drive me toward success both then and now. I thank her for all of her support. Moreover, the support of the faculty at Penn State during my four years as an undergraduate and graduate student were crucial in getting me to where I am today. Their trust, professionalism, and expertise in all fields of atmospheric science provided me the opportunity to not only attain a broad knowledge base, but also prosper as a young scientific researcher. The most notable of these is Euguene Clothiaux. While I have never done research with Eugene, he has also been interested in my work both then and now. I look forward to future conversations with him.

The support I have received also goes beyond that of just people within the academic and scientific communities. I am grateful for the friends that have made my graduate student experience an enjoyable one. I will always remember running up mountains with Simon Cooper, backpacking with Luigi Perotti and Madeline Miller, taking coffee breaks with Lauren Edgar, and chatting with Racheal Bliley on the phone. They all truly made this experience wonderful.

Purposely, I have refrained from including family thus far. I honestly feel that there are no words to fully express my thanks to mom and dad. Their love, support, and encouragement have been second to none over the years. Through good times and bad, they have *always* been by my side, always there for me. They have always been there to provide advice and a helping hand. I am proud to be their son. I look forward to returning the favor.

Through five years, a lot can change. I thank my sister for those conversations on the phone over the years and for giving me a beautiful niece whom I love dearly. I also owe a lot to Justine; she is truly the most amazing person in my life and every day my life feels truly complete knowing that she is a part of it. I thank her too for listening to me and helping me through the rough times, especially toward the end of my time at Caltech.

Not every change is a good thing. I sadly lost someone who meant the world to me nearly half way through my studies at Caltech. I recall that one of the last things I ever said to her was in response to her telling me that she would not be here to see me graduate. I told her that she would. Sadly, I was wrong. My grandmother meant so much to me. She was always there to listen regardless of whether times were good or bad. She had a smile that could light up the world and a heart that loved so many over her long life. She taught me something very important about life without even knowing that she had done so: Happiness can never be measured by the money in your pocket, the size of your house, or the car you drive. Instead, happiness comes from the heart, knowing that you are loved and that you share that love with others. That's a lesson that I will hold close to my heart for as long as I live.

# Abstract

Basic questions regarding the interaction between changes in human activity and the atmosphere remain unanswered. Among these, the link between aerosol particles and cloud formation and development, especially in an altered climate, is a large point of uncertainty in recent climate projections. This should come as no surprise given the uncertainty in model parameters required to predict droplet activation, even in the most detailed models used for climate predictions. Here, a detailed spectral mixed-phase microphysics scheme and a state-of-the-art continuous two-dimensional (2-D) aerosol-droplet microphysics scheme have been developed and coupled to the Weather Research and Forecasting (WRF) model to more closely analyze the effects of aerosol perturbations on single clouds or cloud systems with the hope of ultimately improving numerical parameterizations used by microphysics schemes in general circulation models (GCMs).

The continuous 2-D aerosol-droplet model is developed to explicitly treat the entire spectrum of aerosol, haze droplets, cloud droplets, and drizzle drops while allowing the solute mass spectrum to evolve within the droplets. In other words, the aerosol mass is conserved and regeneration of aerosol particles upon droplet evaporation is physically accurate without any *a priori* assumptions. The model is tested by performing simulations of marine stratocumulus and the results are compared with those from the aforementioned bin and bulk models. It is shown that microphysical processing of aerosols alone results in a large shift in the aerosol spectrum toward larger particles (via collision-coalescence of droplets). This could have potentially large effects on the activation of regenerated particles. Future studies with the model will address the need for better parameterizations of the aerosol regeneration process.

The spectral mixed-phase microphysics scheme is used in conjunction with a two-moment bulk

microphysics model to study the effect of aerosol perturbations on deep convective clouds. The bin model shows that with an increase in aerosol number concentration comes an invigoration and a decrease in precipitation. On the other hand, the bulk model suggests that the storm ought to weaken and precipitation will increase in a more polluted environment. The invigoration predicted by the bin model is a result of the suppression of the collision-coalescence process that permits more droplets to be lofted above the freezing level, hence increasing the bulk freezing rate aloft. The additional freezing and subsequent deposition acts to increase the latent heating and thus increase buoyancy. However, the cloud particles in the polluted cases are now smaller and more numerous and consequently have a shorter evaporation/sublimation timescale and a longer sedimentation timescale. The ultimate result is for precipitation to decrease in conjunction with a moistening of the mid- to upper-troposphere. The difference in the sign of the aerosol effect between the two models is thought to be related to the saturation adjustment scheme used in the bulk model and is addressed by including an explicit treatment of condensation and activation within the bulk model, similar to the algorithm utilized in the bin model. The results of the inter-model comparison demonstrate the significance of the saturation adjustment assumption on the sign and magnitude of the aerosol effect on deep convective clouds.

# Contents

# List of Tables

# List of Figures

# Chapter 1

# Introduction and Motivation

Aerosol particles, specifically those that act as cloud condensation nuclei (CCN) and/or ice nuclei (IN) are a fundamental constituent of Earth's atmosphere and play a vital role in the formation of clouds. Under normal atmospheric conditions, water vapor is unable to homogeneously condense into spherical droplets due to the large free energy barrier requirement (e.g., Rogers and Yau, 1989; Pruppacher and Klett, 1997). By introducing particles that are hygroscopic, i.e., CCN, the formation of water droplets can occurs readily at relatively small supersaturations within the atmosphere. Moreover, homogeneous freezing of liquid cloud droplets occurs spontaneously only for temperatures below about -38°C. Between 0 and -38°C, heterogeneous nucleation of ice particles occur due to the existence of IN in the atmosphere. When supercooled liquid droplets coexist with sufficient IN number concentrations, ice can form via three modes: contact mode, immersion mode, and condensation mode. On the other hand, ice crystals can form by the direct deposition of water vapor onto the surface of IN. Due to the fundamental relation between aerosols and clouds, changes in aerosol number concentration can lead to changes in cloud optical properties, precipitation, buoyancy, etc.

The effect of increased anthropogenic aerosol emissions on clouds has been addressed in countless studies for more than a half century (e.g., Gunn and Phillips, 1956; Squires, 1958; Twomey, 1977; Albrecht, 1989). Yet, on a global scale, the magnitude to which an increase in aerosol loading alters the cloud radiative forcing and ultimately Earth's radiation budget is poorly constrained (e.g., IPCC, 2007). It has been customary to distinguish specific aerosol indirect effects on clouds and determine a corresponding radiative forcing for each effect. However, IPCC (2007) presents the predicted radiative forcing for only the first aerosol indirect effect, namely between -0.3 and -1.8 W $m^{-2}$. (This is the effect whereby an increase in aerosol number concentration leads to an increase in cloud droplet number and a decrease in size and collision-coalescence. This leads to an increase in the cloud optical depth and a consequential increase in albedo.) No set range was established for other direct effects in IPCC (2007). Constraining the cloud radiative forcing is prudent for improving climate predictions and requires a detailed understanding and physical representation of the important physical processes relating aerosols and clouds.

Beyond the potential radiative impacts of an increase in aerosol loading are the potential impacts

on precipitation. Albrecht (1989) showed that in warm, stratiform clouds, an increase in precipitation can lead to a reduction in collision-coalescence and thus an increase in cloud lifetime in conjunction with a decrease in surface precipitation. Naturally, in a more complicated system, e.g., clouds containing both ice and liquid, determining whether an increase in aerosol loading leads to an increase or decrease in precipitation is challenging and remains uncertain. In fact, numerous recent studies have specifically addressed this issue without any definitive conclusion as to the sign of the change in precipitation due to increased aerosol number concentration (e.g., Khain et al., 2004; Khain and Pokrovsky, 2004; Khain et al., 2005; Wang, 2005; Koren et al., 2005; Grabowski, 2006; Seifert et al., 2006; Teller and Levin, 2006; Van den Heever et al., 2006; Fan et al., 2007; Tao et al., 2007; Van den Heever and Cotton, 2007; Khain et al., 2008; Lee et al., 2008a,b; Rosenfeld et al., 2008; Fan et al., 2009; Khain and Lynn, 2009; Koren et al., 2010; Noppel et al., 2010; Ekman et al., 2011; Lee, 2011; Lebo and Seinfeld, 2011a; Grabowski and Morrison, 2011; Seifert et al., 2012). Furthermore, recent studies have proposed that an increase in aerosol loading may actually invigorate convection in deep convective clouds, specifically supercell systems (e.g., Khain and Lynn, 2009; Lebo and Seinfeld, 2011a). Again, the sign of the effect on the convective updrafts for elevated aerosol concentrations is not well constrained. Moreover, changes in updraft velocities can lead to other changes in cloud properties, e.g., increased condensate loading, increased anvil extent, changes in anvil optical depth, etc. Numerical modeling of deep convective systems to determine the effects of aerosol perturbations requires both a detailed cloud microphysics scheme *and* a physically consistent aerosol activation algorithm.

Here, in Chapter 2, we address aerosol-cloud interactions in warm clouds via a new state-of-the-art two-dimensional (2-D) spectral aerosol-cloud microphysics model (Lebo and Seinfeld, 2011b). The model predicts both solute mass and liquid water mass over a 2-D mesh of cloud particles. In doing so, the model can retain all information about the activated aerosol and physically predict the evolution of the solute size distribution due to cloud microphysical processing. It is conventional in 1-D bin microphysics models to remove aerosol particles upon the activation of a cloud droplet and thus all information is lost about the aerosol. In the new 2-D spectral scheme, the solute mass is

conserved in addition to the water mass. As a result, aerosol activation and regeneration are both consistent and physically accurate. A discussion on the effects of regeneration mechanisms in other cloud models is provided.

In Chapter 3, we discuss a detailed mixed-phase 1-D bin microphysics model coupled to an explicit aerosol activation scheme designed to study the effect of increased aerosol loading on deep convection. Here a comparison between the modeled supercells using bin and bulk microphysics schemes is given. It is demonstrated that the bin model predicts an invigoration in convection due to an increase in latent heat release aloft, which provides a positive buoyancy contribution. However, the convective updrafts predicted by the bulk model are shown to be quite insensitive to an aerosol perturbation. Moreover, we discuss a detailed mechanism by which the convective tower can be invigorated while the cumulative precipitation is reduced for elevated aerosol number concentrations. The chapter concludes with a thorough analysis of IN effects on deep convection, and the potential for an increase in CCN to lead to increased rainfall intensity even though the domain-averaged precipitation decreases.

It was hypothesized that the differences between the simulated results of the bin and bulk models presented in Chapter 3 arise from the use of a saturation adjustment scheme in the bulk model. The saturation adjustment scheme is used to predict condensation and evaporation whereby at the end of the model time step, if a surplus of water vapor exists, the saturation ratio is brought to 1 and the excess vapor is condensed. On the other hand, if there is a deficit in water vapor, the saturation ratio is brought to 1 by evaporating the available cloud water. In doing so, the model does not account for number and size of cloud droplets in determining the condensation/evaporation rate and thus prevents the model from accurately predicting the changes that occur in polluted conditions. In Chapter 4 we address this issue by implementing an explicit calculation of the supersaturation over the time step, analogous to that of the bin model but within the bulk model. Simulations of a supercell are performed and robustness is determined via numerous perturbations to the initial conditions. The results suggest that the saturation adjustment scheme erroneously predicts excess condensation at lower levels, especially in a clean environment, and thus p[revents the model from

predicting an increase in buoyancy, like that which is predicted by the bin and bulk model without saturation adjustment. In fact, the increase in convective mass flux for the bin and bulk model without saturation adjustment are shown to be 4.73% and 5.09%, respectively, while the bulk model with saturation adjustment predicts a decrease of -3.50%. Moreover, the effect of an increase in aerosol loading for all model configurations on the strength of the cold pool and thus low-level convergence is discussed. Lastly, a discussion of the potential impact of the saturation adjustment scheme on other cloud types is also provided.

## 1.1 Bibliography

Albrecht, B.: Aerosols, cloud microphysics, and fractional cloudiness, Science, 245, 1227–1230, doi:10.1126/science.245.4923.1227, 1989.

Ekman, A. M. L., Engstrom, A., and Soderberg, A.: Impact of two-way aerosol-cloud interaction and changes in aerosol size distribution on simulated aerosol-induced deep convective cloud sensitivity, J. Atmos. Sci., 68, 685–697, 2011.

Fan, J., Zhang, R., Li, G., and Tao, W.-K.: Effects of aerosols and relative humidity on cumulus clouds, J. Geophys. Res., 112, doi:10.1029/2006JD008136, 2007.

Fan, J., Yuan, T., Comstock, J. M., Ghan, S., Khain, A., Leung, L. R., Li, Z., Martins, V. J., and Ovchinnikov, M.: Dominant role by vertical wind shear in regulating aerosol effects on deep convective clouds, J. Geophys. Res., 114, doi:10.1029/2009JD012352, 2009.

Grabowski, W. W.: Indirect Impact of Atmospheric Aerosol in Idealized Simulations of Convective-Radiative Quasi Equilibrium., J. Climate, 19, 4664–4682, 2006.

Grabowski, W. W. and Morrison, H.: Indirect Impact of Atmospheric Aerosol in Idealized Simulations of Convective-Radiative Quasi Equilibrium. Part II: Double-moment microphysics, J. Climate, 24, 1897–1912, 2011.

Gunn, R. and Phillips, B. B.: An experiment investigation of the effect of air pollution on the initiation of rain, J. Meteor., 14, 272–280, 1956.

IPCC: Summary for Policymakers, in: Climate Change 2007: The Physical Science Basis. Contribution of Working Group I to the Fourth Assessment Report of the Intergovernmental Panel on Climate Change, edited by Solomon, S., Qin, D., Manning, M., Chen, Z., Marquis, M., Averyt, K. B., Tignor, M., and Miller, H. L., Cambridge University Press, 2007.

Khain, A. and Lynn, B.: Simulation of a supercell storm in clean and dirty atmosphere using weather research and forecasting model with spectral bin microphysics, J. Geophys. Res., 114, doi:10.1029/2009JD011827, 2009.

Khain, A. and Pokrovsky, A.: Simulation of effects of atmospheric aerosols on deep turbulent convective clouds using a spectral microphysics mixed-phase cumulus cloud model. Part II: Sensitivity study, J. Atmos. Sci., 61, 2983–3001, 2004.

Khain, A., Pokrovsky, A., Pinsky, M., Seifert, A., and Phillips, V.: Simulation of effects of atmospheric aerosols on deep turbulent convective clouds using a spectral microphysics mixed-phase cumulus cloud model. Part I: Model description and possible applications, J. Atmos. Sci., 161, 2963–2982, 2004.

Khain, A., Rosenfeld, D., and Pokrovsky, A.: Aerosol impact on the dynamics and microphysics of deep convective clouds, Quart. J. Roy. Meteor. Soc., 131, 2639–2663, doi:10.1256//qj.04.62, 2005.

Khain, A., BenMoshe, N., and Pokrovsky, A.: Factors Determining the Impact of Aerosols on Surface Precipitation from Clouds: An Attempt at Classification, J. Atmos. Sci., 65, 1721–1748, 2008.

Koren, I., Kaufman, Y. J., Rosenfeld, D., Remer, L. A., and Rudich, Y.: Aerosol invigoration and restructuring of Atlantic convective clouds, Geophys. Res. Let., 32, doi:10.1029/2005GL023187, 2005.

Koren, I., Remer, L. A., Altaratz, ., Martins, J. V., and Davidi, A.: Aerosol-induced changes of convective cloud anvils produce climate warming, Atmos. Chem. Phys., 10, 5001–5010, doi:10.5194/acp-10-5001-2010, 2010.

Lebo, Z. J. and Seinfeld, J. H.: Theoretical basis for convective invigoration due to increased aerosol concentration, Atmos. Chem. Phys., 11, 5407–5429, doi:10.5194/acp-11-5407-2011, 2011a.

Lebo, Z. J. and Seinfeld, J. H.: A continuous spectral aerosol-droplet microphysics model, Atmos. Chem. Phys., 11, 12 297–12 316, doi:10.5194/acp-11-12297-2011, 2011b.

Lee, S. S.: Dependence of aerosol-precipitation interactions on humidity in a multiple-cloud system, Atmos. Chem. Phys., 11, 2179–2196, doi:10.5194/acp-11-2179-2011, 2011.

Lee, S. S., Donner, L. J., Phillips, V. T. J., and Ming, Y.: Examination of aerosol effects on

precipitation in deep convective clouds during the 1997 ARM summer experiment, Quart. J. Roy. Meteor. Soc., 134, 1201–1220, doi:10.1002/qj.287, 2008a.

Lee, S. S., Donner, L. J., Phillips, V. T. J., and Ming, Y.: The dependence of aerosol effects on clouds and precipitation on cloud-system organization, shear and stability, J. Geophys. Res., 113, doi:10.1029/2007JD009224, 2008b.

Noppel, H., Blahak, U., Seifert, A., and Beheng, K. D.: Simulations of a hailstorm and the impact of CCN using an advanced two-moment cloud microphysics scheme, Atmos. Res., 96, 286–301, 2010.

Pruppacher, H. R. and Klett, J. D.: Microphysics of Clouds and Precipitation, Kluwer Academic Publishers, Boston, 1997.

Rogers, R. R. and Yau, M. K.: A Short Course in Cloud Physics, Butterworth-Heinemann, 1989.

Rosenfeld, D., Lohmann, U., Raga, G. B., O'Dowd, C. D., Kulmala, M., Fuzzi, S., Reissell, A., and Andreae, M. O.: Flood or Drought: How do aerosols affect precipitation?, Science, 321, 1309–1313, 2008.

Seifert, A., Khain, A., Pokrovsky, A., and Beheng, K.: A Comparison of Spectral Bin and Two-Moment Bulk Mixed-Phase Cloud Microphysics, Atmos. Res., 80, 146–66, 2006.

Seifert, A., Köhler, C., and Beheng, K. D.: Aerosol-cloud-precipitation effects over Germany as simulated by a convective-scale numerical weather prediction model, Atmos. Chem. Phys., 12, 709–725, doi:10.5194/acp-12-709-2012, 2012.

Squires, P.: The microstructure and Colloidal Stability of Warm Clouds: Part I - The Relation between Structure and Stability, Tellus, 10, 256–261, 1958.

Tao, W.-K., Li, X., Khain, A., Matsui, T., Lang, S., and Simpson, J.: Role of atmospheric aerosol concentration on deep convective precipitation: Cloud-resolving model simulations, J. Geophys. Res., 112, doi:10.1029/2007JD008728, 2007.

Teller, A. and Levin, Z.: The effects of aerosols on precipitation and dimensions of subtropical clouds: a sensitivity study using a numerical cloud model, Atmos. Chem. Phys., 6, 67–80, 2006.

Twomey, S.: The Influence of Pollution on the Shortwave Albedo of Clouds, J. Atmos. Sci., 34, 1149–1152, 1977.

Van den Heever, S. C. and Cotton, W. R.: Urban Aerosol Impacts on Downwind Convective Storms, J. Appl. Meteor. Clim., 46, 828–850, 2007.

Van den Heever, S. C., Carri, G. G., Cotton, W. R., DeMott, P. J., and Prenni, A. J.: Impacts of Nucleating Aerosol on Florida Storms. Part I: Mesoscale Simulations, J. Atmos. Sci., 63, 1752–1775, 2006.

Wang, C.: A modeling study of the response of tropical deep convection to the increase of cloud condensation nuclei concentration: 1. Dynamics and microphysics, J. Geophys. Res., 110, doi:10.1029/2004JD005720, 2005.

# Chapter 2

# A Continuous Spectral Aerosol-Droplet Microphysics Model

## 2.1 Abstract

A two-dimensional (2-D) continuous spectral aerosol-droplet microphysics model is presented and implemented into the Weather Research and Forecasting (WRF) model for large-eddy simulations (LES) of warm clouds. Activation and regeneration of aerosols are treated explicitly in the calculation of condensation/evaporation. The model includes a 2-D spectrum that encompasses wet aerosol particles (i.e. haze droplets), cloud droplets, and drizzle droplets in a continuous and consistent manner and allows for the explicit tracking of aerosol size within cloud droplets due to collision-coalescence. The system of differential equations describing condensation/evaporation (i.e. mass conservation and energy conservation) is solved simultaneously within each grid cell. The model is demonstrated by simulating a marine stratocumulus deck for two different aerosol loadings (100 and $500\,\mathrm{cm}^{-3}$), and comparison with the more traditional microphysics modeling approaches (both 1-D bin and bulk schemes) is evaluated. The simulations suggest that in a 1-D bin microphysics scheme, without regeneration, too few particles are produced and hence the mode of the droplet size spectrum occurs at a larger size relative to the 2-D bin model results. Moreover, with regeneration, the 1-D scheme produces too many small droplets and thus shifts the mode toward smaller sizes. These large shifts in the droplet size distribution can potentially have significant effects on the efficiency of the collision-coalescence process, fall speeds, and ultimately precipitation.

## 2.2 Introduction

Numerical modeling of clouds presents a particularly challenging problem in that the underlying physical processes occur on the micro-scale, while the bulk quantities often observed and predicted by models are on the macro-scale. In large-scale numerical models, e.g. regional climate models and general circulation models (GCM), cloud processes are prognostic but require significant assumptions about the details of the sub-gridscale processes (e.g. Sundqvist, 1988; Beheng, 1994; Del Genio et al., 1996; Rotstayn, 1997; Roeckner et al., 2003; Rotstayn and Liu, 2003a; Zhang et al., 2003; Morrison and Gettelman, 2008). As one moves toward models with smaller domains, e.g. numerical

weather prediction models or cloud resolving models (CRM), relevant dynamical processes are better resolved and this requires more precise numerical cloud models. Frequently, single-moment or two-moment bulk microphysics schemes are employed in these models (e.g. Lin et al., 1983; Rutledge and Hobbs, 1983, 1984; Ferrier, 1994; Walko et al., 1995; Feingold et al., 1998; Rasch and Kristjansson, 1998; Simpson et al., 2003; Hong et al., 2004; Thompson et al., 2004; Morrison et al., 2005; Morrison and Pinto, 2005; Hong and Lim, 2006; Li et al., 2008; Thompson et al., 2008; Wang and Feingold, 2009a,b; Lim and Hong, 2010). These models predict either the first moment of a cloud particle size distribution (i.e. number concentration) or both the first and third moments (i.e. number concentration and mass mixing ratio), respectively. In general, the prognostic equations for changes both in number concentration and mass mixing ratio rely on an assumption regarding the shape of the size distribution of cloud particles. Here, "particles" refers to any of the following: cloud droplets, rain drops, pristine ice, snow (aggregates), graupel, and/or hail. By assuming a functional shape, e.g. a gamma distribution, changes in bulk cloud quantities can be analytically computed. However, such schemes lack the ability to accurately represent the various nonlinear processes within a cloud, i.e. collision-coalescence, aggregation, accretion, riming, etc, since the analytical solutions require gross assumptions regarding not only the size distribution shape, but also, fall speed, collection efficiency, etc.

In recent years, advances in computing efficiency and parallel processing have enabled the use of more detailed cloud microphysics models, i.e. bin (or spectral) microphysics. These models have been developed for applications in both warm and mixed-phase clouds (e.g. Tzivion et al., 1987, 1989; Feingold et al., 1988; Reisin et al., 1996; Stevens et al., 1996; Geresdi, 1998; Geresdi and Rasmussen, 2005; Rasmussen et al., 1987; Khain et al., 2004; Khain and Pokrovsky, 2004; Khain and Lynn, 2009; Fan et al., 2009; Xue et al., 2010; Lebo and Seinfeld, 2011). Instead of tracking a single number concentration and mass for each type of cloud particle, the bin microphysics schemes discretize the distributions into size bins that span the smallest cloud droplets to large rain/graupel/snow/hail particles. The inherent nature of this approach allows for the explicit calculation of the collection processes within clouds based upon pair-wise collisions of cloud particles. Additionally, through size

resolution, other processes, e.g. sedimentation, condensation/evaporation, deposition/sublimation, can be better simulated.

These approaches to simulating clouds, even in the most detailed case of the traditional bin microphysics scheme, still rely on assumptions, specifically regarding aerosol activation (i.e. the process by which a haze droplet or wet aerosol grows beyond its corresponding critical radius, $r_c$, thus becoming a cloud droplet) and aerosol regeneration (this term refers to the mechanism by which an aerosol particle is formed as a cloud droplet evaporates). In reality, wet aerosols, cloud droplets, and drizzle droplets comprise a continuous spectrum defined by both the total size and the contained solute (aerosol) mass. Recently, Xue et al. (2010) demonstrated the significance of aerosol regeneration using a spectral bin microphysics model. Following Mitra et al. (1992), it is assumed that for each droplet that evaporates, one aerosol particle is generated from the solute contained in the droplet. However, the size of the regenerated aerosol is not known, since after the activated aerosol particle grows within the cloud droplet spectrum, information regarding the size of the activated aerosol is lost. Furthermore, the evaporation of cloud droplets is often simulated by predicting the amount of mass lost to the gas phase within a time step for a given droplet size, shifting the distribution, and rebinning the new cloud droplets into the Eulerian bins (Tzivion et al., 1989; Reisin et al., 1996; Khain et al., 2004; Lebo and Seinfeld, 2011). Thus, information regarding the size of the droplet before evaporation is lost after a single time step, making it difficult to use droplet size as a proxy for the regenerated aerosol size. In all, these assumptions regarding activation and regeneration represent a shortcoming in the current spectral bin microphysics models.

In previous works (e.g. Xue et al., 2010; Lebo and Seinfeld, 2011), the size distribution of the regenerated aerosols is prescribed to be lognormal (either with a single mode or bimodal). And since the actual size of the regenerated aerosols is not known, the shape of the regenerated lognormal distribution must also be predefined (often the shape parameters of the original distribution are used). This assumption introduces a bias in the modeled droplet number concentration that can be either positive or negative (i.e. leads to too many or too few cloud droplets), as will be explained shortly. In Fig. 2.3 a schematic of the relevant cloud microphysical process that control both the

droplet size and solute mass are shown. Aerosol particles located in subsaturated regions will exist as haze particles. Upon activation, condensational growth increases the droplet mass while the solute mass remains constant. If the droplets are sufficiently large, collision-coalescence can become an important mechanism for not only cloud droplet growth, but also solute mass growth. Also, the solute mass in a droplet may have changed during the time in cloud due to collection, scavenging of aerosols, or in-situ chemical reaction. Thus, a shift in the size distribution toward larger sizes is expected, especially, in relatively clean environments where collision-coalescence is significant and efficient. Modeling the evolution of solute mass along with cloud droplet number concentration and mass is desirable.

The activation/regeneration problem can be summarized as follows (Fig. 2.3). An initial aerosol size ($D_s$) distribution ($N_s$) undergoes activation (left to right, red, solid); larger cloud condensation nuclei (CCN) are more easily activated since a lower ambient supersaturation is required. These particles are then removed from the aerosol size distribution, leaving the non-activated particles. From this point, the manner in which the regeneration step is represented can affect the droplet (and aerosol) size distribution in two ways:

1. Negative Bias – In regions of entrainment, if all of the droplets within a grid box evaporate, the number concentration of regenerated aerosol particles ($N_{reg}$) is identical to the original cloud droplet number concentration ($N_d$). A traditional approach is that these particles are described by the parameters used for the initial aerosol size distribution and are added to the existing distribution (black, dashed). However, during the activation process, the smaller aerosols do not activate and thus should not be regenerated. Here, we see that the aforementioned assumptions regarding aerosol regeneration begin to artificially enhance the aerosol number concentration in the smaller size bins (i.e. those particles that did not activate and likely will not activate). With subsequent evaporation/regeneration events this bias grows, and continuous activation and regeneration will lead to a significant, yet artificial, increase in small aerosol particles that are unlikely to activate since the available water vapor surplus is consumed by the larger aerosols and cloud droplets (thus reducing the supersaturation below that which

would allow the smaller aerosol particles to activate). Consequently, fewer droplets are formed during activation and $N_d$ is ultimately underpredicted, i.e. there is a negative bias in $N_d$.

2. Positive or Negative Bias – In the event that all of the droplets in a grid cell are not evaporated, large droplets will remain, while smaller droplets will completely evaporate (Pruppacher and Klett, 1997). The smaller, now evaporated droplets, were most likely formed on aerosol particles near to the cutoff size for activation (i.e. the critical supersaturation of these aerosols is just below the ambient supersaturation when activation occured) and should consequently return to the bins containing the smallest activated aerosols. Instead, these droplets are evaporated and the regenerated aerosol is spread over all sizes. This treatment produces excess small aerosols (similar to that shown above for the Negative Bias) but also produces excess larger aerosols. The larger aerosols are more likely to activate in a subsequent time step than their smaller counterparts (since the critical supersaturation for these particles is smaller). By spreading the distribution out over all sizes, particles will activate to form new cloud droplets in the presence of small supersaturations (even though, if the aerosols were placed in the correct location, the critical supersaturation ought to be too large for subsequent activation to occur). Here, a competition exists between the negative skewness caused by overproducing smaller aerosols and positive skewness caused generating excess larger aerosols. The former will suppress $N_d$ while the latter will enhance $N_d$.

An approach to reproducing or recycling aerosol particles was presented by Kogan et al. (1995) to attempt to account for the fact that smaller droplets (likely formed from smaller aerosol particles) will evaporate first and more readily. Here, the regenerated aerosols are assumed to go to the smallest size bin in the aerosol distribution until it attains its pre-activated value (i.e. the number concentration that was set during the model initialization), then the second smallest bin is filled, and so on. This method, albeit more precise in that it will not artificially produce excess small particles, still lacks the ability to reproduce the ambient aerosol field after droplet evaporation, especially in conditions where the collision-coalescence process is a significant sink of small aerosols and a source of larger aerosols (as shown below).

Another method for simulating aerosol effects on clouds is to assume that the aerosol number concentration is fixed (e.g. Lu and Seinfeld, 2005, 2006; Sandu et al., 2008; Chen et al., 2011). Although this assumption circumvents the aerosol regeneration problem, fixing the aerosol number concentration may result in excess droplet formation. After activation, only those particles that are less likely to activate remain. On the next time step, if a supersaturation exists, as long as it is less than that of the previous time step, no new aerosols should activate (unless particles in the larger size categories are replenished by advection). But, in the case of fixed aerosol number concentration, the possibility exists for aerosol particles to activate and increase $N_d$, leading to a positive bias in $N_d$. Such a bias can lead to an artificial suppression of drizzle formation, increasing the LWP, or more vigorous evaporation in regions of entrainment since the droplets will be smaller (assuming the LWC is unchanged) acting to decrease the LWP. Obviously, these effects can offset one another, but in the case that they do not, the predicted LWP will likely not be correct.

To more accurately simulate the evolution of the continuous field that encompasses the spectrum from wet aerosols to drizzle droplets and address in detail the activation/regeneration problem in cloud models, we present here the implementation of a 2-D continuous spectral aerosol-droplet microphysics scheme coupled to a 3-D dynamical core for studying warm cloud microphysics. Recently, Ovchinnikov and Easter (2010) described a detailed 2-D fixed-bin (i.e. Eulerian) cloud microphysics scheme including chemistry, in which activated aerosols and interstitial wet aerosol particles are tracked within each grid point. The method does not include collision-coalescence and incorporates a linearized approximation to the droplet vapor growth equation. Collision-coalescence is an essential process for drizzle formation, and will alter the regenerated aerosol distribution, by shifting the solute mass to larger sizes.

The new method, as described in detail below, requires no a priori assumptions regarding aerosol activation and regeneration, since the treatment is explicitly accounted for via the representation of condensation/evaporation. Moreover, the solutions to the supersaturation (mass) and energy (temperature) equations are performed in a consistent, continuous, and simultaneous (i.e. latent heating and changes in the vapor surplus/deficit are computed with condensation/evaporation)

manner including the effects of droplet curvature and solute mass on the condensation/evaporation rate of wet aerosol particles and cloud droplets. A detailed calculation of the collision-coalescence process is included to accurately represent both the evolution of the droplet spectrum due to pair-wise collisions, as well as the shift in the aerosol size distribution resulting from collision (either pair-wise collisions of cloud droplets or aerosol and cloud droplets, i.e. scavenging). Thus, the model includes the relevant physics in a manner that requires few assumptions unlike the more traditional 1-D bin microphysics schemes and bulk schemes. The continuous nature of the microphysics scheme allows one to address regeneration as well as determine the effect of cloud microphysics on the aerosol size distribution, an important component in determining the resulting aerosol spectrum after a cloud dissipates and accurately predicting evaporation rates in regions of entrainment.

The remainder of the work is organized as follows: Sect. 2.3 describes the 2-D continuous spectral aerosol-cloud microphysics model in detail as well as the alternative models used for comparative purposes. Section 2.4 discusses the dynamical model that is used as well as the model initialization. Numerical results are presented in Sect. 2.5, while Sect. 2.6 includes a discussion of the most important conclusions and future work.

## 2.3 New 2-D spectral microphysics scheme

The method developed here predicts the number of particles in a two-dimensional space, one dimension for the droplet size (mass or radius) and one for the solute size (mass or radius). One continuous 2-D size spectrum encompasses both aerosol particles and activated droplets and maintains the solute mass within activated droplets over the entire size spectrum. Even the most detailed bin microphysics schemes (e.g. Tzivion et al., 1987, 1989; Reisin et al., 1996; Stevens et al., 1996; Geresdi, 1998; Geresdi and Rasmussen, 2005; Rasmussen et al., 1987; Khain et al., 2004; Khain and Lynn, 2009; Xue et al., 2010) predict cloud particle sizes in just one dimension. Even with a detailed activation scheme that predicts droplet formation from a binned aerosol distribution (e.g. Xue et al., 2010), information regarding the size (and composition) of the aerosol particle after activation (i.e. from the dry aerosol distribution to the cloud droplet distribution) is not preserved. And, since

the solute quantity in each droplet size bin is not computed and tracked, the regeneration of aerosol particles upon droplet evaporation must be parameterized. Although for each drop that evaporates, one aerosol particle is regenerated, aerosol scavenging by cloud/rain droplets, collision-coalescence, and aqueous-phase chemistry alter the solute mass in each droplet, and thus affect the size distribution of regenerated aerosol. In this study we exclude aqueous-phase chemistry in order to focus on the overall effect of collision-coalescence on the solute mass distribution and consequently the regenerated aerosol distribution; however, aqueous-phase chemistry can, in principle, be included in the model. The 2-D method presented here requires no special assumptions and includes all important aerosol/cloud microphysical processes.

We assume mass doubling between droplet bins and aerosol bins, i.e.

$$x_{i+1} \;=\; 2\; x_i \tag{2.1}$$

$$x_{k+1} \;=\; 2\; x_k, \tag{2.2}$$

respectively, where the subscripts $i$ and $k$ refer to the $i$-th bin of the droplet size dimension and the $k$-th bin of the aerosol size dimension. In other words, each particle lies in a bin $i$, $k$. For illustration, we assume that the smallest aerosol diameter is 0.05 µm and the smallest droplet diameter is 0.05 µm (sensitivity simulations show that the results are qualitatively similar for changes in the size of the smallest bins). We include 15 bins in the aerosol dimension and 36 bins in the droplet dimension such that the upper edge of the largest droplet size bin is 204.8 µm. Note that the smallest droplet size category corresponds to that of the smallest aerosol size bin. In the case that the ambient air is relatively dry, i.e., below the deliquescence point for the aerosol type, the particle will contain no water and thus its total size corresponds to just the aerosol size.

In any Eulerian bin microphysics scheme, the number of bins is always determined by the user. However, for specific cases, the number of bins should be extended toward larger sizes or can be reduced to only include smaller sizes. For example, to simulate Arctic stratus, Harrington et al. (2000) employed 25 bins while for simulations of deep convective clouds, Khain and Lynn (2009)

and Lebo and Seinfeld (2011) used 33 and 36 bins, respectively, to capture large droplets and graupel. In determining the number of bins necessary for the study at hand, one must consider the differences in such things as terminal fall speed, activation, collection efficiency, etc., of the added or removed bins. In the case of the number of aerosol bins, we restricted the calculations to 15 bins. Simulations (not shown) with 20 bins were performed. There was no qualitative difference between the simulations using 15 and 20 bins. In fact this should be expected since the actual size of the aerosol upon regeneration and subsequent re-activation ought to only be important when the critical supersaturation of the newly formed particle is approximately that of the ambient supersaturation attained in the cloud during the simulation. Since the critical supersaturation of aerosol particles is not a linear function of size, adding bins with smaller sizes will act to increase the computational expense, with little to no change in the cloud properties since these particles are likely to not activate during the simulation. On the other hand, adding bins with larger sizes will also have little to no effect on the cloud properties since these particles have a very low critical supersaturation and thus will likely re-activate in the presence of *any* supersaturation. Thus, the chosen aerosol binning is dependent upon the ambient supersaturation within the cloud. For future studies of other cloud types, e.g., shallow convection, deep convection, etc., the aerosol size distribution will have to be extended to encompass particles with higher critical supersaturations since the ambient supersaturation in these cloud types is often higher than in the marine stratocumulus case chosen to demonstrate the model's implementation.

### 2.3.1 Condensation/evaporation

Condensation and evaporation are simulated by solving the set of ordinary differential equations that describe vapor deposition onto the particles, water mass conservation, energy conservation, and ambient supersaturation. The vapor deposition equation is defined as (Pruppacher and Klett (1997)):

$$\frac{dr_{i,k}}{dt} = \frac{Gs}{r_{i,k}} \left[ 1 - \frac{A}{r_{i,k}} + \frac{B_k}{r_{i,k}^3} \right] \tag{2.3}$$

where,

$$G = \left[\frac{R_v\ T}{D_v^*\ e_s} + \frac{\Delta H_v}{K_T^*\ T}\left(\frac{\Delta H_v}{R_v\ T} - 1\right)\right]^{-1} \tag{2.4}$$

$$A = \frac{2\ \sigma_w}{\rho_l\ R_v\ T} \tag{2.5}$$

$$B_k = \frac{3\ i\ m_{s_k}}{4\ \pi\ \rho_l}\ \frac{M_w}{M_s}. \tag{2.6}$$

Here, $r_{i,k}$ is the radius of a droplet in bin $i,k$, $R_v$ is the gas constant for water vapor, $D_v^*$ is the diffusion coefficient of water vapor as a function of temperature ($T$) and pressure ($P$) including kinetic effects, $e_s$ is the equilibrium vapor pressure over liquid water, $\Delta H_v$ is the enthalpy of vaporization for water, $K_T^*$ is the thermal conductivity of air as a function of $T$ including kinetic effects, $\sigma_w$ is the surface tension of liquid water, $\rho_l$ is the density of liquid water, $i$ is the ionic dissociation factor, $m_{s_k}$ is the solute mass in aerosol bin $k$, $M_w$ is the molar mass of water, and $M_s$ is the molar mass of the solute (assumed to be ammonium sulfate for the cases presented herein). Following Pruppacher and Klett (1997), we express $D_v^*$ and $K_T^*$ as

$$D_v^* = \frac{D_v}{\left[\frac{r_{i,k}}{r_{i,k} + \lambda_v} + \frac{D_v}{r_{i,k}\ \alpha_c}\sqrt{\frac{2\ \pi\ M_w}{RT}}\right]} \tag{2.7}$$

and

$$K_T^* = \frac{K_T}{\left[\frac{r_{i,k}}{r_{i,k} + \lambda_T} + \frac{K_T}{r_{i,k}\ \alpha_T\ \rho_a\ c_p}\sqrt{\frac{2\ \pi\ M_a}{RT}}\right]} \tag{2.8}$$

where $D_v$ is the unmodified diffusivity, $\lambda_v$ is the vapor jump length (assumed to be equal to the mean free path of air molecules), $\alpha_c$ is the condensation accommodation coefficient, $K_T$ is the unmodified thermal conductivity of air, $\lambda_T$ is the thermal jump distance, $\alpha_T$ is the thermal accommodation coefficient, $c_p$ is the heat capacity of air at constant pressure, $R$ is the universal gas constant and $M_a$ is the molar mass of air. In the absence of ice, the mass conservation equation can be written simply as balance between the decrease (increase) of the vapor mixing ratio ($q_v$) due to condensation

(evaporation) changing the liquid water mixing ratio ($q_l$):

$$\frac{dq_v}{dt} \;=\; -\,\frac{dq_l}{dt} \tag{2.9}$$

where

$$\frac{dq_l}{dt} \;=\; \frac{4\,\pi\rho_w}{\rho_a}\;\sum_{i=1}^{N}\;\sum_{k=1}^{M}\; r_{i,k}^2\;\frac{dr_{i,k}}{dt}\;N_{i,k} \tag{2.10}$$

in which $\rho_a$ is the ambient air density, $N$ and $M$ are the total number of bins in the droplet and aerosol dimensions, respectively, and $N_{i,k}$ is the number concentration of particles in bin $i$, $k$ in units of $\mathrm{kg}^{-1}$. Energy conservation is represented by

$$\frac{dT}{dt} \;=\; \frac{\Delta H_v}{c_p\;(1\;+\;q_v)}\;\frac{dq_l}{dt}. \tag{2.11}$$

Here, the ambient temperature is modified due to latent heating induced by phase changes. Lastly, the supersaturation ($s$) equation is represented by (Korolev and Isaac, 2003):

$$\frac{ds}{dt} \;=\; (s\;+\;1)\;\left[-\left(\frac{1}{q_v}\;+\;\frac{\Delta H_v^2}{c_p\;R_v\;T^2}\right)\;\frac{dq_l}{dt}\right]. \tag{2.12}$$

Equations (2.3), (2.9), (2.11), and (2.12) comprise a set of

$$N_{equ} = \frac{M}{2}\,(M+1) + M\,(N-M) + 3 \tag{2.13}$$

ordinary differential equations (where $N_{equ}$ is the number of equations). The solution to the set of equations is found by employing the Variable Order Differential Equation (VODE) solver of Brown et al. (1989). The solver is initialized with the ambient $q_v$, $T$, $s$, and $N_{i,k}$ on each time step. The solver predicts the values of the given variables at the end of the time step and $q_v$, $T$, and $s$ are updated accordingly. The droplets are rebinned into the Eulerian bins defined during the model initialization. This is done by assuming that the droplet distribution in each aerosol row of the 2-D mesh is piecewise linear. The new number concentration in each Eulerian bin is found by numerically

integrating the piecewise linear distribution. It is important to note that during a time step, the condensation/evaporation algorithm conserves both water mass (i.e. the sum of the water vapor and droplet mixing ratios is fixed) and aerosol mass. The aerosol mass is conserved, since, as shown in Fig. 2.3, condensation/evaporation moves droplets left and right in the 2-D space (up and down movements, or shifts in the aerosol size bin, is not permitted). This is justified since, physically, in the absence of aqueous phase chemistry, the soluble aerosol mass in a droplet will not change during condensation/evaporation.

### 2.3.2 Sedimentation

The terminal fall speeds required to compute sedimentation are calculated following Beard (1976) in which the particles are categorized into different regimes based upon their Reynolds number. The change in mass and number within a grid box due to sedimentation is computed then by predicting the mass and number that fall into the box from above and subtracting the mass and number that fall out of the box and into the box below. At the lowest level, the loss of mass through the bottom boundary is considered precipitation. This algorithm is analogous to that which is used in the 1-D bin and bulk models. Therefore, the only difference between the representation of sedimentation amongst the models is in the calculation of the terminal fall speeds (the bulk model has the least complex and fastest calculation while the new continuous spectral scheme is more accurate and computationally expensive).

### 2.3.3 Collision-coalescence and aerosol scavenging

The proposed 2-D microphysics scheme does not distinguish between collisions of cloud droplets and collisions of aerosol particles with cloud droplets since the entire particle spectrum is continuous (i.e. the aerosol is *included* in the droplet size). Moreover, due to the large difference in timescales between the collection process and vapor deposition, we separate the collection calculations from the vapor deposition. The former occurs over 10s of minutes (e.g. Tzivion et al., 1987; Bott, 1998) while the latter occurs over the course of a few seconds (e.g. Chuang et al., 1997; Pruppacher and Klett,

1997) Another reason for doing so is that the collection process does not affect the ambient water vapor mixing ratio (note that the equilibrium vapor pressure will change slightly since larger drops require less water vapor in the gas phase to maintain equilibrium), temperature, or supersaturation directly. The calculations are performed as follows.

For numerical implementation, we employ the flux method of Bott (1998). (Bott, 2000 proposed a method by which the 2-D collection problem can be reduced to a 1-D problem and then extrapolated back to 2-D. We find that it is best to apply the 1-D method of Bott, 1998 in two-dimensions to minimize the loss of information when the problem is simplified to a 1-D collection problem.) Collisions between every pair of bins are explicitly calculated. We follow the parabolic flux method proposed in Bott (1998) to limit upstream numerical diffusion.

We can express the loss of particles in bin $i, k$ due to collisions with particles in bin $j$, $l$ ($\Delta N_{(i,k)-(j,l)}$) as

$$\Delta N_{(i,k)-(j,l)}\,|_{loss} \;=\; N_{i,k}\; N_{j,l}\; K_{i,j}\; \Delta t \tag{2.14}$$

where $N_{i,k}$ and $N_{j,l}$ are the number of particles in bins $i$, $k$ and $j$, $l$, respectively, $K_{i,j}$ is the collection kernel for the collisions between the $i$-th and $j$-th droplet bins (the solute is assumed to have a negligible impact on the kernels), and $\Delta t$ is the time step. Assuming the collection kernel is symmetric,

$$\Delta N_{(i,k)-(j,l)}\,|_{loss} \;=\; \Delta N_{(j,l)-(i,k)}\,|_{loss} \;=\; \Delta N^{(n,m)}_{(i,k)-(j,l)}\,|_{gain} \tag{2.15}$$

in which $\Delta N^{(n,m)}_{(i,k)-(j,l)}|_{gain}$ represents the gain of particles in bin $n$, $m$ due to collisions between droplets in bins $i$, $k$ and $j$, $l$. The subscripts $n$ and $m$ correspond to the droplet and aerosol bins, respectively, that contain the particles formed by collisions between particles in bins $i$, $k$ and $j$, $l$. Note that the well known problem occurs in which the newly formed droplets do not necessarily coincide with a 2-D bin size. Thus, following Bott (1998) the new particles are added to bin $n$, $m$ such that

$$N'_{n,m} \;=\; N_{n,m} \;+\; \Delta N^{(n,m)}_{(i,k)-(j,l)}\,|_{gain} \tag{2.16}$$

where the $'$ denotes an intermediary number concentration used to compute the flux to surrounding

bins. Unlike the pure 1-D collection scenario, wherein a single flux through the upper boundary of the bin must be computed, the 2-D case requires 3 fluxes. Here, we can write the updated number concentrations in the bins affected by collisions between bins $i$, $k$ and $j$, $l$ as

$$N_{n,m} \;=\; N'_{n,m} \;-\; f_{n+1/2,m} \;-\; f_{n,m+1/2} \tag{2.17}$$

$$N_{n+1,m} \;=\; N_{n+1,m} \;+\; f_{n+1/2,m} \;-\; f_{n+1,m+1/2} \tag{2.18}$$

$$N_{n,m+1} \;=\; N_{n,m+1} \;+\; f_{n,m+1/2} \tag{2.19}$$

$$N_{n+1,m+1} \;=\; N_{n+1,m+1} \;+\; f_{n+1,m+1/2} \tag{2.20}$$

where $f$ denotes the flux through the boundary given by the subscript. For example, $f_{n+1/2,m}$ is the flux from bin $n$, $m$ to $n+1$, $m$. First, $f_{n+1/2,m}$ is computed and used to calculate the following

$$N''_{n,m} \;=\; N'_{n,m} \;-\; f_{n+1/2,m} \tag{2.21}$$

$$N'_{n+1,m} \;=\; N_{n+1,m} \;+\; f_{n+1/2,m} \tag{2.22}$$

where the added $'$'s denote an intermediary number concentration. These values are then used to compute the flux through the $m+1/2$ boundary, i.e. $f_{n,m+1/2}$ and $f_{n+1,m+1/2}$. For the 2-D case, similar to Bott (1998) we can express $f_{n+1/2,m}$ as a polynomial expression of order 2

$$f_{n+1/2,m} \;=\; w^{(1)}_{(i,k)-(j,l)} \sum_{s=0}^{2} \frac{a_{n,m,s}}{(s \;+\; 1)\; 2^{s+1}} \left[1 \;-\; (1 \;-\; 2\; c_{n,m})^{s+1}\right] \tag{2.23}$$

in which

$$w^{(1)}_{(i,k)-(j,l)} \;=\; \frac{N'}{N'_{n,m}} \tag{2.24}$$

$$a_{n,m,0} \;=\; -\,\frac{1}{24}\,\left[N_{n+1,m} \;-\; 26\; N'_{n,m} \;+\; N_{n-1,m}\right] \tag{2.25}$$

$$a_{n,m,1} \;=\; \frac{1}{2}\;(N_{n+1,m} \;-\; N_{n-1,m}) \tag{2.26}$$

$$a_{n,m,2} \;=\; \frac{1}{2}\;\left[N_{n+1,m} \;-\; 2\;N'_{n,m,} \;+\; N_{n-1,m}\right] \tag{2.27}$$

$$c_{n,m} \;=\; \frac{x' \;-\; x_{n,m}}{x_{n+1,m} \;-\; x_{n,m}} \tag{2.28}$$

where $N' = \Delta N^{(n,m)}_{(i,k)-(j,l)}|_{gain}$, $x'$ is the mass of a droplet formed by collisions between bins $i$, $k$ and $j$, $l$, $w^{(1)}_{(i,k)-(j,l)}$ is a weighting function, and $c_{n,m}$ can be thought of as a Courant number. The coefficients $a_{n,m,s}$ are computed by fitting the mass distribution curve to a polynomial of order 2 following Bott (1998). Similar expressions can be derived for the remaining two fluxes to get:

$$f_{n,m+1/2} \;=\; w^{(2)}_{(i,k)-(j,l)}\;\sum_{s=0}^{2}\;\frac{a'_{n,m,s}}{(s\;+\;1)\;2^{s+1}}\;\left[1\;-\;(1\;-\;2\;c_{n,m})^{s+1}\right] \tag{2.29}$$

in which

$$w^{(2)}_{(i,k)-(j,l)} \;=\; \frac{N' \;-\; f_{n+1/2,m}}{N''_{n,m}} \tag{2.30}$$

$$a'_{n,m,0} \;=\; -\,\frac{1}{24}\;\left[N_{n,m+1} \;-\; 26\;N'_{n,m} \;+\; N_{n,m-1}\right] \tag{2.31}$$

$$a'_{n,m,1} \;=\; \frac{1}{2}\;\left(N_{n,m+1} \;-\; N_{n,m-1}\right) \tag{2.32}$$

$$a'_{n,m,2} \;=\; \frac{1}{2}\;\left[N_{n,m+1} \;-\; 2\;N'_{n,m,} \;+\; N_{n,m-1}\right] \tag{2.33}$$

$$c_{n,m} \;=\; \frac{y' \;-\; y_{n,m}}{y_{n,m+1} \;-\; y_{n,m}} \tag{2.34}$$

and

$$f_{n+1,m+1/2} \;=\; w^{(3)}_{(i,k)-(j,l)}\;\sum_{s=0}^{2}\;\frac{a_{n+1,m,s}}{(s\;+\;1)\;2^{s+1}}\;\left[1\;-\;(1\;-\;2\;c_{n+1,m})^{s+1}\right] \tag{2.35}$$

where

$$w^{(3)}_{(i,k)-(j,l)} \;=\; \frac{f_{n+1/2,m}}{N'_{n+1,m}} \tag{2.36}$$

$$a_{n+1,m,0} \;=\; -\,\frac{1}{24}\;\left[N_{n+1,m+1} \;-\; 26\;N'_{n+1,m} \;+\; N_{n+1,m-1}\right] \tag{2.37}$$

$$a_{n+1,m,1} \;=\; \frac{1}{2}\;\left(N_{n+1,m+1} \;-\; N_{n+1,m-1}\right) \tag{2.38}$$

$$a_{n+1,m,2} \;=\; \frac{1}{2}\;\left[N_{n+1,m+1} \;-\; 2\;N'_{n+1,m} \;+\; N_{n+1,m-1}\right] \tag{2.39}$$

$$c_{n+1,m} = \frac{y' - y_{n+1,m}}{y_{n+1,m+1} - y_{n+1,m}}. \quad (2.40)$$

Here, the weighting functions ($w^{(2)}_{(i,k)-(j,l)}$ and $w^{(3)}_{(i,k)-(j,l)}$ for the fluxes through the $n$, $m+1/2$ and $n+1$, $m+1/2$ boundaries, respectively) represent the updated change in droplet number concentration in bin $n$, $m$ and $n+1$, $m$ according to the flux $f_{n+1/2,m}$. Furthermore, $y$ refers to the aerosol masses ($y'$ is the aerosol mass created by collisions between droplets in bins $i$, $k$ and $j$, $l$. A diagram showing these calculations, demonstrating the directions in which mass "flows" due to collection for the various fluxes shown above, is presented in Fig. 2.2.

Lastly, we note that collisions between droplets (or even large CCN) and small aerosol particles (i.e., radius $<2\mu$m) are very rare due to gravitational settling alone. For particles in this size range, the collection is more likely to be a result of Brownian diffusion to the droplets and large CCN and/or temperature and density gradients, i.e., themophoresis and diffusiophoresis, respectively. However, the temperature and density gradients within the cloud are not significant enough for thermophoresis or diffusiophoresis to be a significant mechanism for the loss of small aerosols. Moreover, simulations performed with Brownian diffusion included in the 2-D continuous bin scheme (not shown) resulted in a negligible effect on the various cloud properties presented below. It is important to note that Brownian diffusion, thermophoresis, and diffusiophoresis are not included in most 1-D bin or bulk models. Including such processes in the spectral scheme would warrant their inclusion in the other schemes as well and require numerous parameterizations.

### 2.3.4 1-D bin microphysics model

For comparative purposes, we will present results using the traditional 1-D bin microphysics approach. The particular form of the 1-D bin model is that described in Lebo and Seinfeld (2011), and the ice phase is excluded in the numerical calculations performed here. The 1-D bin model is configured for simulations in which aerosol particles are regenerated upon droplet evaporation as described in the Introduction (i.e. the regenerated aerosol size distribution is prescribed with the same shape parameters as the initial distribution).

### 2.3.5 Bulk microphysics model

A two-moment bulk microphysics model (Morrison et al., 2005; Morrison and Pinto, 2005) is employed in order to compare with the detailed 2-D microphysics scheme presented above. The bulk model is altered to include a detailed spectral representation of the aerosol size distribution following Lebo and Seinfeld (2011). As is the case of the 1-D bin scheme, simulations are performed in both the presence and absence of aerosol regeneration. In both the bulk model and the 1-D bin model, the regenerated aerosol size distribution is assumed to be lognormal with the same geometric mean diameter and standard deviation as the initial size distribution.

In addition to the modified version of the bulk microphysics scheme, we include for comparative purposes, a set of simulations performed with the bulk microphysics scheme without any modifications, i.e. no aerosol coupling (fixed droplet number concentration, $N_d$). This microphysical option, obviously the fastest, lacks any link between aerosol particles and cloud droplets.

## 2.4 Simulation of marine stratocumulus dynamics

In order to compare the various microphysics models, we present simulations of a marine stratocumulus deck using an LES model. The stratified and closed nature of marine stratocumulus presents a good testbed for the 2-D continuous spectral warm-phase microphysics model. Also, marine stratocumulus is a well-studied cloud type via both in-situ measurements and modeling studies (e.g. Stevens et al., 1998, 2003, 2005; Rotstayn and Liu, 2003b; Lu and Seinfeld, 2005, 2006; Bretherton et al., 2007; Sandu et al., 2008, 2009; Hill et al., 2008, 2009; Ackerman et al., 2009; Shao and Liu, 2009; Wang et al., 2009; Wang and Feingold, 2009b; Wang et al., 2010, 2011).

We employ the Weather Research and Forecasting (WRF) model, version 3.1.1 (Skamarock et al., 2008) for the dynamical core for the LES. All three microphysics schemes described in Sect. 2.3 are coupled to WRF. The model is initialized with the liquid water potential temperature ($\theta_l$) and total water mixing ratio ($q_{tot}$) shown in Fig. 2.1 based on the First International Satellite CLoud Climatology Project Regional Experiment (FIRE I) from Duynkerke et al. (2004) and as

incorporated in Chen et al. (2011). Soundings from FIRE I have been used in numerous modeling studies of marine stratocumulus (e.g. Hill et al., 2008, 2009; Chen et al., 2011). The sounding depicts a 600 m deep shallow boundary layer that is capped with a 12 K and 3 g kg$^{-1}$ inversion in $\theta_l$ and $q_{tot}$, respectively. The zonal ($u$) and meridional ($v$) wind speeds are prescribed to be -1 and 6 m s$^{-1}$, respectively, throughout the model domain. The LES model is initialized with a random $\pm$0.1 K temperature perturbation to initiate the eddies. For illustrative purposes, only nocturnal conditions are considered. The Rapid Radiative Transfer Model (RRTM) option in WRF is used for the longwave radiative transfer calculations. The monotonic advection scheme is used for the advection of all scalars. Surface latent heating and fluxes are computed following the Monin-Obukhov scheme.

Simulations are performed on a 1 km $\times$ 1 km $\times$ 1.6 km domain with a horizontal and vertical grid-spacing of 66.7 and 40 m, respectively. The vertical resolution chosen for the current study is a bit lower than some of the recent detailed LES studies of marine stratocumulus (e.g. Hill et al., 2009; Chen et al., 2011), however, due to the increased complexity of the microphysics calculations required to explicitly represent the continuous 2-D aerosol-droplet spectrum, we relax the resolution somewhat in favor of a more detailed microphysics scheme. Since the purpose of this work is to illustrate the model's implementation in a 3-D LES model, the resolution should be appropriate to determine changes in the aerosol size distribution due to cloud processing. The model time step is 0.5 s. Periodic boundary conditions are employed on both the zonal and meridional domain boundaries. The first 30 min are excluded from the analysis below due to model spin-up. Results are shown for the subsequent 2 h.

To compare the different microphysics schemes defined in Sect. 2.3 with the 2-D continuous scheme, we perform simulations both with and without aerosol regeneration using the 1-D bin microphysics schemes, as well as a set of simulations with and without aerosol regeneration using the bulk scheme. Lastly, we perform simulations using the bulk microphysics model without aerosol coupling, i.e. fixed $N_d$. For the purpose of the these simulations, we fix $N_d$ at 100 and 400 cm$^{-3}$ to represent the "Clean" and "Polluted" cases. These values are chosen so as to represent the number of droplets expected to activate in an environment with an aerosol number concentration of 100 and

$500\,\mathrm{cm}^{-3}$, respectively. The suite of simulations is defined in Table 2.1, including details on the assumptions regarding activation and regeneration of aerosol particles. In those simulations with explicit aerosol activation, the model is initialized with a lognormal aerosol distribution:

$$n^d\ (D_p)\ \equiv\ \frac{dN}{d\ \ln\ D_p}\ =\ \frac{N_a}{\sqrt{2\ \pi}\ \ln\ \sigma}\ \exp\ \left[-\frac{\ln^2\ \left(\frac{D_p}{D_g}\right)}{2\ \ln^2\ \sigma}\right] \tag{2.41}$$

where, $N_a$ is the total aerosol number concentration, $\sigma$ and $D_g$ are the standard deviation and geometric mean diameter, respectively, and $D_p$ is the aerosol particle diameter. For the purposes of illustration, we let $D_g = 0.1\,\mu\mathrm{m}$ and $\sigma = 1.8$.

In the 2-D continuous bin scheme, the initial aerosol distribution is binned in the 2-D space according to dry aerosol size and equilibrium wet size. The equilibrium size is computed by solving the equation for the equilibrium saturation ratio over a sphere of an aqueous solution using the bisection method. For grid points in which the saturation ratio ($S$) is greater that 0.95, we assume that the relative humidity (RH) is 95 % for the purpose of initializing the model.

## 2.5 Results

### 2.5.1 Comparison of microphysics schemes

For comparison, we show the domain-averaged liquid water path (LWP) and conditionally-averaged droplet number concentration ($N_\mathrm{d}$) in Fig. 2.4. Table 2.2 shows the LWPs at the end of the simulations and the changes relative to the LES_2D for the same CCN number concentration. For the most part, the models suggest a LWP of 46 to $62\,\mathrm{g\,m}^{-2}$ after 2.5 h. The LES_Bulk_NoReg case with $N_\mathrm{d} = 100\,\mathrm{cm}^{-3}$ is an outlier (orange, solid), predicting a LWP less than $30\,\mathrm{g\,m}^{-2}$ for most of the simulation. The reason for this disparity lies in the fact that if aerosols are not regenerated when a droplet evaporates (whether it be at cloud top due to entrainment or at cloud base due to sedimentation into subsaturated air), the evaporation serves as a sink for aerosol particles. Thus, instead of generating more aerosol particles that can activate and keep the droplet number concentration replenished, lack of regeneration leads to a gross underprediction of $N_\mathrm{d}$ (Hereinafter, it

should be noted that all comparative statements refer to results relative to those from the 2-D continuous bin scheme, unless otherwise noted). In this case, the droplets will tend to be larger and thus the collision-coalescence process is artificially enhanced. The autoconversion parameterization (Khairoutdinov and Kogan, 2000) is solely a function of the bulk $N_{\rm d}$ and cloud liquid water content (LWC, $q_{\rm c}$). The autoconversion rate is proportional to $N_{\rm d}^{-1.79}$. Thus, a decrease in $N_{\rm d}$ results in a strong increase in the autoconversion rate, and enhanced drizzle formation. The drizzle drop formation occurs near cloud top, as expected since this region of the cloud contains the highest LWC. Ultimately, this leads to a decrease in the cloud top height (Fig. 2.5c) and a decrease in the LWC (due to smaller cloud depth and drizzle loss of condensed water). Interestingly, the LES_Bulk_NoAer performs much better since the assumption that $N_{\rm d}$ is fixed circumvents the aerosol problem in its entirety and acts to force $N_{\rm d}$ to stay relatively high (almost as if aerosols were being regenerated and activated again). However, the LWP is overpredicted in this case (Fig. 2.4 and Table 2.2).

Moreover, from Fig. 2.4f, we see the effect of the assumption of constant droplet number concentration. Comparison amongst the bin schemes suggests that this assumption overpredicts $N_{\rm d}$ by a factor of 2 in the "Clean" case and factor of 2 to 8 in the "Polluted" case. The addition of an explicit aerosol activation scheme produces LWPs that are in better agreement with the bin models. However, the bulk model is still not able to capture the change in $N_{\rm d}$ during the simulation (Fig. 2.4). These effects combine to produce an unrealistic profile of the domain-averaged total condensed water ($q_{\rm t}$) profile for the LES_Bulk_NoReg cases (Fig. 2.6c). Here, we see evidence of the overpredicted autoconversion rate, suppressing the cloud top LWC and drizzle leading to a reduction in the mean LWC. Again, the simulations performed with an explicit binned-aerosol activation scheme better capture the vertical profile of $q_{\rm t}$, regardless of the regeneration assumption.

Figures 2.4b, d, and e show that in all but the LES_Bulk_NoAer case, there is a rapid decrease in $N_d$. The decrease is largest in the simulations performed with bulk microphysics owing to its simplistic representation of the collision-coalescence process. One would expect that the decrease in $N_d$ ought to be largest for the "Clean" cases since the particles ought to grow large enough such that the collision-coalescence process becomes quite efficient. However, Figs. 2.4b, d, and e suggest

otherwise. Here however, it is difficult to distinguish between the loss of cloud droplets due to collection and the loss due to evaporation. In the "Clean" case, the in-cloud mean supersaturation ought to be higher and thus increasing the capability for smaller aerosols to remain activated. However, in the "Polluted" case, all aerosol particles initially activate within the cloud, but, as the larger, now more numerous, particles grow, the depletion in the water vapor mixing ratio causes the smaller droplets to evaporate. Hence, $N_d$ decreases rapidly due to a combination of evaporation and collection. Moreover, the decrease in $N_d$ is also partially related to the fact that as the cloud droplets are converted to rain droplets, the below-cloud layer becomes populated with small concentrations of sedimentating drops that ultimately reduce the average number concentration.

With the two bin microphysics schemes, we find that there is little agreement on the direction of the aerosol effect on the LWP. From Fig. 2.4a, the 2-D continuous bin model predicts that the LWP increases with increasing aerosol concentration (by $6\,\mathrm{g\,m^{-2}}$ at the end of the simulations). This is in agreement with previous modeling studies (e.g. Albrecht, 1989; Ackerman et al., 2003; Wood et al., 2009) and in-situ observations (Radke et al., 1989; Ferek et al., 2000). The increase in LWP results from changes near cloud top to an increase in aerosol loading. An increase in CCN number concentration lead to a monotonic increase in $N_\mathrm{d}$ and thus a less efficient collision-coalescence process. As a result, the droplets that reside near cloud top are *smaller* under polluted conditions and thus have a smaller terminal fall speed than analogous droplets in the "Clean" scenario. Consequently, the cloud top region moistens and stays elevated (Figs. 5a and 2.6a). A similar effect is seen in the simulations performed with the 1-D bin microphysics scheme without aerosol regeneration (Fig. 2.5b, blue). On the other hand, the simulations performed with the 1-D bin scheme including aerosol regeneration suggest that the LWP decreases with increased aerosol loading (Fig. 2.4, red and Fig. 2.5b). The reason for the switch in the sign of the effect on the LWP is due to an increase in entrainment at the cloud top-free troposphere interface. Figure 2.7 shows the horizontal- and temporal-averaged vertical velocity variance ($\overline{w'w'}$), a proxy for the strength of turbulent mixing. For the LES_1D_Reg case (red, dashed), there is an increase in $\overline{w'w'}$ at the inversion level ($z = 600\,\mathrm{m}$) relative to the "Clean" case (red, solid). This increase in mixing is caused

by increased evaporation in the entrainment regions (regeneration produces more numerous, smaller aerosol particles that are more likely to evaporate), leading to an increase in entrainment and a positive feedback loop occurs with a further increase in evaporation near cloud top. Ultimately, this leads to a decrease in the LWP (the differences in modeled LWP are discussed in more detail below). This is corroborated by the decrease in $q_t$ in Fig. 2.6b and the decrease in LWP in Fig. 2.4. This effect is commonly referred to as the entrainment – evaporation effect for non-drizzling clouds (i.e. Wang et al., 2003; Xue and Feingold, 2006; Hill et al., 2008). On the other hand, the *increase* in LWP demonstrated by the 2-D continuous bin scheme for an increase in aerosol loading is suggestive of the cloud-lifetime effect (Albrecht, 1989), in which an increase in aerosol loading leads to more numerous, smaller droplets that mitigate the collision-coalescence process. Consequently, drizzle is suppressed and the LWP increases (Fig. 2.4a).

Owing to the inherent nature of the assumptions regarding aerosol regeneration and activation in the current 1-D bin schemes, the cloud droplet number concentration and LWP predicted could be biased (either positively or negatively) as discussed in the Introduction. In fact, the aerosol size distribution is constantly being modified by cloud processes (both microphysical and chemical, although the latter is not considered in the current study), thus the regenerated aerosol will not necessarily conform to the size distribution of the originally activated aerosol (see Sect. 1). The 2-D continuous bin microphysics scheme suggests that there is a negligible change in turbulent mixing at cloud top with an increase in aerosol loading (Fig. 2.7a) and thus increases in LWP (Fig. 2.4a), $q_t$ near cloud top (Fig. 2.6a) and cloud top height (Fig. 2.5a) are observed.

Changes in aerosol loading near cloud base initiate a number of effects on marine stratocumulus dynamics. An increase in the CCN number concentration leads to smaller, more numerous droplets, slowing the collection process and suppressing drizzle. This leads to a decrease in both below-cloud evaporative cooling and latent heating within the cloud and consequently an increase in turbulent mixing near cloud base. More mixing implies more entrainment and an increase in evaporation that acts to decrease the LWP. This so-called drizzle-entrainment effect, counteracts the cloud lifetime effect mentioned above. Figure 2.7 demonstrates the increase in $\overline{w'w'}$ both within the cloud and

at cloud base. Accordingly, as suggested by Lu and Seinfeld (2005) and Wood (2007), this leads to a decrease in $q_t$ due to increased evaporation near cloud base. However, the decrease in $q_t$ near cloud base due to increased aerosol loading is *smaller* than the opposing increase in $q_t$ at cloud top. Thus, the overall effect is to increase the LWP of the cloud. Moreover, changes in cloud top may be mitigated by changes at cloud base (or even at cloud edges), thus a detailed model is necessary to simulate aerosol effects on cloud properties. The compensating effects of increased aerosol loading on cloud top and cloud base need not always favor increased LWC near cloud top (and thus an increase in LWP). The case presented here is representative of marine stratocumulus, but other factors can play a role in cloud dynamics near the boundaries, for example, sensitivity of marine stratocumulus to free tropospheric humidity (e.g. Ackerman et al., 2004), sea surface temperature (SST) (e.g. Lu and Seinfeld, 2005), diurnal heating (e.g. Hill et al., 2008; Sandu et al., 2009), entrainment rates (e.g. Wang et al., 2003; Xue and Feingold, 2006; Bretherton et al., 2007; Hill et al., 2009), and point sources, e.g. ships (e.g. Wang et al., 2011) under various aerosol loadings have been explored.

The reasons for the disparity in the sign of the effect on the LWP of increased aerosol loading between the 2-D continuous bin microphysics scheme and the 1-D bin scheme are three-fold. (1) The underlying assumptions involving regeneration of aerosol particles in the 1-D bin scheme erroneously produce particles that are either smaller or larger than their actual size after cloud microphysical processing. (2) The terminal fall speed ($v_t$) calculations are quite different. The 1-D bin model uses a simple (and efficient) size relation for $v_t$ (i.e. $v_t = AD_d^B$, where $A$ and $B$ are empirical constants and $D_d$ is the droplet size in a given bin in the 1-D model). Conversely, we have included the detailed calculation of $v_t$ following Beard (1976) to more accurately represent the nonlinear nature of $v_t$ as a function of droplet size. For intra-model consistency, the detailed calculations of $v_t$ are also used to compute the collection kernels. And (3), the 1-D bin microphysics model does not include the effect of solute mass on condensation/evaporation. From Köhler Theory, we expect that a droplet containing a relatively large amount of solute will be less likely to evaporate since its critical supersaturation ($s_c$) is small (i.e. less than the ambient supersaturation within the cloud). Moreover, droplets formed on large CCN can be large enough to be considered a droplet (i.e. its diameter is

more than 3 µm) even in a subsaturated environment. In the absence of collision-coalescence, the slowed evaporation near cloud top due to increased solute mass ought to be rather insignificant since there are very few large aerosol particles present in the initial aerosol size distribution. However, as we show below, the collision-coalescence process is very efficient, especially in relatively clean environments, and consequently there is a significant increase in both the mean droplet size *and* solute mass. Since the highest LWC is found near cloud top, collection of cloud droplets is often most efficient in this region and thus one would expect to find that the increase in larger aerosol particles to be most substantial here. Hence, in the "Clean" scenario, the 1-D bin microphysics model does not agree with the the 2-D continuous bin scheme.

### 2.5.2 Cloud microphysics effects on the aerosol size spectrum

The 2-D continuous model allows for the analysis of microphysical effects on the aerosol size distribution. Larger aerosol particles are more readily activated, especially in regions of relatively high CCN number concentration, i.e. regimes in which the activation process (or formation of cloud droplets from haze particles) is vapor-limited and not CCN-limited. In relatively clean environments, most, if not all, CCN activate to form cloud droplets. However, as the number concentration of CCN increases, the fraction of particles that ultimately activate decreases. In the transition region, from vapor-limited activation to CCN-limited activation, the size distribution of the ambient aerosol becomes important. Moreover, the collision-coalescence process is still relatively efficient and consequently cloud microphysical processing ought to lead to the formation of larger aerosol particles, i.e. particles that are more readily activated after regeneration. The 2-D continuous microphysics scheme is designed to explicitly and physically represent the change in the aerosol size spectrum due to cloud microphysical processing.

As sketched in Fig. 2.3, cloud microphysical processing results in a shift in the aerosol size spectrum towards larger sizes; there is no cloud microphysics process by which aerosols become smaller. The increase in the mean size of the aerosol spectrum depends on the effectiveness of the

collision-coalescence. The cloud radar reflectivity ($Z$) defined as (Rogers and Yau, 1989)

$$Z \;=\; 10 \;\log\; \left[ \sum_i \; \sum_k \; \int_0^\infty \; N_{i,k} D_k^6 \; \mathrm{d}D_k \right] \tag{2.42}$$

where $D_k$ is the droplet diameter in the $k$-th droplet bin shows the effect of the microphysical processes (Fig. 2.8). Higher values of $Z$ (i.e. less negative) correspond to the production of larger cloud droplets and drizzle droplets. In the "Clean" case, $Z$ increases from its minimum of $-38\,\mathrm{dBZ}$ at 35 min to $-19\,\mathrm{dBZ}$ at the end of the simulation (an increase of 19 dBZ) while in the "Polluted" case, $Z$ increases from $-44\,\mathrm{dBZ}$ at 60 min to $-32\,\mathrm{dBZ}$ at the end of the simulation (an increase of 12 dBZ). Linear regression lines are shown in Fig. 2.8 for the final 50 min of simulation time and the corresponding slopes ($m$) are displayed to demonstrate the differences in collection efficiency between the "Clean" and "Polluted" cases; $Z$ increases at $10.6\,\mathrm{dBZ\,h^{-1}}$ during the final 50 min in the "Clean" case, while at only $1.9\,\mathrm{dBZ\,h^{-1}}$ in the "Polluted" case. Moreover, the increase in $Z$ from its minimum to its maximum in the "Clean" scenario is 58 % larger than that of the "Polluted" scenario, clearly demonstrating the increase in efficiency of the collision-coalescence process in relatively clean conditions. Given the substantial increase in $Z$, even within a short period of time, it is expected that the change in the aerosol spectrum ought to be significant.

The enhancement in radar reflectivity is corroborated in Fig. 2.9 in which we show droplet distributions for the 2-D continuous bin model and the 1-D microphysics scheme with and without regeneration. Figure 2.9 clearly shows the reduction in the number concentration due to suppressed collision coalescence in the "Polluted" case compared with the "Clean" scenario. Furthermore, we see from the 1-D bin microphysics results, the effect of the regeneration assumption on the droplet size distribution. Specifically, at 150 min, in the "Polluted" (dashed) scenario, Fig 2.9 shows that the 1-D bin model with regeneration produces many more smaller particles compared to the 2-D continuous bin scheme. The potential for the model to overpredict the number concentration was alluded to above and, demonstrated here, results in a large suppression in the formation of drizzle drops relative to the 2-D continuous scheme. Moreover, in the absence of a regeneration parameterization in the

1-D bin model, the mode of the droplet size spectrum is higher in comparison to the 2-D continuous bin scheme. This is a direct result of the fact that without a regeneration scheme, the droplet number concentration is likely to be underpredicted, hence producing larger droplets (assuming the liquid water content does not change much). Figure 2.9 alone demonstrates the large differences between the bin microphysical modeling approaches. These differences in the droplet size spectrum can potentially have a significant impact on the efficiency of the collision coalescence process as well as the terminal fall speeds (and ultimately precipitation).

In Fig. 2.10 we show the relative CCN number concentration at various times in the simulations ($R_{\rm CCN}$). These calculations are done relative to the mean size distribution after the 30 min of spinup (this ensures that the results presented in Fig. 2.10 are not significantly affected by the initial thermal perturbation). Thus, $R_{\rm CCN}$ is defined as:

$$R_{\rm CCN}(t) \;=\; \frac{N_{\rm CCN}(t)}{N_{\rm CCN}\;(t\;=\;30\;\min)} \tag{2.43}$$

where $N_{\rm CCN}(t)$ is the CCN (aerosol) number concentration at time $t$ and $N_{\rm CCN}$ $(t = 30\,\min)$ is the CCN number concentration at $t = 30\,\min$. If we first focus our attention on the "Clean" case in Fig. 2.10 (solid) and move from 45 min (black) to 150 min (red), we find that even after 2 h, the collection process still significantly affects the aerosol size spectrum (as suggest by the monotonic increase in $Z$ from Fig. 2.8). In fact, after 150 min of simulation time (or, 2 h after the point at which the relative concentrations are defined), there is a substantial increase in particles in bins 10–14, reaching a maximum in bin 14 with $R_{\rm CCN}$ $(t = 150\,\min) = 9.2$. Thus, there is an increase, by nearly an order of magnitude, in the number of particles in this bin, solely as a result of the collision-coalescence process. The collection of cloud droplets (either via collision-coalescence or aerosol scavenging) is the sole mechanism for this increase (i.e. we can rule out sedimentation and advection), since the calculations are horizontal averages within the boundary layer and Fig. 2.7a suggest that there is little mixing across the cloud top inversion (the source of fresh aerosol from above is negligible), and the cloud does not produce precipitation at the surface. This increase arises at the expense of

smaller aerosol particles. At the end of the simulation, only about 40 % of the particles in bins 1 through 6 remain relative to the number concentrations at $t = 30$ min. (In traditional 1-D bin and bulk microphysics models with aerosol regeneration included, it is assumed that there is no change in the size distribution parameters of the regenerated aerosol.) Under relatively clean conditions, the arithmetic mean aerosol size increases from 0.119 µm at 30 min to 0.138 µm 2 h later. In other words, the mean size increases by 16 % in 2 h for the "Clean" scenario.

The increase in the CCN number concentration from the "Clean" to the "Polluted" case limits the production of larger cloud droplets and drizzle drops (Fig. 2.8) and consequently limits the conversion of aerosol particles to larger CCN. From Fig. 2.10a (dashed), we find that there is a rather small change in the number concentrations in the larger bins until about 90 min into the simulations (60 min after the chosen time to compute $R_{\rm CCN}$) since the collision-coalescence process is far less efficient in a polluted environment. However, at the end of the simulation, we find that the number concentration in bin 14 increases by a factor of 4 (albeit, less than half that shown for the "Clean" case above). Moreover, the number concentration of aerosol particles in bins 1 through 5 is about half that of the number present at 30 min into the simulation due to collection (collision-coalescence and/or aerosol scavenging). In other words, after 2 h of cloud microphysical processing the number of small aerosol particles is reduced by one-half. In this case, the mean aerosol size increases from 0.1175 µm at 30 min to 0.133 µm 2 h later, an increase of about 10 % (roughly two-thirds of the increase in the mean aerosol size shown for the "Clean" case above). These changes in the aerosol size distribution are significant and suggest that the assumptions used regarding aerosol regeneration in traditional 1-D bin microphysics models (and even detailed bulk microphysics scheme) can lead to inaccuracies in the predicted LWP, distribution of LWC within the cloud, and an underestimation of $N_{\rm d}$.

The changes in the CCN number concentration presented here are obviously a factor of the meteorological conditions imposed. However, the collision-coalescence rate is controlled dominantly by $N_{\rm d}$ and $q_{\rm t}$ and consequently the change in aerosol distribution is also mostly affected by changes in $N_{\rm d}$ and $q_{\rm t}$. For clouds within the marine boundary layer, $q_{\rm t}$ is not significantly altered for an

increase in the aerosol loading from 100 to 500 $\mathrm{cm}^{-3}$. However, the droplet number concentration *is* significantly larger. Thus, the droplet number concentration, which is inherently linked to the ambient CCN number concentration, should be the most significant factor in determining the collision-coalescence rate and consequently the change in the aerosol distribution due to cloud processing. Moreover, one can expect that for a thinner cloud (i.e. less than 250 m deep), $q_\mathrm{t}$ will be reduced, leading to a decrease in the size of the cloud droplets and less collision-coalescence. This will result in a smaller effect on the aerosol size distribution shift toward larger sizes. On the other hand, in a thicker cloud, (i.e. more than 300 m deep), $q_\mathrm{t}$ will be elevated, increasing the size of the cloud droplets, increasing the collision-coalescence rate, and potentially further enhancing the production of larger aerosol particles.

## 2.6 Conclusions

A 2-D continuous spectral aerosol-droplet microphysics model is presented and compared to the traditional microphysics approaches (i.e. 1-D bin models and bulk models). Unlike the now standard 1-D bin microphysics schemes, the aerosol size spectrum and the droplet size spectrum are joined together to create a 2-D continuous distribution encompassing both wet aerosol particles (i.e. haze particles), cloud droplets, and drizzle droplets. This approach requires no a priori assumptions regarding the activated size of nucleated droplets and the size of regenerated aerosol particles (i.e. those aerosol particles that are formed upon the evaporation of cloud droplets). The former is normally calculated by computing the nucleated droplet equilibrium size for small aerosol particles or by multiplying the aerosol size by a factor between 3 and 8 for larger aerosol particles (Kogan, 1991; Khain et al., 2000; Xue et al., 2010; Lebo and Seinfeld, 2011). Upon activation, an aerosol particle is lost. The regeneration process presents an additional complication and shortcoming in the traditional 1-D microphysics approach. While it is often assumed that each evaporated droplet forms one aerosol particle, the size of the newly formed aerosol particle is unknown and must be assumed. Yin et al. (2005), Wang et al. (2010), and Xue et al. (2010) demonstrate the significance of including aerosol regeneration in detailed cloud models, however the actual size of the regenerated

particles is not known. The 2-D continuous bin microphysics scheme can be extended to include aqueous-phase chemistry and generate parameterizations for regenerated aerosol sizes.

We show that the collection process is a significant source of large aerosol particles, especially in relatively clean environments where the collision-coalescence process is rather efficient (an increase in large aerosols by nearly a factor of 10 after 2 h of cloud processing is shown). In the absence of aqueous-phase chemistry and collision-coalescence, the aerosol size spectrum is stagnant (assuming that the cloud is not precipitating to the surface). However, the collision-coalescence process is a sink for cloud droplets and a source for larger cloud droplets and drizzle drops (and consequently is a sink of small aerosol particles and a source of larger aerosol particles). Without tracking the solute mass in a continuous aerosol-droplet spectrum, the regenerated aerosol distribution will have a bias and the evaporating of cloud droplets and subsequent activation of the regenerated aerosol will be erroneous. We demonstrate that the sign of the change in LWP due to an increase in aerosol loading is positive using the 2-D continuous bin model while it is negative using the 1-D bin model with regeneration. The 1-D model is not capable of accurately predicting the retarded evaporation of droplets containing larger solute mass (that resulted from collection within the cloud) and thus overpredicts the evaporation-entrainment effect near cloud top (e.g. Wang et al., 2003; Xue and Feingold, 2006; Hill et al., 2008).

The 2-D continuous spectral aerosol-droplet microphysics model is designed to simultaneously account for the depletion (production) of water vapor and heating (cooling) during condensation (evaporation). Traditionally (e.g. Tzivion et al., 1989; Reisin et al., 1996; Harrington et al., 2000; Khain and Lynn, 2009; Xue et al., 2010), the supersaturation change over the course of a time step is approximated and used to compute the condensation or evaporation of cloud droplets. The total change in mass is then used to compute the amount of latent heat release, and subsequently the ambient temperature is updated. However, in reality, the process is not step-wise but instead continuous, and coupled. To avoid inconsistencies the simulated condensation/evaporation, the Variable Order Differential Equation (VODE) solver is employed embedded within the scheme in order to solve the coupled set of differential equations account for condensation/evaporation in each bin,

mass conservation, energy conservation, and supersaturation. The setup is computationally expensive, but ensures the accurate prediction of condensation/evaporation including both the curvature effect and solute effect (i.e. Köhler Theory is explicitly included).

In determining the practical applications of the 2-D continuous spectral aerosol-droplet microphysics scheme, it is important to consider two key questions: (1) is collision-coalescence a significant process for modulating $N_{\mathrm{d}}$? and (2) is regeneration important? The former is often answered by considering the ambient CCN number concentration and cloud depth (a measure of the adiabatic LWC). Thus, for relatively low CCN number concentrations in moist environments, collision-coalescence is an efficient mechanism for drizzle formation and it was shown that the bulk model performs worst in comparison to the 2-D bin model. The 1-D model is better able to capture the collection process, but, the model is negatively biased in terms of the predicted LWP, without regeneration, while positively biased when regeneration is accounted for. We show that regardless of the activation assumption, the 1-D bin model underpredicts $N_{\mathrm{d}}$ since, without regeneration, droplet evaporation results in a loss of aerosol and, with regeneration, the aerosols are preferentially relocated to the smaller bins that are less likely to activate on subsequent time steps. On the other hand, for relatively high CCN number concentrations, (i.e. where collision-coalescence is less efficient), the bulk model performs rather well in comparison to the explicit 2-D bin model. The 1-D model with regeneration is not able to represent the increase in LWP with increased aerosol loading that is suggested by the 2-D bin model. Again, the 1-D model underpredicts $N_{\mathrm{d}}$ and the coinciding dynamical feedback at cloud top causes a decrease in cloud top height and a decrease in LWP. To answer the second question, one can speculate that within a thicker stratiform cloud (i.e. the volume to surface area ratio of the cloud as a whole is larger), the relative importance of regeneration decreases since it is less likely that a parcel of air will interact with drier, entrained air. Conversely, in a thinner stratiform cloud, regeneration will likely be even more important than shown for the illustrated scenario. However, in the cases of cumulus and deep convective clouds, the turbulent nature of these clouds presents an environment conducive to entrainment and complete evaporation of droplets, even though the cloud itself is rather thick. Understanding the effects of regeneration on these clouds using the model

presented here is a subject for future investigation.

It is shown that the 2-D bin model, with the explicit treatment of aerosol regeneration and scavenging, predicts an increase in LWP with increased aerosol loading while the 1-D bin model with regeneration predicts the opposite effect, demonstrating the significance of including a physically-based representation of regeneration (in addition to include solute effects on condensation/evaporation). The suite of simulations performed here suggests that using traditional microphysical models in the absence of aerosol regeneration on short timescales (i.e. $<3$ h) at night may provide results similar to the more detailed, 2-D bin method (i.e. predicted LWPs within 10 % of the 2-D bin method prediction). Attempting to account for regeneration, especially when collision-coalescence is significant (and thus greatly affects the solute mass distribution), introduces a negative bias on the droplet number concentration as well as additional, erroneous feedbacks (i.e. increased entrainment at cloud top, decreased LWP, etc.).

Moreover, the simulations suggest that the droplet size distribution becomes skewed in a 1-D bin microphysics scheme toward either smaller or larger sizes in the presence and absence of an aerosol regeneration parameterization, respectively. These large shifts in the droplet size distribution can potentially have significant effects on the efficiency of the collision-coalescence process, fall speeds, and ultimately precipitation.

In situations where the efficiency of collision-coalescence and regeneration is challenging to determine a priori, the 2-D continuous spectral aerosol-cloud microphysics model, in conjunction with an explicit 1-D bin microphysics model, can serve as a useful tool in determining the significant of regeneration on the chosen case and model setup.

The model, in its current state, lacks the ability to simulate mixed-phase microphysics and thus cannot be combine to studies related to, for example, mixed-phase stratiform clouds in the Arctic or deep convection. Including mixed-phase microphysics within a 2-D spectral microphysics model is computationally too expensive at present. However, one can speculate that in deep convective clouds where entrainment and detrainment of air into and out of the convective core is prevalent, regeneration could potentially play a significant role in subsequent microphysical processes (both

regeneration from evaporated cloud drops and sublimated ice crystals, snow, and/or graupel). Increased instability and turbulent motions within these systems creates an environment conducive to efficient collision-coalescence, and consequently large shifts in the aerosol mass distribution. More work is needed in this regard to determine the precise importance of regeneration in mixed-phase clouds.

## 2.7 Acknowledgements

This work was supported by the Office of Naval Research grant N00014-10-1-0200. Computations were carried out on the CITerra Dell Cluster of the Geological and Planetary Sciences Division at Caltech.

**Table 2.1:** ]

Model Configurations and Microphysics Descriptions.

| Designation | Type | Microphysics | Aerosol Activation | Aerosol Regeneration | Reference |
|---|---|---|---|---|---|
| LES_2D | LES | 2-D Bin | Explicit | Explicit | Current Study |
| LES_1D_Reg | LES | 1-D Bin | Parameterized | Parameterized | Lebo and Seinfeld (2011) |
| LES_1D_NoReg | LES | 1-D Bin | Parameterized | No | Lebo and Seinfeld (2011) |
| LES_Bulk_Reg | LES | 2-Moment Bulk | Parameterized | Parameterized | Morrison et al. (2005)<br>Morrison and Pinto (2005)<br>Lebo and Seinfeld (2011) |
| LES_Bulk_NoReg | LES | 2-Moment Bulk | Parameterized | No | Morrison et al. (2005)<br>Morrison and Pinto (2005)<br>Lebo and Seinfeld (2011) |
| LES_Bulk_NoAer* | LES | 2-Moment Bulk | No | No | Morrison et al. (2005)<br>Morrison and Pinto (2005) |

* In this scenario, the bulk microphysics scheme of Morrison et al. (2005) and Morrison and Pinto (2005) is run without any modifications, i.e. no aerosol coupling (fixed droplet number concentration).

**Table 2.2:** LWP and relative change in comparison to the corresponding simulation performed with the 2-D bin microphysics scheme.

| | LWP $[\mathrm{g\,m^{-2}}]^*$ | | | | | |
|---|---|---|---|---|---|---|
| $N_{\mathrm{CCN}}$ $[\mathrm{cm^{-3}}]$ | LES_2D | LES_1D_Reg | LES_1D_NoReg | LES_Bulk_Reg | LES_Bulk_NoReg | LES_Bulk_NoAer |
| 100 | 49.6 | 54.8 (10.5 %) | 52.3 (5.4 %) | 57.0 (14.9 %) | 29.7 (−40.1 %) | 55.5 (11.9 %) |
| 500 | 54.5 | 48.3 (−11.4 %) | 53.0 (−2.8 %) | 59.9 (9.9 %) | 50.0 (−8.3 %) | 56.0 (2.8 %) |

* The LWP is domain- and temporal-averaged for the final 30 min of the simulations. Relative changes are shown in parenthesis and are computed relative to the LES_2D simulations with the same $N_{\mathrm{CCN}}$.

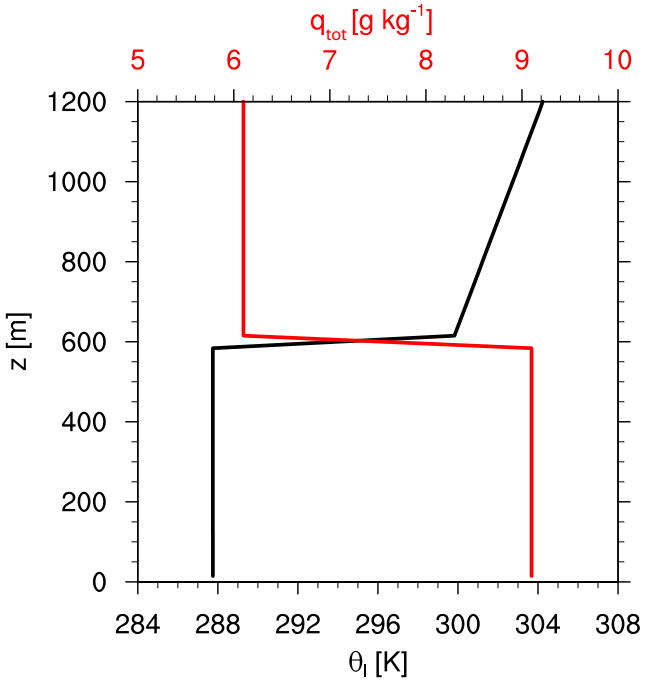


**Figure 2.1:** Liquid potential temperature (black) and total water mixing ratio (red) used to initialize the model in the marine stratocumulus example.

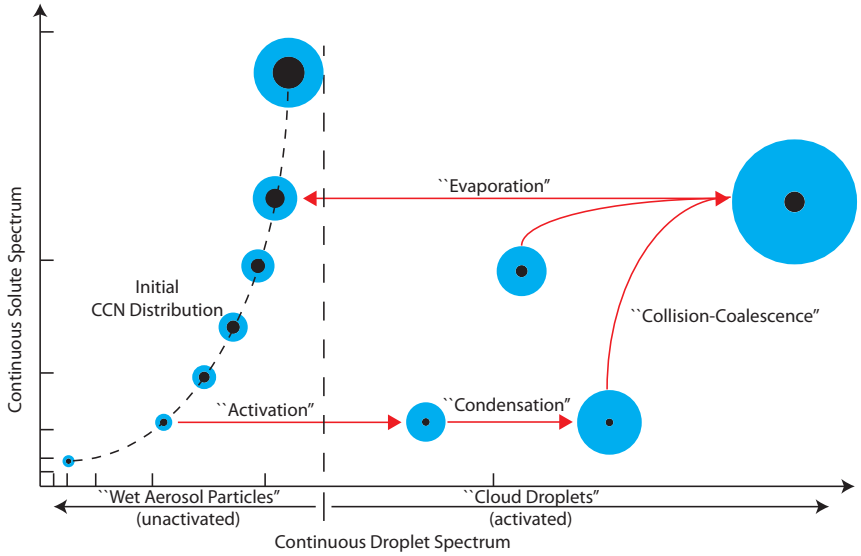


**Figure 2.2:** Schematic of the 2-D collection problem for a mesh of particles with droplet mass $x_{\mathrm{d}}$ and solute mass $x_{\mathrm{s}}$. The calculations are performed in the following order: (1) droplets in bins $i$, $k$ and $j$, $l$ collide to form a droplet of mass $x_{i,k} + x_{j,l}$ in bin $n$, $m$. (2) The newly formed particles are added to $n$, $m$ to get $N'_{n,m}$. 3) The flux through the $n+1/2$, $m$ boundary is computed and the particles are moved from bin $n$, $m$ to $n+1$, $m$ according to $f_{n+1/2,m}$. (4) The fluxes through the $n$, $m+1/2$ and $n+1$, $m+1/2$, i.e., $f_{n,m+1/2}$ and $f_{n+1,m+1/2}$, respectively, are then computed and the number concentrations in the surround 4 bins are updated accordingly.

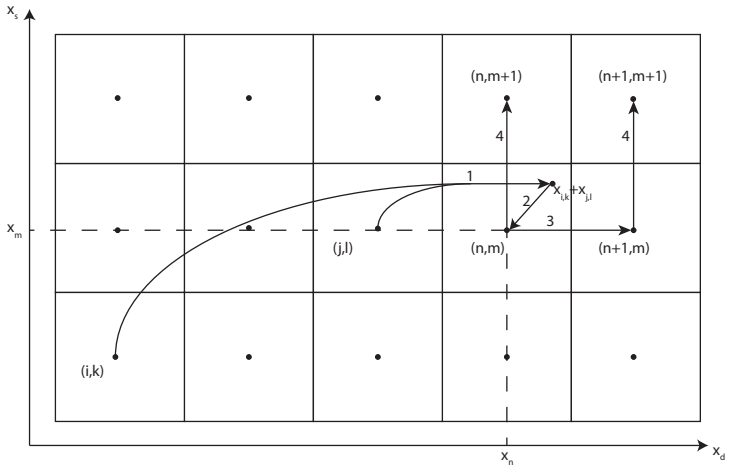


**Figure 2.3:** Schematic of the microphysical process represented in the continuous 2-D spectral aerosol-droplet microphysics scheme.

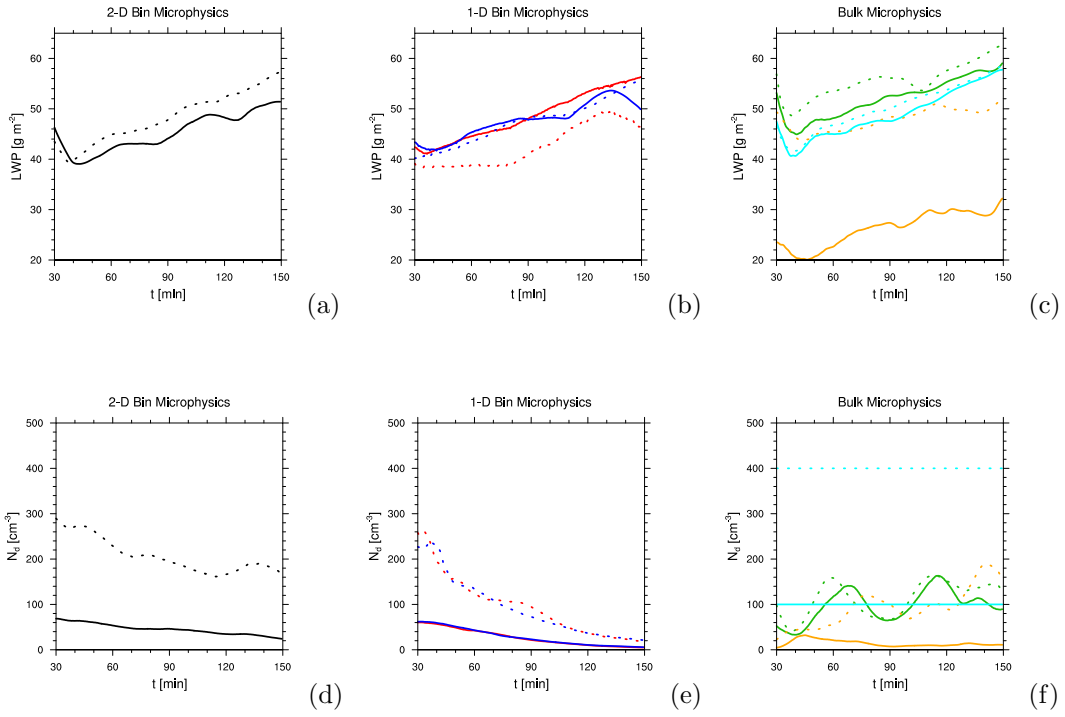


**Figure 2.4:** Liquid water path (LWP) and droplet number concentration ($N_{\mathrm{d}}$) for the set of simulations defined in Table 2.1: LES_2D – **(a)** and **(d)** (black), LES_1D_Reg – **(b)** and **(e)** (red), LES_1D_NoReg – **(b)** and **(e)** (blue), LES_Bulk_Reg – **(c)** and **(f)** (green), LES_Bulk_NoReg – **(c)** and **(f)** (orange), and LES_Bulk_NoAer – **(c)** and **(f)** (cyan). Both the "Clean" (solid) and "Polluted" (dashed) cases are shown for all scenarios.

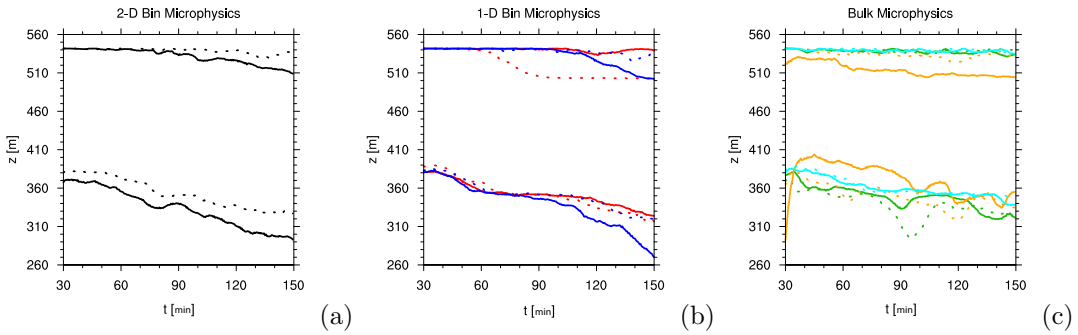


**Figure 2.5:** Cloud top (top curves) and cloud base (bottom curves) for the suite of simulations described in Table 2.1, i.e. LES_2D – **(a)**, black, LES_1D_Reg – **(b)**, red, LES_1D_NoReg – **(b)**, blue, LES_Bulk_Reg – **(c)**, green, LES_Bulk_NoReg – **(c)**, orange, and LES_Bulk_NoAer – **(c)**, cyan. Both the "Clean" (solid) and "Polluted" (dashed) cases are shown for all scenarios.

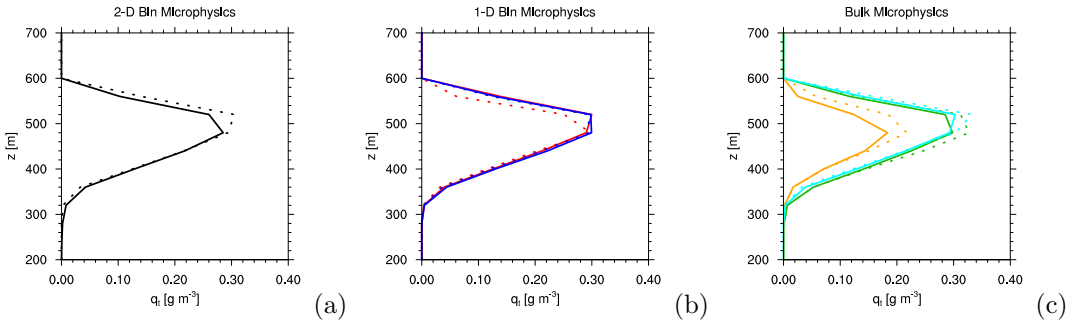


**Figure 2.6:** Total condensed water ($q_\mathrm{t}$). Colors are as in Fig. 5. Note that these are horizontally-averaged profiles of $q_\mathrm{t}$ at 2 h into the simulations.

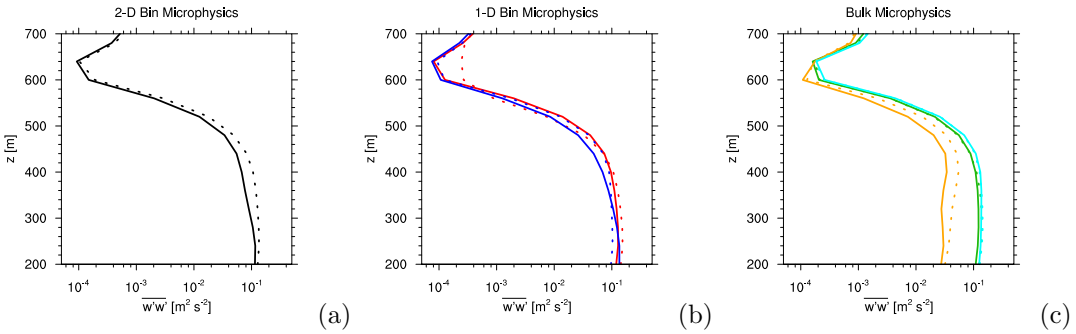


**Figure 2.7:** ]
Vertical velocity variance ($\overline{w'w'}$). The vertical profiles are averaged over the last 2 h of the simulations. Colors are as in Fig. 2.5.

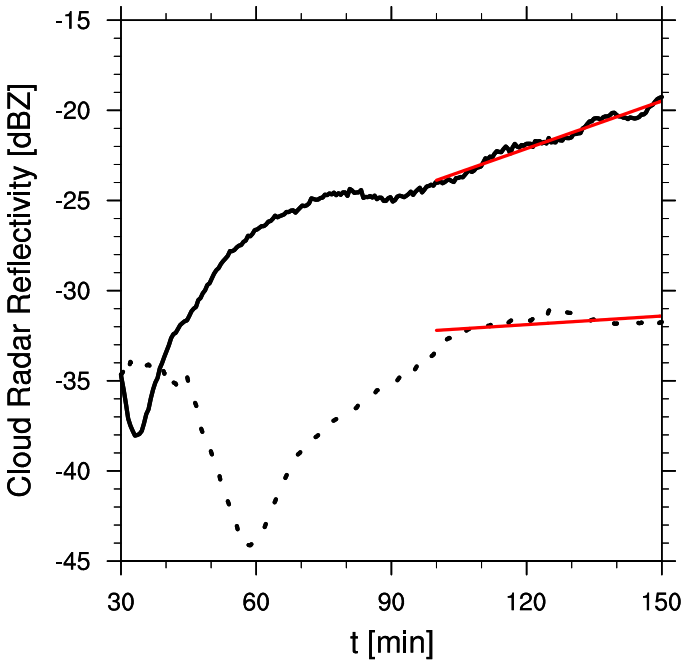


**Figure 2.8:** Cloud radar reflectivity in dBZ for the simulations performed with the 2-D continuous bin microphysics scheme under "Clean" (solid) and "Polluted" (dashed) conditions. Reflectivities are averaged horizontally throughout the domain and vertically within the boundary layer.

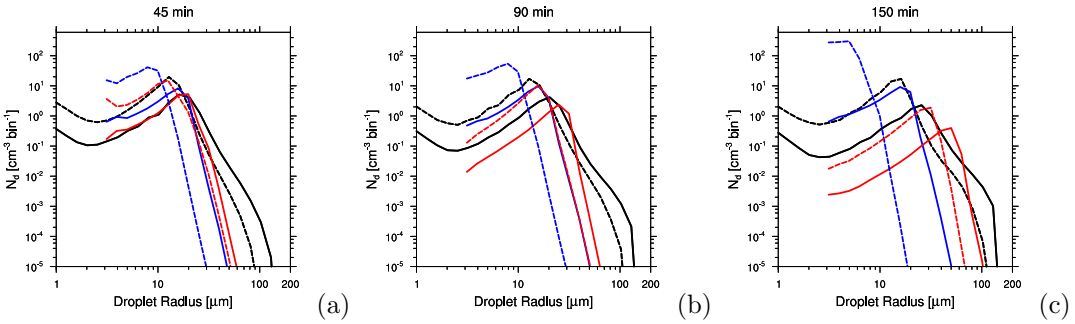


**Figure 2.9:** Droplet size distributions at 45 **(a)**, 90 **(b)**, and 150 **(c)** min of simulation time. Spectra for simulations performed with the 2-D continuous bin scheme (black) as well as the 1-D bin microphysics model with regeneration (blue) and without regeneration (red) are shown for the "Clean" (solid) and "Polluted" (dashed) scenarios.

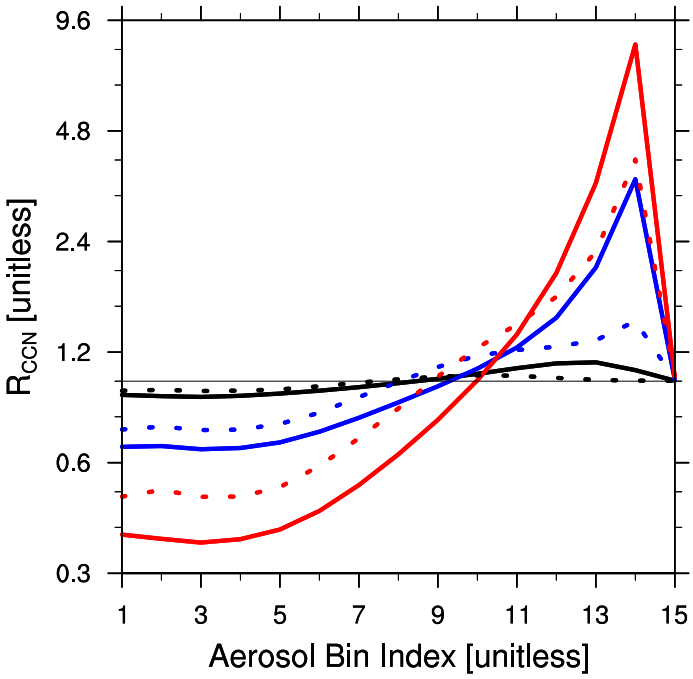


**Figure 2.10:** Relative change in the CCN number concentration ($N_{\mathrm{CCN}}$) after 45 min (black), 90 min (blue), 150 min (red). Both the "Clean" (solid) and "Polluted" (dashed) cases are shown. Note that the y-axis is a log-scale and that the area under the curves relative to the line $R_{\mathrm{CCN}} = 1$ need not be 0. In fact it should not be 0 since we use mass doubling between bins such that, for example, the diameter of particles in bin 8 are half that of particles in bin 11. Shown are the horizontally-averaged values within the boundary layer.

## 2.8 Bibliography

Ackerman, A. S., Toon, O. B., Stevens, D. E., and Coackley Jr., J. A.: Enhancement of cloud cover and suppression of nocturnal drizzle in stratocumulus polluted by haze, Geophys. Res. Let., 30, doi:10.1029/2002GL016634, 2003.

Ackerman, A. S., Kirkpatrick, M. P., Stevens, D. E., and Toon, O. B.: The impact of humidity above stratiform clouds on indirect aerosol climate forcing, Nature, 432, 1014–1017, 2004.

Ackerman, A. S., vanZanten, M. C., Stevens, B., Savic-Jovic, V., Bretherton, C. S., Chlond, A., Golaz, J.-C., Jiang, H., Khairoutdinov, M., Krueger, S. K., Lewellen, D. C., Lock, A., Moeng, C.-H., Nakamura, K., Petters, M. D., Snider, J. R., Weinbrecht, S., and Zulauf, M.: Large-eddy simulations of a drizzling, stratocumulus-topped marine boundary layer, Mon. Wea. Rev., 137, 1083–1110, doi:10.1175/2008MWR2582.1, 2009.

Albrecht, B.: Aerosols, cloud microphysics, and fractional cloudiness, Science, 245, 1227–1230, doi:10.1126/science.245.4923.1227, 1989.

Beard, K. V.: Terminal velocity and shape of cloud and precipitation drops aloft, J. Atmos. Sci., 33, 851–864, 1976.

Beheng, K. D.: A parameterization of warm cloud microphysical conversion processes, Atmos. Res., 33, 193–206, 1994.

Bott, A.: A flux method for the numerical solution of the stochastic collection equation, J. Atmos. Sci., 55, 2284–2293, 1998.

Bott, A.: A flux method for the numerical solution of the stochastic collection equation: Extension to two-dimensional particle distributions, J. Atmos. Sci., 57, 284–294, 2000.

Bretherton, C. S., Blossey, P. N., and Uchida, J.: Cloud droplet sedimentation, entrainment efficiency, and subtropical stratocumulus albedo, Geophys. Res. Let., 34, doi:10.1029/2006GL027648, 2007.

Brown, P. N., Bryne, G. D., and Hindmarsh, A. C.: VODE: A variable coefficient ODE solver, J. Sci. Stat. Comput., 10, 1038–1051, 1989.

Chen, Y.-C., Xue, L., Lebo, Z. J., Wang, H., Rasmussen, R. M., and Seinfeld, J. H.: A comprehensive numerical study of aerosol-cloud-interactions in marine stratocumulus, Atmos. Chem. Phys., 11, 9749–9769, doi:10.5194/acp-11-9749-2011, 2011.

Chuang, P. Y., Charlson, R. J., and Seinfeld, J. H.: Kinetic limitations on droplet formation in clouds, Nature, 390, 94–96, 1997.

Del Genio, A. D., Yao, M.-S., Kovari, W., and Lo, K. K.-W.: A prognostic cloud water parameterization for global climate models, J. Climate, 9, 270–304, 1996.

Duynkerke, P. G., de Roode, S. R., van Zanten, M. C., Calvo, J., Cuxart, J., Cheinet, S., Chlond, A., Grenier, H., Jonker, P. J., Kohler, M., Lenderink, G., Lewellen, D., Lappen, C.-L., Lock, A. P., Moeng, C.-H., Muller, F., Olmeda, D., Piriou, J.-M., Sanchez, E., and Sednev, I.: Observations and numerical simulations of the diurnal cycle of the EUROCS stratocumulus case, Quart. J. Roy. Meteor. Soc., 604, 3269–3296, 2004.

Fan, J., Yuan, T., Comstock, J. M., Ghan, S., Khain, A., Leung, L. R., Li, Z., Martins, V. J., and Ovchinnikov, M.: Dominant role by vertical wind shear in regulating aerosol effects on deep convective clouds, J. Geophys. Res., 114, doi:10.1029/2009JD012352, 2009.

Feingold, G., Tzivion, S., and Levin, Z.: Evolution of raindrop spectra. Part I: solution to the stochastic collection/breakup equation using the method of moments, J. Atmos. Sci., 45, 3387–3399, 1988.

Feingold, G., Walko, R. L., Stevens, B., and Cotton, W. R.: Simulations of marine stratocumulus using a new microphysical parameterization scheme, Atmos. Res., 47, 505–528, 1998.

Ferek, R. J., Garret, T., Hobbs, P. V., Strader, S., Johnson, D., Taylor, J. P., Nielsen, K., Ackerman, A. S., Kogan, Y., Liu, Q., Albrecht, B. A., and Babb, D.: Drizzle suppression in ship tracks, J. Atmos. Sci., 57, 2707–2728, 2000.

Ferrier, B. S.: A double-moment multiple-phase four-class bulk ice scheme. Part I: Description, J. Atmos. Sci., 51, 249–280, 1994.

Geresdi, I.: Idealized simulation of the Colorado hailstorm case: Comparison of bulk and detailed microphysics, Atmos. Res., 45, 237–252, 1998.

Geresdi, I. and Rasmussen, R. M.: Freezing drizzle formation in stably stratified layer clouds. Part II: The role of giant nuclei and aerosol particle size distribution and solubility, J. Atmos. Sci., 62, 2037–2057, 2005.

Harrington, J. Y., Feingold, G., and Cotton, W. R.: Radiative impacts on the growth of a population of drops within simulated summertime Arctic stratus, J. Atmos. Sci., 57, 766–785, 2000.

Hill, A. A., Dobbie, S., and Yin, Y.: The impact of aerosols on non-precipitating marine stratocumulus. Model description and prediction of the indirect effect, Quart. J. Roy. Meteor. Soc., 134, 1143–1154, doi:10.1002/qj.278, 2008.

Hill, A. A., Feingold, G., and Jiang, H.: The influence of entrainment and mixing assumption on aerosol-cloud interactions in marine stratocumulus, J. Atmos. Sci., 66, 1450–1464, 2009.

Hong, S.-Y. and Lim, J.-O. J.: The WRF single-moment 6-class microphysics scheme (WSM6), J. Korean Meteor. Soc., 42, 129–151, 2006.

Hong, S.-Y., Dudhia, J., and Chen, S.-H.: A revised approach to ice microphysical processes for the bulk parameterization of clouds and precipitation, Mon. Wea. Rev., 132, 103–1120, 2004.

Khain, A. and Lynn, B.: Simulation of a supercell storm in clean and dirty atmosphere using weather research and forecasting model with spectral bin microphysics, J. Geophys. Res., 114, doi:10.1029/2009JD011827, 2009.

Khain, A. and Pokrovsky, A.: Simulation of effects of atmospheric aerosols on deep turbulent convective clouds using a spectral microphysics mixed-phase cumulus cloud model. Part II: Sensitivity study, J. Atmos. Sci., 61, 2983–3001, 2004.

Khain, A., Ovtchinnikov, M., Pinsky, M., Pokrovsky, A., and Krugliak, H.: Notes on the state-of-the-art numerical modeling of cloud microphysics, Atmos. Res., 55, 159–224, 2000.

Khain, A., Pokrovsky, A., Pinsky, M., Seifert, A., and Phillips, V.: Simulation of effects of atmospheric aerosols on deep turbulent convective clouds using a spectral microphysics mixed-phase cumulus cloud model. Part I: Model description and possible applications, J. Atmos. Sci., 161, 2963–2982, 2004.

Khairoutdinov, M. and Kogan, Y.: A new cloud physics parameterization in a Large-Eddy Simulation model of marine stratocumulus, Mon. Wea. Rev., 128, 229–243, 2000.

Kogan, Y. L.: The simulation of a convective cloud in a 3D model with explicit microphysics. Part I: Model description and sensitivity experiments, J. Atmos. Sci., 48, 1160–1189, 1991.

Kogan, Y. L., Khairoutdinov, M. P., Lilly, D. K., Kogan, Z. N., and Liu, Q.: Modeling of stratocumulus cloud layers in a large-eddy simulation model with explicit microphysics, J. Atmos. Sci., 52, 2923–2940, 1995.

Korolev, A. and Isaac, G.: Phase transformation of mixed-phase clouds, Quart. J. Roy. Meteor. Soc., 129, 19–38, doi:10.1029/qj.01.203, 2003.

Lebo, Z. J. and Seinfeld, J. H.: Theoretical basis for convective invigoration due to increased aerosol concentration, Atmos. Chem. Phys., 11, 5407–5429, doi:10.5194/acp-11-5407-2011, 2011.

Li, G., Wang, Y., and Zhang, R.: Implementation of a two-moment bulk microphysics scheme to the WRF model to investigate aerosol-cloud interaction, J. Geophys. Res., 113, doi:10.1029/2007JD009361, 2008.

Lim, K.-S. S. and Hong, S.-Y.: Development of an effective double-moment cloud microphysics scheme with prognostic cloud condensation nuclei (CCN) for weather and climate models, Mon. Wea. Rev., 138, 1587–1612, 2010.

Lin, Y.-L., Farley, R. D., and Orville, H. D.: Bulk parameterization of the snow field in a cloud model, J. Clim. Appl. Meteor., 22, 1065–1092, 1983.

Lu, M.-L. and Seinfeld, J. H.: Study of the aerosol indirect effect by large-eddy simulation of marine stratocumulus, J. Atmos. Sci., 62, 3909–3932, 2005.

Lu, M.-L. and Seinfeld, J. H.: Effect of aerosol number concentration on cloud droplet dispersion: A large-eddy simulation study and implications for aerosol indirect forcing, J. Geophys. Res., 111, doi:10.1029/2005JD006419, 2006.

Mitra, S. K., Brinkmann, J., and Pruppacher, H. T.: A wind tunnel study on the drop-to-particle conversion, J. Aerosol Sci., 23, 245–256, 1992.

Morrison, H. and Gettelman, A.: A new two-moment bulk stratiform cloud microphysics scheme in the community atmosphere model, version 3 (CAM3). Part I: Description and numerical tests, J. Climate, 21, 3642–3659, 2008.

Morrison, H. and Pinto, J. O.: Mesoscale modeling of springtime Arctic mixed-phase stratiform clouds using a new two-moment bulk microphysics scheme, J. Atmos. Sci., 62, 3683–3704, 2005.

Morrison, H., Curry, J. A., and Khvorostyanov, V. I.: A new double-moment microphysics parameterization for application in cloud and climate models. Part I: Description, J. Atmos. Sci., 62, 1665–1677, 2005.

Ovchinnikov, M. and Easter, R. C.: Modeling aerosol growth by aqueous chemistry in a nonprecipitating stratiform cloud, J. Geophys. Res., doi:10.1029/2009JD012816, 2010.

Pruppacher, H. R. and Klett, J. D.: Microphysics of Clouds and Precipitation, Kluwer Academic Publishers, Boston, 1997.

Radke, L. F., Coakley Jr., J. A., and King, M. D.: Direct and remote sensing observations of the effects of ships on clouds, Science, 245, 1146–1149, 1989.

Rasch, P. J. and Kristjansson, J. E.: A comparison of the CCM3 model climate using diagnosed and predicted condensate parameterizations, J. Climate, 11, 1587–1614, 1998.

Rasmussen, R. M., Geresdi, I., Thompson, G., Manning, K., and Karplus, E.: Freezing drizzle formation in stably stratified layer clouds: The role of radiative cooling of cloud droplets, cloud condensation nuclei, and ice initiation, J. Atmos. Sci., 59, 837–860, 1987.

Reisin, T., Levin, Z., and Tzivion, S.: Rain production in convective clouds as simulated in an axisymmetric model with detailed microphysics. Part I: Description of the model, J. Atmos. Sci., 53, 497–519, 1996.

Roeckner, E., Bäuml, G., Bonaventura, L., Brokopf, R., Esch, M., Giorgetta, M., Hagermann, S., Kirchner, I., Kornblueh, L., Manzini, E., Rhodin, A., Schlese, U., Schulzweida, U., and Thompins, A.: The atmospheric general circulation model ECHAM5, Part I: Model description, Max-Planck-Institute for Meteorology, 2003.

Rogers, R. R. and Yau, M. K.: A Short Course in Cloud Physics, Butterworth-Heinemann, 1989.

Rotstayn, L. D.: A physically based scheme for the treatment of stratiform clouds and precipitation in large-scale models. I: Description and evaluation of the microphysical processes, Quart. J. Roy. Meteor. Soc., 123, 1227–1282, 1997.

Rotstayn, L. D. and Liu, Y.: Sensitivity of the first indirect aerosol effect to an increase of cloud droplet spectral dispersion with droplet number concentration, J. Climate, 26, 3476–3481, 2003a.

Rotstayn, L. D. and Liu, Y.: Cloud droplet spectral dispersion and the indirect aerosol effect: Comparison of two treatments in a GCM, Geophys. Res. Let., 36, doi:10.1029/2009GL038216, 2003b.

Rutledge, S. A. and Hobbs, P. V.: The mesoscale and microscale structure and organization of clouds and precipitation in midlatitude cyclones. VIII: A model for the "seeder-feeder" process in warm-frontal rainbands, J. Atmos. Sci., 40, 1185–1206, 1983.

Rutledge, S. A. and Hobbs, P. V.: The mesoscale and microscale structure and organization of clouds and precipitation in midlatitude cyclones. XII: A diagnostic modeling study of precipitation development in narrow cold-frontal rainbands, J. Atmos. Sci., 41, 2949–2972, 1984.

Sandu, I., Brenguier, J.-L., Geoffroy, O., Thouron, O., and Masson, V.: Aerosol impacts on the diurnal cycle of marine stratocumulus, J. Atmos. Sci., 65, 2705–2718, 2008.

Sandu, I., Brenguier, J.-L., Thouron, O., and Stevens, B.: How important is the vertical structure for the representation of aerosol impacts on the diurnal cycle of marine stratocumulus?, Atmos. Chem. Phys., 9, 4039–4052, doi:10.5194/acp-9-4039-2009, 2009.

Shao, H. and Liu, G.: A critical examination of the observed first aerosol indirect effect, J. Atmos. Sci., 66, 1018–1032, 2009.

Simpson, W.-K. T. J., Baker, D., Braun, S., Chou, M.-D., Ferrier, B., Johnson, D., Khain, A., Lang, S., Lynn, B., Shie, C.-L., Starr, D., Sui, C.-H., Wang, Y., and Wetzel, P.: Microphysics, radiation and surface processes in the Goddard Cumulus Ensemble (GCE) model, Meteor. Atmos. Phys., 82, 97–137, 2003.

Skamarock, W. C., Klemp, J. B., Dudhia, J., Gill, D. O., Barker, D. M., Duda, M. G., Huang, X.-Y., Wang, W., and Powers, J. G.: A description of the advanced research WRF Version 3, National Center for Atmospheric Research, Boulder, Colorado, USA, 2008.

Stevens, B., Feingold, G., Cotton, W. R., and Walko, R. L.: Elements of the microphysical structure of numerically simulated nonprecipitating stratocumulus, J. Atmos. Sci., 53, 980–1006, 1996.

Stevens, B., Cotton, W. R., Feingold, G., and Moeng, C.-H.: Large-eddy simulations of strongly precipitating, shallow, stratocumulus-topped boundary layers, J. Atmos. Sci., 55, 3616–3638, 1998.

Stevens, B., Lenscho, D. H., Faloona, I., Moeng, C.-H., Lilly, D. K., Blomquist, B., Valie, G., Bandy, A., Campos, T., Gerber, H., Haimov, S., Morley, B., and Thornton, D.: On entrainment rates in nocturnal marine stratocumulus, Quart. J. Roy. Meteor. Soc., 129, 3469–3493, doi:10.1256/qj.02.202, 2003.

Stevens, B., Moeng, C.-H., Ackerman, A. S., Bretherton, C. S., Chlond, A., De Roode, S., Edwards, J., Golaz, J., Jiang, H., Khairoutdinov, M., Kirkpatrick, M. P., Lewellen, D. C., Lock, A., Muller,

F., Stevens, D. E., Whelan, E., and Zhu, P.: Evaluation of large-eddy simulations via observations of nocturnal marine stratocumulus, Mon. Wea. Rev., 133, 1443–1462, 2005.

Sundqvist, H.: Parameterization of condensation and associated clouds in models for weather prediction and general circulation simulation, in: Physically-based modelling and simulation of climate and climate change, Part 1, edited by Schlesinger, M. E., pp. 433–462, Kluwer Academic Publishers, 1988.

Thompson, G., Field, P. R., and Rasmussen, R. M.: Explicit forecasts of winter precipitation using and improved bulk microphysics scheme. Part I: Description and sensitivity analysis, Mon. Wea. Rev., 132, 519–542, 2004.

Thompson, G., Field, P. R., Rasmussen, R. M., and Hall, W. D.: Explicit forecasts of winter precipitation using and improved bulk microphysics scheme. Part II: Implementation of a new snow parameterization, Mon. Wea. Rev., 136, 5095–5115, 2008.

Tzivion, S., Feingold, G., and Levin, Z.: An efficient numerical solution to the stochastic collection equation, J. Atmos. Sci., 44, 3139–3149, 1987.

Tzivion, S., Feingold, G., and Levin, Z.: The Evolution of raindrop spectra. Part II: Collisional collection/breakup and evaporation in a rainshaft, J. Atmos. Sci., 46, 3312–3327, 1989.

Walko, R. L., Cotton, W. R., Harrington, J. Y., and Meyers, M. P.: New RAMS cloud microphysical parameterization. Part I: The single moment scheme, Atmos. Res., 38, 29–62, 1995.

Wang, H. and Feingold, G.: Modeling mesoscale cellular structures and drizzle in marine stratocumulus. Part I: Impact of drizzle on the formation and evolution of open cells, J. Atmos. Sci., 66, 3237–3256, 2009a.

Wang, H. and Feingold, G.: Modeling mesoscale cellular structures and drizzle in marine stratocumulus. Part II: The microphysics and dynamics of the boundary region between open and closed cells, J. Atmos. Sci., 66, 3257–3275, 2009b.

Wang, H., Skamarock, W. C., and Feingold, G.: Evaluation of scalar advection schemes in the Advance Research WRF model using large-eddy simulations of aerosol-cloud-interactions, Mon. Wea. Rev., 137, 2547–2558, 2009.

Wang, H., Feingold, G., Wood, R., and Kazil, J.: Modeling microphysical and meteorological controls on precipitation and cloud cellular structures in Southeast Pacific stratocumulus, Atmos. Chem. Phys., 10, 6347–6362, doi:10.5194/acp-10-6347-2010, 2010.

Wang, H., Rasch, P. J., and Feingold, G.: Manipulating marine stratocumulus cloud amount and albedo: A process-modelling study of aerosol-cloud-precipitation interactions in response to injection of cloud condensation nuclei, Atmos. Chem. Phys., 11, 4237–4249, doi:10.5194/acp-11-4237-2011, 2011.

Wang, S., Wang, Q., and Feinfold, G.: Turbulence, condensation, and liquid water transport in numerically simulated nonprecipitating stratocumulus clouds, J. Atmos. Sci., 60, 262–278, 2003.

Wood, R.: Cancellation of aerosol indirect effects in marine stratocumulus through cloud thinning, J. Atmos. Sci., 64, 2657–2669, doi:10.1175/JAS3942.1, 2007.

Wood, R., Kubar, T. L., and Hartmann, D. L.: Understanding the importance of microphysics and macrophysics for warm rain in marine low clouds. Part II: Heuristic models of rain formation, J. Atmos. Sci., 66, 2973–2990, 2009.

Xue, H. and Feingold, G.: Large-eddy simulations of trade wind cumulus: Investigation of aerosol indirect effects, J. Atmos. Sci., 63, 1605–1622, 2006.

Xue, L., Teller, A., Rasmussen, R., Geresdi, I., and Pan, Z.: Effects of aerosol solubility and regeneration on warm-phase orographic clouds and precipitation simulated by a detailed bin microphysics scheme, J. Atmos. Sci., 67, 3336–3354, 2010.

Yin, Y., Carslaw, K. S., and Feingold, G.: Vertical transport and processing of aerosol in a mixed-phase convective cloud and the feedback on cloud development, Quart. J. Roy. Meteor. Soc., 131, 221–245, 2005.

Zhang, M., Lin, W., Bretherton, C. S., Hack, J. J., and Rasch, P. J.: A modified formulation of fractional stratiform condensation rate in the NCAR community atmosphere model (CAM2), J. Geophys. Res., 108, doi:10/1029/2002JD002523, 2003.

# Chapter 3

# Theoretical Basis for Convective Invigoration due to Increased Aerosol Concentration *

*Reproduced with permission from "Theoretical Basis for Convective Invigoration due to Increased Aerosol Concentration" by Z. J. Lebo and J. H. Seinfeld, *Atmos. Chem. Phys., 11*, 5407-5429, doi:10.5194/acp-11-5407-2011. 

## 3.1 Abstract

The potential effects of increased aerosol loading on the development of deep convective clouds and resulting precipitation amounts are studied by employing the Weather Research and Forecasting (WRF) model as a detailed high-resolution cloud resolving model (CRM) with both detailed bulk and bin microphysics schemes. Both models include a physically-based activation scheme that incorporates a size-resolved aerosol population. We demonstrate that the aerosol-induced effect is controlled by the balance between latent heating and the increase in condensed water aloft, each having opposing effects on buoyancy. It is also shown that under polluted conditions, increases in the CCN number concentration reduce the cumulative precipitation due to the competition between the sedimentation and evaporation/sublimation timescales. The effect of an increase in the IN number concentration on the dynamics of deep convective clouds is small and the resulting decrease in domain-averaged cumulative precipitation is shown not to be statistically significant, but may act to suppress precipitation. It is also shown that even in the presence of a decrease in the domain-averaged cumulative precipitation, an increase in the precipitation variance, or in other words, and increase in rainfall intensity, may be expected in more polluted environments, especially in moist environments.

A significant difference exists between the predictions based on the bin and bulk microphysics schemes of precipitation and the influence of aerosol perturbations on updraft velocity within the convective core. The bulk microphysics scheme shows little change in the latent heating rates due to an increase in the CCN number concentration, while the bin microphysics scheme demonstrates significant increases in the latent heating aloft with increasing CCN number concentration. This suggests that even a detailed two-bulk microphysics scheme, coupled to a detailed activation scheme, may not be sufficient to predict small changes that result from perturbations in aerosol loading.

## 3.2 Introduction

Changes in ambient concentrations of cloud condensation nuclei (CCN) and ice nuclei (IN) potentially alter cloud properties that may ultimately lead to modifications in cloud radiative forcing and/or precipitation. Traditionally, aerosol-cloud interactions have been discussed primarily in terms of (IPCC, 2007): (1) The "1st aerosol indirect effect" (Twomey, 1977), in which all else being equal, an increase in the CCN number concentration will result in a higher cloud droplet number concentration and hence smaller particles. More numerous smaller particles act to increase the cloud optical depth and thus the cloud albedo that ultimately results in a reduction of the shortwave radiative flux that reaches the surface (cooling effect at the surface). (2) The "2nd aerosol indirect effect" (Albrecht, 1989), in which changes in the CCN number concentration may affect cloud lifetime and precipitation efficiency. An increase in the CCN number concentration will result in smaller cloud droplets, for which the collection kernels and collection efficiencies are substantially smaller in comparison to their larger counterparts, thus mitigating the collision-coalescence process and suppressing precipitation. Ultimately, the additional CCN particles are hypothesized to increase the longevity of the cloud and reduce the surface heating by shortwave radiation (cooling effect at the surface). With that said, it is now recognized that a division into the 1st and 2nd indirect effects is an oversimplification of the continuous cascade of processes that ensue in response to a perturbation in the aerosol number concentration.

Considerable attention has been given to the effects of aerosol particles on cloud properties for warm stratiform clouds (e.g., Ackerman et al., 2004; Lu and Seinfeld, 2006; Sandu et al., 2008; Hill et al., 2008, 2009; Wang and Feingold, 2009a,b; Wang et al., 2010). The extent to which these processes hold in mixed-phase and/or cold clouds is not well established. The ice phase presents significant complexities not present in warm clouds (i.e., riming, aggregation, accretion, heterogeneous and homogeneous freezing, melting, etc.), and the mixed-phase processes are the predominant mechanisms by which rain forms (not directly by collision-coalescence of liquid droplets into larger, rain drops). Recently, the potential effects of polluted environments on the formation and development of deep convective clouds have received attention via both modeling studies using

a 3D CRM with bulk microphysics (e.g., Van den Heever et al., 2006; Van den Heever and Cotton, 2007), 3D CRM with bin microphysics (e.g., Khain et al., 2008; Khain and Lynn, 2009), 2D CRM with bin microphysics (e.g., Fan et al., 2009) and, less commonly, observational analyses (e.g., Koren et al., 2005, 2010).

Conceptual hypotheses have been put forth by Rosenfeld et al. (2008a) and Stevens and Feingold (2009) for the invigoration of deep convective clouds by increased aerosol loading. These works are discussed in further detail below. Briefly however, via different reasoning, both works conclude that an increase in aerosol number concentration should act to increase surface precipitation. Rosenfeld et al. (2008a) suggest that a decrease in invigoration of deep convection may occur due to the direct effect of aerosols acting to limit the downward shortwave radiative flux at the surface, mitigating surface warming and leading to weaker convection. Although the ability for aerosol perturbations to invigorate deep convective clouds makes sense conceptually, modeling studies are still not in agreement as to the sign of the effect on precipitation owing to increased pollutants. For example, Van den Heever et al. (2006) showed using a 3D CRM with bulk microphysics that adding aerosol particles in the form of CCN, giant CCN (GCCN), and/or IN causes a decrease in domain-average cumulative precipitation in reference to a clean environment observed during the Cirrus Regional Study of Tropical Anvils and Cirrus Layer-Florida Area Cirrus Experiment (CRYSTAL-FACE). On the other hand, Khain and Lynn (2009) demonstrated an increase in precipitation with an increase in CCN concentration using a spectral bin microphysics model but with low spatial resolution and abbreviated simulation time. In the same study, a decrease in precipitation with an increase in CCN number concentration was shown using a simple two-moment bulk microphysics scheme simulated on the same dynamic framework.

One can imagine though that the effect of an increase in the ambient aerosol concentration on surface precipitation (as well as cloud radiative forcing) in deep convective clouds may not be monotonic and likely depends significantly on the environmental conditions (i.e., Rosenfeld et al., 2008a). Khain et al. (2008) attempted to classify the effects of increased aerosol concentrations on precipitation for a wide range of cloud types and locations showing that, for example, deep convective

clouds in dry environments should exhibit a decrease in precipitation with an increase in the aerosol number concentration. On the other hand, in moist environments, an increase in the aerosol loading was shown to increase precipitation or provide a negligible change depending on the specific cloud type. Moreover, Fan et al. (2009) studied the importance of the magnitude of the vertical wind shear on the aerosol-induced changes in deep convective clouds. The study showed that in a relatively high shear environment, an increase in the CCN number concentration produced a decrease in vertical velocity and cumulative precipitation.

Additional studies have looked at the potential implications of aerosol perturbations on the anvil cloud development and microphysical characteristics. The cloud resolving model (CRM) study of Van den Heever et al. (2006) showed that the anvil clouds atop the simulated deep convective clouds cover less area but contain higher amounts of condensed water when the aerosol number concentration is elevated. This results in more intense, localized precipitation. More recently, satellite data analysis has shown that regions with higher aerosol concentrations statistically correlate with areas of larger cloud extent, i.e., broader anvils (Koren et al., 2010). By broadening the anvil, the cloud becomes thinner and thus reduces the cloud albedo while the outgoing longwave radiation is relatively unchanged since the cloud top temperature does not change much. In turn, this combination results in an increase in the solar radiation reaching the surface. Little observational evidence is available at this time (due to the inherent complexities in measuring small concentrations of IN in regions of very high instability and remote locations) to determine clearly the overall effect of aerosol perturbations on anvil cloud development.

Measurements of IN number concentration were performed during CRYSTAL-FACE within a period of enhanced dust particle concentration (DeMott et al., 2003; Sassen et al., 2003). DeMott et al. (2003) reported that during CRYSTAL-FACE, IN number concentrations were observed to be as high as $1\,\mathrm{cm}^{-3}$ ($10^3\,\ell^{-1}$). Later, Van den Heever et al. (2006) and Teller and Levin (2006) demonstrated a decrease in precipitation with an increase in IN concentration using 3-D and 2-D CRMs, respectively. However, these studies do not fully represent the potential effects of IN on deep convective cloud development since the freezing process is parameterized based on the empirical relation of

Meyers et al. (1992) in which the IN number concentration is expressed as an exponential function of temperature and/or supersaturation. For low temperatures (i.e., less than about $-30\,^{\circ}\mathrm{C}$), the IN number concentration, as predicted by the empirical relations, becomes erroneously large and will likely significantly impacts the model predictions.

Microphysical calculations of deep convective cloud (e.g., Khain et al., 2004, 2008; Teller and Levin, 2006; Khain and Lynn, 2009) and multi-cloud systems (e.g., Lee and Feingold, 2010; Lee, 2011) invigoration in response to aerosol changes have been performed in recent years . Potential shortcomings exist in the method by which the CCN concentration is implemented and in the representation of the IN number concentration by the empirical Twomey (1959) relationship to predict the number of activated aerosol particles as a function of supersaturation. The empirical constants in this relation are specific to individual cloud types, i.e., the coefficients that apply for the convective core may not be adequate for other regions of the deep convective cloud, e.g., detrained stratocumulus. Moreover, some of the previous studies have used two-dimensional models (e.g., Khain et al., 2004, 2008; Teller and Levin, 2006) and others that have simulated all three dimensions (e.g., Khain and Lynn, 2009) have been performed at rather low spatial resolution, i.e., $\geq 2\,\mathrm{km}$ in the horizontal. It is natural to ask if with limited computational resources, should one simulate deep convective clouds using detailed bin microphysics or instead use a detailed two-moment bulk scheme at much higher spatial resolution? And, if one accounts for the activation of cloud droplets and nucleation of ice particles in a more physically coherent manner, what are the effects of aerosol particles on precipitation in deep convective clouds? These points are addressed in this study.

The remainder of this work is organized as follows: Sect. 3.3 presents hypotheses regarding aerosol effects on deep convective clouds. This is followed in Sect. 3.4 by a detailed description of the bulk and bin microphysics models that are employed in this study. Section 3.5 provides information relevant to the chosen dynamical model as well as details on the model initialization and simulations. Sections 3.6.1 and 3.6.2 discuss our findings regarding the influence of CCN and IN on deep convective clouds, respectively, and include a detailed comparison of the simulations performed with both the bulk and bin microphysics schemes. Moreover, Sects. 3.6.3 and 3.6.4

review the effects of aerosol perturbations on cloud top height and rainfall intensity, respectively. Lastly, Sect. 3.7 concludes the work and serves to outline the most important findings of this study.

## 3.3 Theoretical basis and hypotheses

Here, we highlight and discuss recent work in the realm of aerosol invigoration of deep convective cloud. Our purpose here is to present the relevant hypotheses related to this work in a concise framework.

### 3.3.1 Rosenfeld, et al., 2008

Rosenfeld et al. (2008a) argue that the effect of an increased concentration of sub-cloud aerosol, and hence cloud condensation nuclei (CCN), on convective clouds is to invigorate updrafts and produce an increase in precipitation as a result of upward heat transport via phase change. The argument is based on the results of a bulk thermodynamic parcel model, in which in the baseline simulation it is assumed that all water condenses and is immediately precipitated; hence, no energy is required to lift the hydrometeors (for the purpose of this study, hydrometeors are defined to be liquid cloud drops, pristine ice crystals, dendritic snow crystals, and rimed ice, or graupel). In other words, the work required, here in the form of mechanical energy, to lift condensed forms of water is zero. It is assumed, in addition, that the liquid water freezes at $-4\,^{\circ}\mathrm{C}$ such that when the hydrometeors freeze at and above the level where this temperature is attained, a release of latent heat occurs, providing positive buoyancy. Rosenfeld et al. (2008a) argue that an increase in aerosol number concentration will serve to delay the onset of the collision-coalescence process, and energy is required to lift the parcel containing liquid hydrometeors to lower temperatures. Further increases in the aerosol concentration require the parcel to be lifted to even higher levels before collision-coalescence ensues. If collision-coalescence is delayed up to the freezing level, droplets are assumed to freeze, releasing latent heat, and then precipitating from the parcel, removing water mass and generating positive buoyancy. Hydrometeors are assumed to immediately freeze and precipitate if the parcel is lifted even farther. Rosenfeld et al. (2008a) argue that the addition of aerosol particles above that which would occur

in a relatively clean environment (i.e., increasing the aerosol number concentration from $\approx$100 cm$^{-3}$ to $\geq$1000 cm$^{-3}$) can increase the released gravitational energy, which is equivalent to changing the effective convective available potential energy (CAPE) of the parcel by >1000 J kg$^{-1}$. The effect of the resultant increase in CAPE and mitigation of the collision-coalescence process is to delay the onset of precipitation, but increase the total precipitation. Rosenfeld et al. (2008a) also discussed that the increase in evaporative cooling within the downdrafts near the surface provides additional additional upward heat transport leading to convective invigoration.

The concentration of CCN required to delay collision-coalescence until the parcel reaches the $-4\,^{\circ}$C isotherm is determined from the depth ($D$) above cloud base needed for precipitation to begin as derived from aircraft measurements (Rosenfeld et al., 2008b; Freud et al., 2008; vanZanten et al., 2005). The result is an aerosol concentration of about 1200 cm$^{-3}$, assuming standard values for tropical deep convective clouds. Since typical CCN concentrations tend to lie between 100 and 200 cm$^{-3}$ and between 600 and 1700 cm$^{-3}$ in clean and polluted marine regions, respectively (Andreae, 2009), the CCN concentration of 1200 cm$^{-3}$ at which invigoration should reach a maximum is relevant for anthropogenically influenced locations. For concentrations of CCN above 1200 cm$^{-3}$, collision-coalescence is delayed beyond the freezing level, more energy is required to lift the parcel, and the invigoration effect is mitigated. For higher CCN concentrations, less incoming solar radiation reaches the surface, reducing surface warming, which in turn, stabilizes the boundary layer, hence limiting convective development.

### 3.3.2 Stevens and Feingold, 2009

In addition to invigoration of updrafts within and below deep convective clouds, Stevens and Feingold (2009) proposed that an increase in CCN may act to increase cloud top height (i.e., cloud depth). The basis for this hypothesis is that an increase in CCN should act both to increase cloud droplet number concentration ($N_c$) and to reduce cloud droplet effective radius ($r_e$) in warm clouds, hence delaying the onset of precipitation. This allows hydrometeors to be advected to higher levels, increasing the amount of condensed water within the cloud, in turn increasing evaporation at cloud top, hence

cooling and destabilizing the cloud top region. Updrafts near cloud top are invigorated, increasing cloud depth. Since deeper clouds are expected to have more liquid water, an increase in precipitation is expected. However, the microphysical complexity of cold clouds (i.e., those containing ice in some form) adds another dimension, hence the effect of increased aerosols no longer follows such a straightforward pathway.

### 3.3.3 Khain et al., 2008

Khain et al. (2008) attempt to classify the effect of aerosol levels on precipitation from clouds of all types. Using a 2-D CRM with spectral microphysics, Khain et al. (2008) show that deep clouds in both tropical and moist urban areas tend to display an increase in precipitation with increasing aerosol levels. The effect of increased aerosol levels on supercell storms is shown to either decrease or increase precipitation depending upon whether the environment is dry or moist, respectively.

## 3.4 Numerical simulation

We explore the effects of aerosol perturbations on deep convective clouds by using the Weather Research and Forecasting (WRF) model Version 3.1 (Skamarock et al., 2008) as a CRM. The dynamical core of the WRF model is augmented by a detailed mixed-phase bin microphysics scheme following Tzivion et al. (1987), Tzivion et al. (1989), Feingold et al. (1988), Reisin et al. (1996), and Khain et al. (2004). In addition, we provide comparisons between predictions of the detailed bin model and those of a modified two-moment five-class (i.e., cloud, rain, pristine ice, snow, and graupel) bulk microphysics scheme (Morrison et al., 2005; Morrison and Pinto, 2005). The bin scheme and the modifications to the bulk scheme are described in detail below.

### 3.4.1 Bin microphysics scheme

The mixed-phase bin microphysics scheme divides each hydrometeor spectrum into 36 bins (i.e., $x_{j_1}, x_{j_2}, \ldots, x_{j_{36}}$, where $j$ corresponds to the hydrometeor type: c, i, s, and g for liquid cloud droplets, pristine ice, snow, and graupel, respectively, and $x$ is the mass) with mass doubling between bins

such that

$$x_{k+1} = 2x_k \tag{3.1}$$

in which $k$ corresponds to the lower boundary of bin number $k$. The mass of the smallest bin is defined to be $1.598\times10^{-14}$ kg (Reisin et al., 1996), which, for liquid droplets (with density $\rho_{\mathrm{l}}$=1000 kg m$^{-3}$) corresponds to a diameter of 3.125 µm. Additionally, we assume fixed bulk densities for the frozen species, i.e., $\rho_{\mathrm{i}}$=900 kg m$^{-3}$, $\rho_{\mathrm{s}}$=200 kg m$^{-3}$, $\rho_{\mathrm{g}}$=500 kg m$^{-3}$. The choice of 36 bins allows hydrometeors to attain appreciable sizes for precipitation to occur while minimizing the risk of creating numerical instability due to very large particles falling through grid boxes within a single time step. With these assumptions, the droplets, pristine ice, snow, and graupel can grow to 10.1 mm, 10.5 mm, 17.3 mm, and 12.8 mm, respectively. These sizes are adequate to accurately represent the formation of hail (i.e., large graupel) and the changes in hail formation due to aerosol perturbations that have been shown to be important in previous studies (e.g., Andrejczuk et al., 2004; Khain et al., 2011).

#### 3.4.1.1 Collision-coalescence, accretion, riming, and aggregation

The collision-coalescence process is represented by the moment-conserving numerical solution to the stochastic collection equation of Tzivion et al. (1987) for the first two moments of each distribution, namely the number concentration ($N_{j_k}$) and mass mixing ratio ($M_{j_k}$). For collisions amongst liquid droplets, we use the Long (1974) collection kernel. For ice-ice, ice-snow, ice-graupel, snow-graupel, snow-snow, liquid-ice, liquid-snow, liquid-graupel, graupel-graupel collisions we use the gravitational collection kernel.

Collisions among liquid droplets simply produce larger droplets. As a result, the first moment of the size distribution, the mass, is conserved within the liquid category while the zeroth moment, the number concentration, is reduced. Collisions among other particles, e.g., ice-liquid, ice-ice, etc., are not as straightforward because the collisions may lead to the formation of particles in a different category. Hence, the gain and loss terms for each hydrometeor type and category must be determined following the rules defined in Table 3.1 (Reisin et al., 1996; Khain et al., 2004). Note that $m_{\mathrm{l}}$, $m_{\mathrm{s}}$, and $m_{\mathrm{i}}$ correspond to the masses of the liquid, snow, and ice particles involved in a collision.

#### 3.4.1.2 Vapor condensation/deposition and evaporation/sublimation

The simulation of condensation and evaporation of water to and from liquid drops, as well as deposition and sublimation, can depend strongly on the chosen time step and are highly sensitive to small fluctuations in the supersaturation (both with respect to liquid water as well as ice). Tzivion et al. (1989) formulated the condensational forcing ($\tau$) due to a vapor surplus or deficit ($\Delta q_{\mathrm{v}}$) as the integral of the surplus/deficit over a timestep ($\Delta t$) as

$$\tau = G(P,T)\int_{t}^{t+\Delta t} \Delta q_{\mathrm{v}} dt \tag{3.2}$$

in which $G(P,T)$ is a known function of pressure ($P$) and temperature ($T$) defined in Pruppacher and Klett (1997) and Seinfeld and Pandis (2006) and $\Delta q_{\mathrm{v}}$ is defined as

$$\Delta q_{\mathrm{v}} = q_{\mathrm{v}} - q_{\mathrm{s}} \tag{3.3}$$

where $q_{\mathrm{s}}$ is the saturated water vapor mixing ratio. Due to condensation/evaporation and deposition/sublimation, and the resulting latent heating, within a timestep, $\Delta q_{\mathrm{v}}$ is not necessarily constant over the timestep. We use the method of Harrington et al. (2000) to predict the evolution of $q_{\mathrm{v}}$, and consequently, $\Delta q_{\mathrm{v}}$, over the course of each timestep. By utilizing Eq. (3.2) we can capture the changes in the vapor surplus within a timestep as a result of phase changes, i.e., condensation/evaporation and deposition/sublimation. The full solution to the condensation equation as derived by Tzivion et al. (1989) for linearized distributions within bins is cumbersome and computationally expensive. Therefore, we employ the method of Stevens et al. (1996) in which the mass and number within a given bin are distributed following a top hat distribution. Moreover, we include gas kinetic effects on the growth of the hydrometeors following Clark (1974) and Stevens et al. (1996) in which the mass growth equation can be expressed as

$$\frac{dm}{dt} = \frac{m^{2/3}}{m^{1/3} + \ell} G(P,T)\Delta q_{\mathrm{v}} \tag{3.4}$$

in which $\ell$ represents a length scale for vapor growth defined as

$$\ell = \ell_\circ \left( \frac{4}{3} \pi \rho_\mathrm{w} \right)^{1/3} \tag{3.5}$$

in which $\ell_\circ$ is assumed to be 6.4 µm. There exists an analytic solution to Eq. (3.4), and this solution is used for the remapping of the bins due to condensation/evaporation and deposition/sublimation.

#### 3.4.1.3 Cloud droplet activation and regeneration

The aerosol size distribution is assumed to follow a single-mode lognormal distribution (Seinfeld and Pandis, 2006),

$$n^d \left( D_\mathrm{p} \right) \equiv \frac{dN}{d \ln D_\mathrm{p}} = \frac{N_\mathrm{a}}{\sqrt{2\pi} \ln \sigma} \exp \left[ - \frac{\ln^2 \left( \frac{D_\mathrm{p}}{D_\mathrm{g}} \right)}{2 \ln^2 \sigma} \right] \tag{3.6}$$

where, $N_\mathrm{a}$ is the total aerosol number concentration, $\sigma$ and $D_\mathrm{g}$ are the standard deviation and geometric mean diameter, respectively, and $D_\mathrm{p}$ is the particle diameter. For the purposes of this study, we let $D_\mathrm{g} = 0.1$ $\mu$m and $\sigma = 1.8$. The aerosol distribution is discretized into 36 mass-doubling bins. The first bin corresponds to an aerosol particle in which $D_\mathrm{p} = 1$ nm. The total number concentration is set during the model initialization and the aerosol particles that remain after advection are advected throughout the domain. The number of activated aerosol particles ($N_\mathrm{act}$) is computed during each time step by integrating the size distribution over particles with critical supersaturations that are less than the ambient supersaturation,

$$N_\mathrm{act} = \int_0^S n^s(s') ds' \tag{3.7}$$

where $S$ is the ambient supersaturation and $n^s(s')$ is the critical supersaturation distribution. The activated aerosols are removed from the corresponding aerosol bin and moved to the cloud droplet distribution. The activated size of the newly formed droplets is computed following Kogan (1991), Khain et al. (2000), and Xue et al. (2010) in which the activated droplet size is assumed to be a factor of $k(D_\mathrm{p})$ larger than the aerosol of size $D_\mathrm{p}$. The smallest of the activated aerosols are

assumed to enter the first bin of the droplet distribution whereas larger aerosols are moved to the bin corresponding to their predicted activated droplet size. Aerosol scavenging was shown to have a negligible effect on cloud properties by Geresdi and Rasmussen (2005) and is thus not included in the current scheme. The evaporation of cloud droplets leads to the regeneration of aerosol particles. Xue et al. (2010) demonstrated the significance of aerosol regeneration on cloud microphysical properties. Without including the regeneration of aerosols, the number of cloud droplets activated during a simulation can be erroneously underestimated thus increasing the mean size and ultimately leading to artificially enhanced precipitation. The number of aerosols that are formed in one timestep is assumed to be equivalent to the number of cloud droplets that evaporate following Xue et al. (2010). For the purposes of this study, we assume that the effect of collision-coalescence on the regenerated aerosol size distribution is negligible.

#### 3.4.1.4 Freezing and melting

Supercooled cloud drops can freeze to form ice crystals via heterogenous (i.e., contact nucleation, immersion freezing, deposition freezing, etc.) and homogeneous freezing. We must turn to previous studies (Bigg, 1953; Fletcher, 1962; Vali, 1975; Cooper, 1986; Meyers et al., 1992) that have shown via various techniques that the ice nuclei (IN) number concentration (and inherently the number of frozen drops) can be diagnosed by empirically derived using the ambient environmental conditions. The expression derived by Bigg (1953) for the rate of change of frozen drops with time can be used to express the number of frozen drops in a bin during a time step ($N_{\mathrm{f}_k}$) due to both homogeneous freezing of cloud droplets (for $T<-37\,^{\circ}\mathrm{C}$) and immersion freezing ($-37\,^{\circ}\mathrm{C}<T<-5\,^{\circ}\mathrm{C}$) as (Reisin et al., 1996),

$$N_{\mathrm{f}_k} = N_{\mathrm{c}_k}(t)\left(1-\exp\left[-\frac{\overline{m_{\mathrm{c}_k}}}{\rho_{\mathrm{l}}}A'\exp\left(B'\left(T_{\circ}-T\right)\right)\Delta t\right]\right) \tag{3.8}$$

where $N_{\mathrm{c}_k}(t)$ is the number of cloud drops in bin $k$ at the start of the time step, $\overline{m_{\mathrm{c}_k}}$ is the average droplet mass in bin $k$, and $A'$ and $B'$ are constants defined as $10^{-4}\,\mathrm{cm}^{-3}\,\mathrm{s}^{-1}$ and $0.66\,\mathrm{K}^{-1}$, respectively, from Orville and Kopp (1977). The frozen mass in bin $k$ is simply $N_{\mathrm{f}_k}\overline{m_{\mathrm{c}_k}}$. Here, we use Eq. (3.8) only for homogeneous nucleation of ice crystals. The nucleation of ice crystals due to

immersion freezing is caused by IN being immersed within a cloud droplet. These IN become active at various temperatures. Vali (1975) showed that the number of active immersion IN ($N_{\rm im}$) can be expressed as a function of temperature in degrees Celsius ($T_{\rm c}$) by

$$N_{\rm im} = N_{\rm im_\circ} (0.1 T_{\rm c})^{\gamma} \tag{3.9}$$

in which it is assumed that $N_{\rm im_\circ}$=$10^7\,{\rm m}^{-3}$ and $\gamma$=4.4 for convective clouds. Furthermore, for deposition and condensation freezing, we use the formula of Meyers et al. (1992) to relate the number of deposition and condensation IN ($N_{\rm d}$) to that of the ambient supersaturation with respect to ice ($S_{\rm ice}$) as

$$N_{\rm d} = N_{\rm d_\circ} \exp\left[-0.639 + 12.96 S_{\rm ice}\right] \tag{3.10}$$

where $N_{\rm d_\circ}$=$10^{-3}\,{\rm m}^{-3}$. We distribute evenly the number of droplets that freeze due to deposition and contact freezing.

All frozen hydrometeors are assumed to melt over the course of a single timestep when the ambient temperature of the grid box containing such particles is greater than 0 °C. Sensitivity simulations with more sophisticated, and hence more computationally expensive, melting routines that attempt to account for heat transfer within the frozen species demonstrated a qualitatively insignificant change in the results presented here.

#### 3.4.1.5 Sedimentation

All hydrometeors are assumed to sediment at their terminal fall speeds ($v_{t_j}$, $j$ corresponding to the particle type). As alluded to above, fall speeds for snow are computed from the mass-fall speed relationships determined by Locatelli and Hobbs (1974) for aggregates of unrimed side planes. For consistency, we use the same mass-fall speed relationships for graupel and hail as in the bulk microphysics scheme (Morrison et al., 2005; Morrison and Pinto, 2005). The mass-fall speed relationships for hail are used to predict sedimentation of particles in the tail of the graupel distribution. The terminal fall speed of ice crystals is computed following Heymsfield and Kajikawa (1987). For the

purpose of this study, it is assumed that particles in the ice category are pristine crystals in the shape of thin hexagonal plates (type P1a). Terminal velocities are computed by relating the crystal Davies or Best number ($X$) to the crystal Reynolds number ($N_{Re}$) by (Heymsfield and Kajikawa, 1987),

$$X = C_{\rm d} N_{Re}^2 = \frac{2mD_{\rm i}^2 g}{\rho_{\rm i}\nu^2 A} \tag{3.11}$$

where $m$ is the crystal mass, $D_{\rm i}$ is the crystal dimension, $g$ is the acceleration due to gravity, $\nu$ is the kinematic viscosity of air, and $A$ is the crystal cross-sectional area normal to the direction of motion. Moreover, we can express $N_{Re}$ as

$$N_{Re} = \frac{v_{\rm t_i} D_{\rm i}}{\nu}. \tag{3.12}$$

Using the $X-N_{Re}$ parameterization of Heymsfield and Kajikawa (1987), i.e.,

$$N_{Re} = \alpha X^{\beta} \tag{3.13}$$

and the definitions of $X$ and $N_{Re}$, we can write $v_{\rm t_i}$ in terms of the crystal equivalent hexagonal diameter ($D_{\rm i_{eq}}$) as

$$v_{\rm t_i} = \frac{\nu\alpha}{D_{\rm i_{eq}}} \left[ \frac{2mD_{\rm i_{eq}}^2 g}{\rho_{\rm i}\nu^2 A} \right]^{\beta} \tag{3.14}$$

where, for a hexagonal plate,

$$A = \frac{3\sqrt{3}}{2} D_{\rm i_{eq}}^2. \tag{3.15}$$

Lastly, Heymsfield and Kajikawa (1987) define $D_{\rm i_{eq}}$ to be equivalent to $D_{\rm i}\sqrt{\gamma}$ where $\gamma$ is the crystal area ratio (i.e., the ratio of the crystal area to that of a crystal with the same dimensions). We take $\gamma$=0.9.

### 3.4.2 Bulk microphysical scheme

For the two-moment bulk microphysics scheme, we use that of Morrison et al. (2005) and Morrison and Pinto (2005), included with the WRF model. The scheme has a fixed cloud drop number concentration ($N_c$), and the freezing process is parameterized following Cooper (1986). In order to more accurately represent the aerosol effect on cloud properties in the bulk model, we have modified the scheme to include explicit droplet activation as well as to include the freezing mechanisms included in the bin scheme described above. In other words, the aerosol population is initiated following a lognormal size distribution and binned into 36 mass doubling bins. The activated droplet size is computed as in the bin scheme and the total liquid water mixing ratio and number concentration that activate are computed and added to the bulk quantities. On the first timestep that aerosol particles are activated, the model fits a gamma distribution to the discretized droplet distribution. Computing the activation in this manner limits the differences between the bin and bulk schemes, especially pertaining to the link between CCN and cloud droplets (as well as IN and ice formation).

## 3.5 Experimental setup

The WRF model, modified as described in Sect. 3, is initialized with an idealized sounding typical for continental locales conducive to deep convective development (Figs. 3.1 and 3.2). Two soundings are used in order to analyze the extent to which an aerosol-induced effect on deep convection is dependent upon the ambient moisture content, i.e., the water vapor mixing ratio ($q_v$) or relative humidity (RH). The ambient RH is permitted to change with height similar to that of Khain and Lynn (2009), except that in the present study, the RH at the surface is 95% in the moist scenarios and the RH for the drier scenarios is simply 5% less than that of the moist cases (hereinafter these scenarios are referred to as the highRH and lowRH simulations, respectively). Therefore, the RH at the surface is 90% for the lowRH simulations. Recently, Fan et al. (2009) showed that aerosol effects act to reduce precipitation in deep convective clouds in high shear environments. However, the purpose of this study is not to analyze the dependence of aerosol-induced invigoration of deep

convective clouds on wind shear. As a result, we limit the vertical wind shear by utilizing the standard quarter circle shear wind profile derived from Weisman and Klemp (1982) (Fig. 3.2) so as not to influence the results by anomalously large vertical wind shear. Convection is initiated in the domain with a perturbation (bubble) in the potential temperature field of 3 °C located in the center of the domain in the north-south direction, and offset to the west in the east-west direction. The horizontal and vertical radii of the bubble are 10 km and 2 km, respectively. Khain and Lynn (2009) looked at the dependency of the aerosol induced effects on deep convective clouds using surface relative humidities of 95% and 85% for the moist and dry cases, respectively. We have increased the surface relative humidity in the lowRH cases since the cumulative domain-averaged precipitation in our simulations was insufficient to draw any definitive, statistically significant, conclusions at the lower RH.

It is important to note that unlike previous studies (e.g., Khain and Lynn, 2009), we choose to use a fixed timestep that is consistent for *all* simulations presented. Doing so does, in fact, increase the computation expense of performing such simulations (by nearly a factor of 2), in comparison to using an adaptive timestep method, in which a large fraction of each simulation is performed with a rather large timestep (i.e., at least twice that chosen here for the fixed timestep). However, the additional expense is necessary since the simulated results can differ both quantitatively and qualitatively when switching from a fixed timestep to an adaptive timestep method. In fact, simulations performed on a smaller domain demonstrate that the effect of even a small perturbation in the ambient aerosol concentration (i.e., from 100 to 200 $\mathrm{cm}^{-3}$) can be qualitatively different when a fixed timestep is chosen over that where the timestep is allowed to evolve based upon the stability of the model itself. We find that it is necessary to used a fixed timestep to study the effect of aerosol perturbations on the stability of deep convective clouds because if the timestep is allowed to change with the model's stability, and the cloud contained within the polluted environment is in fact more unstable than its clean counterpart, the timestep will be *smaller* for the polluted simulation. Our sensitivity simulations show that the difference in the timestep can be as much as 2 s during the period of time in which convection is strongest. Since sedimentation is computed as simply the mass flux

into and and out of a grid box multiplied by the timestep itself, the downward flux of condensed water integrated over a timestep is dependent upon the timestep. In other words, a longer timestep may allow more cloud water to fall out of a particular gridbox before other relevant microphysical processes can occur (i.e., collisions). Hence, the cumulative precipitation can be different between simulations with different aerosol number concentrations due to the difference in the timestep chosen by the model. To remove this uncertainty, we have chosen to fix the timestep at 4 s for all cases.

Another potential shortcoming of previous works (e.g., Fan et al., 2009; Khain and Lynn, 2009) is the choice of boundary conditions. Periodic boundary conditions are often used. However, CRM simulations of transient deep convective cells are not consistent with such boundary conditions. In other words, by choosing periodic boundary conditions, the western boundary of the domain is forced by the eastern boundary, which is physically implausible. We employ open boundaries, so that the advection of mass out of the eastern boundary does not affect the properties along the western boundary and thus artificially modify the cloud and ultimately precipitation patterns.

Many previous studies that have attempted to analyze aerosol-induced effects on deep convective clouds or compare spectral microphysics to bulk microphysics utilized two-dimensional (2-D) models (e.g., Khain et al., 2004, 2008; Khain and Pokrovsky, 2004; Seifert et al., 2006; Phillips et al., 2007). We use a three-dimensional (3-D) domain. The horizontal domain length is 250 km in both the $x$- and $y$-direction while the vertical domain extends from the surface to 20 km. This vertical depth allows us to simulate into the lower stratosphere which is important for properly depicting anvil formation near the tropopause. The horizontal grid spacing is set to 1000 m, and there are 60 stretched grid points in the vertical. The vertical grid spacing is less than 150 m at the surface and stretches to 400 m and 1500 m at 10 km above the surface and at the top of the model, respectively. A time step of 4 s is used to ensure numerical stability. The duration of the simulations is 6 h. The duration of the simulations are limited by the domain size. In order to limit the effect of reflection off of the boundaries and or advection along the boundaries, we must limit the simulations to 6 h. We understand that even at the resolution used in the current work, although higher than that of previous studies in which 3D CRM simulations using bin microphysics was used, still higher

resolution would be beneficial in order to fully capture the three-dimensional dynamical feedbacks and energetics resulting from changes in the cloud microphysics. However, the hard disk space and computational time required to perform such simulations with the bin microphysics model are beyond the magnitude of our current resources.

To analyze the potential effects of CCN and IN on deep convective clouds we perform a set of three simulations with varying concentrations of CCN and IN. These simulations are defined as: (1) "Clean" – $N_{\mathrm{CCN}}$=100 $\mathrm{cm}^{-3}$, (2) "Semi-Polluted" – $N_{\mathrm{CCN}}$=200 $\mathrm{cm}^{-3}$, and (3) "Polluted" – $N_{\mathrm{CCN}}$=500 $\mathrm{cm}^{-3}$. The "Clean" scenario will be used as the base case. To analyze the potential impact of changes in the aerosol loading when the added particles act as good IN, we perform additional simulations in which we multiply the predicted IN number concentrations for immersion, deposition, and condensation IN by a factor of 2. Regardless of the microphysics scheme employed for the IN sensitivity tests, the CCN number concentration is doubled from the "Clean" case to 200 $\mathrm{cm}^{-3}$. Hereinafter, the cases with increased IN number concentrations are referred to as "IN-Polluted". The purpose of the "Semi-Polluted" and "IN-Polluted" cases is to show the effect of an increase in aerosol concentration when the particles act only as CCN and when they are CCN and IN, respectively.

In summary, the model used in the present study differs from those of previous works, (e.g., Fan et al., 2009; Khain and Lynn, 2009). First, we simulate the evolution of deep convective clouds at a much higher resolution than previous studies using a comparable CRM setup. It is prudent to increase the spatial resolution so as to capture the important dynamical feedbacks that may result from differential heating caused by phase changes. Moreover, one likely underestimates the maximum supersaturation within in a grid cell at coarse resolution. In order to predict the cloud drop number concentration, an accurate depiction of the supersaturation is required. We have addressed this issue in the modified bulk scheme by using the explicit activation of a bin-resolved aerosol population. Sensitivity simulations (not shown) exhibit large discrepancies in the bulk cloud water variables, cumulative precipitation, and dynamical feedbacks (i.e., the track of the deep convective cloud) between simulations at low resolution (i.e., $\Delta x$=$\Delta y$$\geq$2000 m) and higher resolutions (i.e.,

$\Delta x$=$\Delta y$<2000 m). Moreover, we have updated the bin microphysics model of Reisin et al. (1996) to include more accurate collection kernels and collection efficiencies for riming processes. It is important to note that a key difference between in the bulk model employed in Khain and Lynn (2009) and the present study is that the prior used a fixed value for $N_c$, while here we predict $N_c$ based on relevant physics, aerosol number concentration, and ambient environmental conditions.

## 3.6 Results: CCN and IN effects on deep convective clouds

We begin with a comparison between bin and bulk simulations of the potential impact on deep convective cloud development and precipitation as a result of increasing the CCN number concentration. It is important to keep in mind that the purpose of this study is not to predict with great precision the amount of precipitation that may result from the given initial environmental conditions, but instead to numerically determine the extent to which the precipitation patterns and magnitude are altered in response to a modified aerosol loading. Unless stated otherwise, changes in the domain-averaged cumulative precipitation due to an increase in the CCN number concentration are statistically significant at the $\alpha = 0.05$ significance level (where $\alpha$ denotes the significance level).

### 3.6.1 CCN effects on precipitation and dynamical feedbacks

#### 3.6.1.1 High relative humidity

The overall effect of a perturbation in the CCN number concentration is to modify the precipitation amounting from a deep convective storm cloud. We quantify the effect as the domain-average cumulative surface precipitation in Fig. 3.3 (highRH simulations only). First, one notices that there is a discrepancy between the total precipitation predicted by the bulk scheme and that of the bin model.

One of the main differences in the inherent assumptions of both microphysics schemes is that the bulk scheme assumes prevents the existence of supersaturation within a gridbox after the microphysical calculations are performed. In other words, the bulk model includes a saturation adjustment

scheme that removes excess water vapor at the end of each time step to reduce the saturation ratio to 1. The bin model includes no such scheme. This difference in the underlying assumptions may force the bulk model to over-predict $q_c$ and thus the total condensed water mixing ratio ($q_t$). The use of a saturation adjustment scheme in the bulk microphysics scheme is useful for low resolution simulations in which the time step is rather large (i.e., larger than the condensational growth timescale of the cloud particles). However, in a detailed CRM, such as the one presented in the current study, the time step is likely shorter than the condensational timescale of the cloud droplets (Chuang et al., 1997), hence the gridbox will remain supersaturated at the end of the timestep. As a result, the results of the bin model ought to be more accurate given the lack of a saturation adjustment scheme within the scheme. Moreover, the difference in precipitation between the simulations performed with each model is acceptable since the overarching goal of this work is to understand how precipitation is affected by changes in the CCN number concentration and not necessarily to fully explain the differences between simulations performed with bin and bulk microphysics.

In Figs. 3.4 and 3.5, cumulative precipitation after 2 h and 4 h of simulation time, respectively, is shown for the suite of scenarios described above under high RH conditions. The two largest differences between the bulk and bin simulations are that the magnitude of the cumulative precipitation near the storm's center is substantially higher for the simulations in which bin microphysics is employed and the precipitation pattern also differs. The latter is seen by comparing, e.g., Fig. 3.5a (bulk) and b (bin) in which we find that the simulation run with bulk microphysics predicts a different trajectory for the northern branch of the system. As the cell splits, the northern cell follows a trajectory more towards due east in the bulk simulation while following a path toward the northeast in the bin simulation. The difference in storm trajectory is likely due to dynamical differences between the two systems, i.e., differences in latent heating and the inherent dynamical feedbacks. The latent heating effects will be discussed in more detail below. However, in general, these differences may be a result of using a simplified approach in a high-resolution model. In other words, as one reduces the model resolution, it should be expected that the deviation of $q_c$ and $N_c$ from some mean state should be reduced, such that the extremes (maxima) are not as large. As a re-

sult, autoconversion will then be reduced and precipitation will ultimately be reduced. Therefore, in order to accurately predict the total precipitation using a bulk microphysics model, sub-grid scale fluctuations should be considered using methods like that proposed by Morales and Nenes (2010) to calculate precisely sub-grid scale supersaturations.

Figure 3.3 shows the domain-averaged cumulative precipitation for the highRH simulations. With the discrepancy between the total amount predicted by the bin model in comparison to that of the bulk scheme aside, we focus on the effect of increased CCN number concentrations on precipitation in each model. The overall effect of a doubling of the CCN number concentration (i.e., from 100 to 200 $\mathrm{cm}^{-3}$), using the bin microphysics scheme, is to decrease precipitation by 10.9% (Table 3.2). We find that a further increase in CCN number concentration (i.e., from 200 to 500 $\mathrm{cm}^{-3}$) causes a further reduction in precipitation predicted using the bin microphysics model, contrary to that which is suggested by the theoretical arguments of Rosenfeld et al. (2008a). Here lies an additional discrepancy between the two microphysics schemes, since the effect of an increase in CCN acts to increase the precipitation predicted by the bulk model. This point will be discussed in more detail below.

In order to understand theoretically how an increase CCN number concentration acts to decrease precipitation from deep convection, we turn our attention to the dynamics of the cloud first to look at the possible invigoration or suppression of convection. We can analyze the invigoration that may result from increased aerosol loading using the buoyancy ($B$) equation (Houze, 1993):

$$B = g\left[\frac{T^\star}{T_\mathrm{a}} - \frac{p^\star}{p_\circ} + 0.61 q_\mathrm{v}^\star - q_\mathrm{t}\right] \tag{3.16}$$

where $T^\star$ is the perturbed temperature from the ambient state ($T_\mathrm{a}$), $p^\star$ is the pressure perturbation from the base state ($P_\circ$), $q_\mathrm{v}^\star$ is the deviation in the ambient water vapor mixing ratio from the reference state, and $q_\mathrm{t}$ is the total condensed water mass mixing ratio. From Eq. (3.16), we see that changes in aerosol concentration can be linked to changes in buoyancy, and consequently vertical velocity, since perturbing the CCN number concentration will lead to changes in $q_\mathrm{t}$ and $T^\star/T_\mathrm{a}$

(through latent heating). However, the effects are counteractive, since an increase in CCN number concentration will increase the number of particles that reach the freezing level, freeze, and grow via vapor deposition, thus increasing the latent heating aloft (i.e., increasing buoyancy). But, the increased heating comes in part from an increase in vapor deposition and thus acts to also increase the $q_{\mathrm{t}}$ (decreasing buoyancy). We see then that if the increase in latent heating outweighs the increase in $q_{\mathrm{t}}$ the cloud will be invigorated. While, on the other hand, if vapor deposition is at least as large as the heating influence on the ambient air, the contributions to buoyancy can be offset and thus no invigoration (or potentially even a decrease in buoyancy) can theoretically occur.

To understand how the performed simulations represent potential changes in buoyancy we show $q_{\mathrm{t}}$ in Fig. 3.6, separated into cloud (solid), rain (dashed), and ice (dotted) water contents. This allows us to analyze the effect of increased aerosol loading on rain water simultaneously. From top to bottom, Fig. 3.6 shows the evolution of the vertical structure of the deep convective cloud in which initially, cloud water is lofted deep into the mixed-phase region, and the ice exists predominantly above 5 km in the bulk simulations and higher yet in the bin simulations. As time progresses, the condensed mass sediments, ice melts to form liquid droplets that act to increase the rain water mixing ratio. As a result, we see that in the bin simulations, the rain water content is suppressed initially while the cloud water content is slightly enhanced (Fig. 3.6b, d, and f). This is a direct result of the fact that smaller particles are less likely to collide, hence reducing the amount of cloud water converted to rain drops, and since the droplets are smaller, their terminal fall speeds are reduced and can be lofted higher in the atmosphere. On the contrary, the bulk model shows a small increase in $q_{\mathrm{r}}$ below the melting level (Figs. 3.6a, c, and e) As time progresses, the peak in the vertical distribution of ice water shifts downward, hence increasing the amount of melt water below the freezing water, ultimately leading to an enhancement in the rain water content for an increase in the CCN number concentration from the bulk model. However, even after 6 h, the bin model shows that $q_{\mathrm{r}}$ is still suppressed in the cases with elevated CCN number concentrations in comparison to the "Clean" case. This prolonged suppression is discussed in detail below.

In order to describe how an increase in the CCN number concentration can alter the rain water

content by a dynamical feedback, we turn to Fig. 3.7a and b, in which the mean vertical velocity ($w$) within the convective core after 2 h of simulation time is shown for all highRH simulations. Here, we define the convective core to contain columns within which the mean vertical velocity between 3.3 km and 11 km is at least $1\,\mathrm{m\,s^{-1}}$. Any significant dynamical invigoration or suppression should appear from such an average. We see that an increase in the CCN number concentration produces a decrease in $w$ is more or less fixed for the simulations using the bulk microphysics scheme (Fig. 3.7a and b). However, the bin results show a slight enhancement in $w$ on the order of 5% to 15% within the warm sector of the cloud (i.e., below about 4 km) due to increases in the CCN number concentration. In conjunction with the fact that the cloud droplets are smaller, hence more likely to be lofted into the mixed-phase region of the cloud and freeze, thus increasing the rate of vapor deposition, this enhancement in $w$ helps increase $q_\mathrm{i}$ and consequently, $q_\mathrm{t}$ (Fig. 3.6b, d, and f).

To confirm that additional vapor deposition is the root cause for the changes in $B$ and hence, $w$, we show domain-averaged latent heating rates in Fig. 3.7c and d for the suite of simulations performed. The simulations performed with the bulk microphysics scheme (i.e., Fig. 3.7c) illustrate that the change in latent heating due to changes in CCN number concentration is quite small, regardless of the magnitude of the CCN perturbation nut negative. From Eq. (3.16) we would expect that such a small change would result in a small decrease in $w$ assuming that $q_\mathrm{t}$ were fixed and if $q_\mathrm{t}$ were to have increased, the possibility for a further decrease in $w$ exists. Since, from Fig. 3.6, we see that $q_\mathrm{t}$ increases when the CCN number concentration is elevated, the result is a decrease in $w$ (Fig. 3.7a and b). In short, the bulk model suggests a limited convective suppression due to increases in CCN number concentration, but does exhibit signs of enhanced precipitation at the surface due to increasing the condensed mass within the mixed-phase region of the cloud.

On the other hand, the latent heating rate for the simulations performed with the bin microphysics scheme elicit a different result. Here, in Fig. 3.7d we see that an increase in the CCN number concentration (solid to dashed or dotted curves) results in an increase in the latent heating and, to a lesser extent, cooling (at some levels, the changes do offset, but, for the most part, the net heating rate increases). The overall result is an increase in the net latent heating rate. This increase in

heating outweighs the negative effect on buoyancy owing to the increase in condensed liquid water in the warm sector of the cloud (Fig. 3.6) and consequently, we find an increase in $w$ (Fig. 3.7b) below 4 km. The increase in $w$ shows that the convective cloud's dynamics are enhanced at low levels. On the other hand, within the mixed-phase region of the cloud and above, there is a negligible change in $w$ (Fig. 3.7b) even though there is an increase in the net latent heating rate (Fig. 3.7d). The reason for this lies in the large increase in $q_{\rm i}$ and thus $q_{\rm t}$ within this region (Figs. 3.6b, d, and f). This increase in $q_{\rm t}$ acts to outweigh the invigoration effect of an increase in latent heating.

The following question is then suggested: why does an increase in CCN number concentration elicit a different response in precipitation in the bin microphysics simulations? And, why is the change in precipitation of a different sign for the bulk and bin microphysics simulations? As noted above, the bulk simulations produce a small change in latent heating rates (Fig. 3.7c) and consequently a slight decrease in $w$ (Fig. 3.7b). Thus, dynamically, the cloud is not invigorated and the resulting increase in precipitation arises from simply a mass balance argument, i.e., what goes up must come down (assuming that the evaporation of cloud/rain water and sublimation of ice/snow/graupel water is small). In other words, the cumulative precipitation increase results from simply adding more condensed water to the system aloft, that ultimately falls to the ground as precipitation. Conversely, we find that the bin model predicts changes to the dynamical nature (and microphysics, to be discussed below) of the convective system that provide a different response to an increase in CCN number concentration.

If we focus our attention on the bin microphysics simulations, Fig. 3.6 portrays an increase in $q_{\rm i}$, and consequently $q_{\rm t}$, for an increase in the CCN number concentration to 500 $\rm cm^{-3}$ that is over and above that which we find for the increase in CCN to 200 $\rm cm^{-3}$. Since the cloud droplets are even smaller in the "Polluted" case, even more droplets reach the freezing level at which point they freeze and grow via vapor deposition. This leads to an increase in condensed mass due to an increase in deposition. Figure 3.7d shows that the latent heating is increased above 7 km for the "Polluted" case in comparison with both the "Clean" and "Semi-Polluted" cases. If all else were equal between the "Polluted" and "Semi-Polluted" cases, we would expect to find an increase in $w$ and thus invigoration.

However, Fig. 3.7d demonstrates that the increase in warming is offset by a substantial increase in cooling above 7 km. Since the particles are smaller (the increase in number and mass is not linear), they are more readily evaporated/sublimated. Therefore, the ice particles are lofted high into the cloud, at which point they can be advected away from the core (smaller particles have a smaller terminal fall speed and thus can remain aloft for more time) and sublimate as they are detrained from the cloud top/anvil region. As a result, the increase in $q_{\rm t}$ for the increase in CCN number concentration moistens the mid- to upper-troposphere rather than increasing precipitation. In other words, as one moves towards a "Polluted" environment, the aerosol-induced effect on deep convection lies in the subtle competition between sedimentation and evaporation/sublimation timescales. Here, the latter is decreased whilst the former is increased, thus providing even more time for particles to evaporate on their way to the surface, resulting in what appears to be a positive feedback loop according to the bin simulations. In order to demonstrate the effect of reduced particles sizes on sedimentation, we use the radar reflectivity factor ($Z$) in dBZ as shown in Fig. 3.8 at 2 h into the simulations. Here, $Z$ is defined as

$$Z = 10 \log \left[ \sum_j \int_0^\infty N_j D_{\rm j}^6 dD_{\rm j} \right] \tag{3.17}$$

where $j$ denotes the different hydrometeor types. After a little algebra, we can write Eq. 3.17 as

$$Z = 10 \log \left[ \sum_j \frac{6}{\pi} \int_0^\infty \frac{\rho_j}{\rho_{\rm a}} q_{\rm j} D_{\rm j}^3 dD_{\rm j} \right] \tag{3.18}$$

where $\rho_{\rm a}$ is air density. We see that changes in $Z$ can be directly related to changes in the mixing ratios of the hydrometeors. From Figs. 3.8b, d, and f, we see that aloft, i.e., in the upper region of the convective core and within the anvil, there is nearly no change in $Z$. But, from Figs. 3.6b, d, and f, there is a consistent increase in condensed water aloft, especially in $q_{\rm i}$. Thus, if $q_{\rm i}$ increases due to increased aerosol loading, while $Z$ remains nearly fixed, the particles $D_{\rm i}$ must be smaller. Hence, the ice falls slower and the ultimate effect is to decrease the melting rate and decrease the domain-averaged cumulative precipitation.

Figure 3.8 also sheds more light on the differences between the simulated bin and bulk model results. In general the maximum $Z$ in each simulation is nearly the same. However, the region of high reflectivity in the bulk results, i.e., $Z > 30\,\mathrm{dBZ}$, is much wider (by a fact or 2 to 3). This results from precipitation from the anvil region of the storm and is likely due to the saturation adjustment assumption mentioned above. From Fig. 3.8 it also becomes clear that the swath of heavier precipitation predicted by the bulk model is relatively unchanged due to increased aerosol loading (i.e., the width of the region in which $Z > 30\,\mathrm{dBZ}$ is nearly fixed) while the bin simulations suggest otherwise. The influence of aerosol loading on rainfall intensity will be discussed in more detail below.

#### 3.6.1.2 Low relative humidity

It has been suggested that various environmental parameters, e.g., vertical wind shear (Fan et al., 2009), ambient relative humidity (Khain et al., 2008; Khain and Lynn, 2009), etc., may influence the aerosol-induced effect on deep convection. Here we extend the work of Khain et al. (2008) and Khain and Lynn (2009) by analyzing the effect on the aerosol-induced invigoration discussed above due to a small change in ambient relative humidity. It was shown previously that a reduction in the RH by 10% throughout the sounding may act to limit any invigoration, or in fact weaken the convective cloud when aerosols are added to the system. Here, we have reduced the RH by just 5% (Fig. 3.1b) to ensure that deep convection forms in all cases, and we permit the simulations to run for 12 h, in order to encapsulate the period of time in which the rain rate attains a maximum.

From Fig. 3.9, we see that like in the highRH cases, precipitation is suppressed in the bin simulations and enhanced in the bulk lowRH simulations for all aerosol perturbations. In other words, the models still disagree on the sign of the aerosol-induced effect on precipitation from deep convective clouds. It should be noted that the change in precipitation from the "Clean" to "Semi-Polluted" case is not statistically significant for $\alpha = 0.01$. Table 3.2 shows the domain-averaged cumulative precipitation at the end of the simulations and the relative changes due to increased aerosol loading. Moreover, Figs. 3.10 and 3.11 show the cumulative precipitation at 2 and 4 h into

the simulations, respectively. Comparing with Figs. 3.4 and 3.5, we see that the main result of decreasing the RH is to reduce the precipitation in the regions of intense rainfall (i.e., Figs. 3.10 and 3.11 show smaller areas in with the precipitation is greater than 70 mm for the bin model and greater than 40 for the bulk model, compared with Figs. 3.4 and 3.5).

Figure 3.12 demonstrates that the rain water content (dashed) is initially suppressed, as expected for increased CCN number concentrations for the bin microphysics simulations. As time progresses, the rain water content is always highest in the "Clean" case (black) for the bin microphysics simulations like in the highRH scenario. Since the rain water content for the "Semi-Polluted" and "Polluted" scenarios never exceeds that for the "Clean" case, it is physically not possible for the domain-averaged cumulative precipitation for the perturbed cases to exceed that of the "Clean" base case.

Following the same line of logic as for the highRH cases, to analyze the dynamical feedback that occurs when the CCN number concentration is perturbed, we show the mean vertical velocity for each polluted scenario and the changes therein due to such perturbations in Fig. 3.13. Here it is shown that $w$ tends to decrease as the CCN number concentration increases for simulations performed with both the bin and bulk microphysics schemes under relatively low RH conditions, unlike that for the highRH cases. In fact, the bulk simulations show a decrease in $w$ of 5 to 20% while the bin simulations suggest a decrease up to 15% within the cloudy part of the convective core (Fig. 3.13b). This elicits the question: Why is convection suppressed for all aerosol perturbation simulations while the precipitation response differs between the bin and bulk simulations?

The key to answering this question is to note first that the mean profile of $w$ is for that of the convective core itself. Hence, details of the changes in evaporation, sedimentation, etc., as a result of increasing the CCN number concentration may not be included in such a figure. Therefore, we show in Fig. 3.13c and d the domain-averaged latent heating profiles for the lowRH simulations. For the bulk simulations under low RH conditions, there is no significant change in latent heating due to increases in CCN number concentration. However, there is a slight increase in $q_t$, thus resulting in a decrease in $B$ and consequently, $w$, as well. Similar to that for the highRH cases, the bin

microphysics scheme predicts more significant changes in latent heating due to changes in aerosol loading. From Figs. 3.7d and 3.13d we see that although the sign of the change in heating rates for increased CCN number concentration is identical for both RH scenarios, the magnitude is not. In fact, the increase in cooling due to an increase in the CCN number concentration is more for the lowRH scenario (since lower RH implies more evaporation/sublimation) for both the "Semi-Polluted" and "Polluted" cases. In other words, evaporation/sublimation is enhanced in the bin model results for a decrease in RH as one may expect. The warming due to phase changes occurs predominantly within the convective core itself, while the cooling occurs at the cloud boundaries and below cloud (from precipitation evaporation/sublimation). It is this increase in evaporation/sublimation aloft (Fig. 3.13) that ultimately leads to a reduction in the domain averaged precipitation (Fig. 3.9) for the lowRH cases using bin microphysics. As mentioned above for bin simulations for the highRH scenario, there exists a competition between evaporation and sedimentation that ultimately controls the sign of the aerosol-induced effect on the precipitation resulting from deep convection. By reducing $q_{\mathrm{v}}$ in the lowRH scenario, we essentially reduce the total condensed water mass in the cloud itself. Hence, all else being equal, particles in the "Clean" case will be smaller under the relatively low RH conditions in comparison to that of higher RH. The same goes for the "Semi-Polluted" and "Polluted" cases. As a result, the sedimentation timescale of the particles aloft is increased while the evaporation timescale is reduced for a decrease in RH. As a result, for even the smallest increase in the CCN number concentration shown (i.e., doubling from 100 to $200\,\mathrm{cm}^{-3}$), the evaporative effect outweighs the sedimentation rate and so consequently, less condensed water is converted to rain water and thus less precipitation is observed at the surface. In fact, the increase in evaporation actually further decreases the sedimentation rate of cloud particles.

The fact that the overall effect of an increase in the CCN number concentration on the cumulative precipitation is inherently tied to the intricate balance between sedimentation and evaporation/sublimation time scales is further corroborated (as was the case for the highRH simulations) by looking at the radar reflectivity factor ($Z$, Fig. 3.14). As described above in Eq. 3.18, an increase in $q_{\mathrm{t}}$ leads to an increase in $Z$ if and only if the particles remain the same size (i.e., more numerous

particles of the same size). On the other hand, as mentioned above, an increase in $q_t$ with no increase in $Z$ signifies that the particles must be smaller, and thus sedimentation is reduced. This is precisely what the bin model simulations suggest (Figs. 3.14b, d, and f). Clearly there is no significant change in $Z$ due to increased aerosol loading while Figs. 3.6b, d, and f suggest that $q_t$ is increased. The changes in particle size are harder to determine for the bulk simulations, especially between the "Clean" and "Semi-Polluted" cases. This should be expected given the smaller relative change in precipitation for increased CCN number concentration compared with the bin model (Table 3.2).

### 3.6.2 IN effects on deep convective clouds

Here we test the sensitivity of each microphysics scheme to the IN number concentration. In order to determine the significance of modifying the ambient IN number concentration we double the number of IN predicted at the ambient temperature in each model. This may prove to be important because, as shown previously by Barahona and Nenes (2009) the number of available IN acts to control whether the predominant freezing mechanism is homogeneous or heterogenous. In other words, as the IN number concentration increases, physically the number of droplets that freeze and consequently grow via vapor diffusion should increase at warmer temperatures, thus depleting the ambient vapor surplus and limiting the number of droplets that freeze via homogeneous freezing at much colder temperatures.

Figure 3.15 illustrates the effect of an increase in the IN number concentration for both microphysics models in conjunction with an increase in the CCN number concentration for the highRH scenario (the results for a reduction in RH are qualitatively consistent with that of the highRH scenario and are thus not shown). Note that the $y$-axes are logarithmically spaced to accentuate the small differences in precipitation due to perturbing the IN number concentration. The sign of the resulting influence on the domain-averaged cumulative precipitation from an increase in IN number concentration agrees for the two microphysics models, i.e., the both models suggest that the precipitation will decrease further when the IN number concentration is increased. Table 3.3 shows the relative change in precipitation as a result of the aforementioned changes in the IN number con-

centration. We should note that the change in the domain-averaged cumulative precipitation from the "Semi-Polluted" to the "IN-Polluted" case is not statistically significant, even if we increase the significance level such that $\alpha = 0.10$.

The decrease in the domain-averaged cumulative precipitation for the simulations with bin microphysics is explained following the same line of reasoning as that which was used above for the decrease observed for an increase in the CCN number concentration in the bin model. From Fig. 3.16, both models suggest a slight increase in $q_{\mathrm{i}}$ due to an increase in the ambient IN number concentration. However, by increasing the IN number concentration, we also increase $N_{\mathrm{i}}$ such that the sizes of the ice particles are now smaller on average and consequently, the particles tend to fall more slowly. The result is a slight decrease in the domain-averaged cumulative precipitation. We see that the precipitation cannot increase beyond that of the "Semi-Polluted" case because the rain water content is always at most about equal between the two cases (Fig. 3.16).

Dynamically, the response to an increase in the IN number concentration is shown to be quite small in comparison to the changes that arise due to increasing the CCN number concentration alone (Fig. 3.17).

### 3.6.3 Cloud top height effects

To shed light on the potential impact of cloud top height in controlling the amount of precipitation that results for a perturbed deep convective cloud (Stevens and Feingold, 2009), we show the change in cloud top height in Fig. 3.18 for the "Semi-Polluted" and "Polluted" cases relative to that of the "Clean" case for both microphysical schemes. There is a rather consistent increase in cloud top height for the simulations performed using the bin microphysics scheme whereas the bulk scheme shows a change in cloud top height of less than 0.5%, up or down, for most of the simulations, regardless of the chose RH scenario. This slight increase in the cloud top height from the bin model is due to the fact that the smaller particles in the polluted cases are more likely to stay lofted and be lofted higher without a change in $w$. However, the reason for a modest change in the cloud top height, as suggested might occur by Stevens and Feingold (2009), is because the clouds in question

in this study are very deep, extending from the lifted condensation level (LCL) to the tropopause. Without a significant increase in vertical velocity near the equilibrium level, i.e., just below the tropopause, allowing moisture to punch higher into the lower stratosphere, it is very difficult to increase the height of such a cloud and hence increase the amount of condensed water mass due solely to adiabatic lifting of moist parcels.

### 3.6.4 Precipitation Intensity

Although it was shown above that the overall result of an increase in the CCN number concentration is to reduce the domain-averaged cumulative precipitation based on bin microphysics (while the bulk model suggest otherwise), this does not mean that the intensity of the rainfall also decreases. To determine the effect of increased aerosol loading on rainfall intensity, we look at the variance of the normalized cumulative precipitation. In other words, the domain-average of the cumulative precipitation is normalized and the variance of the resulting nondimensional precipitation values is computed and shown in Fig 3.19 for all simulations. The dashed lines are shown to demonstrate any potential tendency. A larger normalized variance corresponds to more intense rainfall. Since these are domain-averages, there is a slight increase from the highRH to lowRH scenario as a result of a larger area in which there is no precipitation in the drier case. However, comparing the suite of simulations performed for the highRH scenario, Fig. 3.19 suggests that there is little change in the intensity of the rainfall using the bulk scheme, while on the other hand, the bin results suggest an increase in intensity with increasing CCN number concentration. This result is corroborated in Fig. 3.8b, d, and f we see that the area of highest $Z$ ($Z > 60\,\mathrm{dBZ}$) tends to increase with increased aerosol loading, while the region of moderate $Z$ ($40\,\mathrm{dBZ} < Z < 60\,\mathrm{dBZ}$) tends to decrease. Moreover, Fig. 3.8 a, c, and e shows that there is essentially no change in the size of the area of higher $Z$ (i.e., $Z > 30$) and consequently, the trendline in $Fig.3.19$ has a slope of nearly 0.

When the RH is reduced, Fig. 3.19 suggests no change in the rainfall intensity using the bulk microphysics scheme and the change in intensity using bin microphysics appears to not be monotonic. This change is also reflected in the radar reflectivity contour plots for lowRH (Fig. 3.14). Fig. 3.14a,

c, and e shows that there is little change (as was the case for highRH) in the width of the swath of heavier precipitation (or higher reflectivity, $Z > 30$ dBZ). On the other hand, for the bin microphysics simulations, Fig. 3.14b, d show little change in the extent of the region of higher reflectivity for an increase in $N_{\rm CCN}$ from 100 to 200 $cm^{-3}$ while a further increase in the CCN number concentration reduces the size of the area of higher reflectivity (especially near the surface) but a small are of $Z > 60$ dBZ appears, giving evidence of more intense rainfall. One possible explanation for this non-monotonic effect under low RH conditions could be that a slight increase in the CCN number concentration reduces the size of the cloud particles and thus decreases the evaporation/sublimation time scale, prohibiting enhanced rainfall near the core. However, a further increase in the CCN number concentration, although also decreasing the size of the cloud particles, may also act to enhance riming due to the increase in the number of cloud particles. The enhanced riming near the core could then lead to larger particles with higher reflectivity and ultimately more intense rainfall near the center.

## 3.7 Conclusions

We have presented a high-resolution detailed CRM study (via the WRF model) of the potential effect(s) of aerosol perturbations on the development of deep convective clouds. The study incorporates two different microphysics schemes:

1. Bin Microphysics – a mixed-phase bin microphysics scheme (see Sect. 3.4.1), based on Tzivion et al. (1987, 1989), Stevens et al. (1996), and Reisin et al. (1996), coupled to WRF for very detailed microphysics calculations.

2. Modified Bulk Microphysics – the two-moment six-class bulk microphysics scheme of Morrison et al. (2005) and Morrison and Pinto (2005), modified to include a physically-based activation scheme based upon the explicit calculation of the activation of a bin-resolved aerosol population.

We test the sensitivity of the domain-averaged cumulative precipitation and potential convective invigoration as seen by changes in updraft velocity within the convective core to changes in the ambient aerosol concentration by performing simulations with an increase in the CCN number concentration, as well as a suite of cases in which both the CCN and IN number concentrations are increased. The simulated results are compared to the predictions for the base case (i.e., the "Clean" scenario). The dependence of the aerosol-induced effect on the ambient RH is also analyzed.

Under relatively moist ambient conditions, it is shown that an increase in the CCN number concentration elicits different responses from the two microphysics schemes; the bulk scheme suggests a slight increase while the bin scheme suggests a decrease in the domain-averaged cumulative precipitation. The increase in the CCN number concentration leads to an increase in $q_{\mathrm{i}}$ and consequently, $q_{\mathrm{t}}$ aloft regardless of the microphysics scheme employed. However, the relative increase is much larger for the simulations performed with bulk microphysics. This much larger increase is shown to be a result of more numerous smaller cloud particles that ultimately have a slower sedimentation velocity, leading to a reduction in the precipitation at the surface. It is suggested that the bin model ought to be superior to the bulk model for such high-resolution CRM simulations due to the difference in one key underlying assumption of the two models: the bulk model incorporates a saturation adjustment scheme (i.e., the saturation ratio is assumed to be 1 after the microphysics calculations are performed). For high-resolution simulations with short time steps, as is the case in the present study, the condensational growth timescale may be longer than the time step (Chuang et al., 1997) and thus the grid box may remain supersaturation at the end of a time step. This assumption may lead to an over-prediction of the cloud mass and thus precipitation.

It is also shown that a slight enhancement in updraft velocity occurs for increased aerosol loading using the bin microphysics scheme, while the bulk scheme suggests a slight suppression. The increase in $w$ for the bin simulations aids in keeping cloud particles lofted in the cloud and increasing the sedimentation timescale. On the other hand, the reduction in $w$ allows for the sedimentation timescale to be reduced, thus allowing the particles to reach the surface faster and increase precipitation.

Moreover, when the ambient RH is reduced, it is shown that the two microphysics models still disagree on the sign of the aerosol-induced effect(s) on precipitation; the bin model suggests a significant decrease while the bulk model suggests an increase. As was the case for increasing the CCN number concentration from the "Clean" to "Polluted" scenario under relatively high RH using the bin microphysics scheme, the competition between evaporation/sublimation and sedimentation dominates the sign of the aerosol-induced effect. Here, under dryer conditions, evaporation/sublimation occurs on even a shorter timescale and as a result dominates the sedimentation for all aerosol perturbations. Thus, a decrease in the rain water content and ultimately precipitation is observed. On the contrary, the bulk model suggests a larger decrease in $w$ for an increase in the CCN number concentration which, even though the cloud particles are smaller in the perturbed cases, allows the cloud particles to sediment at a rate at least as large as in the "Clean" case and ultimately increase precipitation.

Changes in the aerosol loading may not necessarily provide particles that act solely as CCN. Some particles are good IN, and thus it is prudent to analyze and understand any and all potential impacts of the IN population on the development of deep convective clouds and the resulting precipitation amount and pattern, at least in terms of testing the model's sensitivity to the predicted IN number concentration. The results presented herein suggest that the influence of additional IN on the domain-averaged cumulative precipitation is not statistically significant. Both models suggest a slight decrease in precipitation regardless of the RH scenario, and this is related to an increase in $N_{\mathrm{i}}$ and thus a decrease in the ice crystal sizes for an increase in the IN number concentration.

Our results demonstrate that any and all changes in the precipitation at the surface are dominated by changes in the mass of condensed water and the competition that exists between evaporation/sublimation and sedimentation and are not related to changes in cloud top height (since it is shown, especially for the simulations performed with bin microphysics, that the cloud top height increases slightly, but the precipitation decreases). For shallow convection, Stevens and Feingold (2009) hypothesized that an increase in cloud top evaporation/sublimation due to smaller particles sizes would act to moisten and cool the layer above the cloud and help to deepen the cloud itself.

Although we find an increase in evaporation/sublimation near the top of the clouds in this study, the result is not to extensively deepen the clouds since the tops are limited in their height by the tropopause. Thus, any increase/decrease in precipitation cannot come from deepening the deep convective cloud, as could be the case for a shallower convective cloud.

Lastly, we present evidence for an increase in rainfall intensity due to an increase in the CCN number concentration. Although the bulk model exhibits no trend in precipitation variance with increased aerosol loading, the bin model shows a clear increase in the precipitation variance as the CCN number concentration increases, especially in a moist environment. We relate the increase in rainfall intensity in the presence of a decrease in domain-averaged cumulative precipitation to an increase in riming within the area of significant rainfall (leading to higher reflectivity) and a decrease in precipitation in the surrounding areas due to decreased sedimentation (caused by reducing the size of the particles for an increase in the aerosol loading).

The present work could be extended to provide a more detailed description of the CCN and IN populations. Recently, work has been done to relate the number of active IN to the number of CCN particles of considerable size (DeMott et al., 2010). Incorporating this approach into the bin microphysics model would allow one to tie together increases in the CCN and IN number concentrations. Furthermore, a detailed comparison with satellite observed cloud water masses, both liquid and ice, would be beneficial in understanding both how CCN and IN particles can and do modify deep convective clouds. Ideally, an ambient vertical profile of aerosol concentration and type collocated with observations of bulk cloud properties and precipitation can build upon the current study.

## 3.8 Acknowledgements

This work was supported by the Office of Naval Research grant N00014-10-1-0200. We thank Jerry Harrington, Hugh Morrison, Adrian Hill, and Graham Feingold for helpful discussions. Computations were carried out on the CITerra Dell Cluster of the Geological and Planetary Sciences Division at Caltech.

**Table 3.1:** Assumptions regarding hydrometeor collisions.

| Collision | Result | Criterion |
|---|---|---|
| Liquid-Liquid | Liquid | |
| Ice-Ice | Snow | |
| Snow-Snow | Snow | |
| Graupel-Graupel | Graupel | |
| Ice-Snow | Snow | |
| Ice-Graupel | Graupel | |
| Ice-Liquid | Ice | $m_\mathrm{i} \geq m_\mathrm{l}$ |
| | Graupel | $m_\mathrm{i} < m_\mathrm{l}$ |
| Snow-Graupel | Graupel | |
| Snow-Liquid | Snow | $m_\mathrm{s} \geq m_\mathrm{l}$ |
| | Graupel | $m_\mathrm{s} \geq m_\mathrm{l}$ |
| Graupel-Liquid | Graupel | |

**Table 3.2:** Domain-averaged cumulative precipitation at the completion of the simulations performed, $t$=6 h.

| Micro. | RH Profile | "Clean" Precip. | "Semi-Polluted" Precip. | $\Delta$ Precip.[a] | "Polluted" Precip. | $\Delta$ Precip.[b] |
|---|---|---|---|---|---|---|
| Bin | highRH | 4.42 mm | 3.94 mm | −10.9% | 3.46 mm | −21.7% (−12.1%) |
| Bulk | highRH | 7.94 mm | 8.16 mm | 2.71% | 8.52 mm | 7.27% (4.45%) |
| Bin | lowRH | 2.39 mm | 2.25 mm | −5.74% | 2.03 mm | −14.9% (−9.74%) |
| Bulk | lowRH | 4.59 mm | 4.69 mm | 2.23% | 4.85 mm | 5.79% (3.49%) |

[a] The relative change in the domain-averaged cumulative precipitation ($\Delta$ Precip.) is computed for the "Semi-Polluted" case compared with that of the "Clean" case.
[b] $\Delta$ Precip. is computed for the "Polluted" case compared with that of the "Clean" case. $\Delta$Precip. between the "Polluted" and "Semi-Polluted" cases is given in parentheses.

**Table 3.3:** Domain-averaged cumulative precipitation at the completion of the simulations performed including potential IN effects, $t$=6 h.

| Micro. | RH Profile | "Clean" Precip. | "Semi-Polluted" Precip. | "IN-Polluted" Precip. | $\Delta$ Precip.[a] |
|---|---|---|---|---|---|
| Bin | highRH | 4.42 mm | 3.94 mm | 3.83 mm | −2.82% (−13.4%) |
| Bulk | highRH | 7.94 mm | 8.16 mm | 8.13 mm | −0.44% (2.38%) |
| Bin | lowRH | 2.39 mm | 2.25 mm | 2.17 mm | −3.67% (−9.2%) |
| Bulk | lowRH | 4.59 mm | 4.69 mm | 4.77 mm | 1.65% (3.91%) |

[a] $\Delta$ Precip. is computed for the "IN-Polluted" case compared with that of the "Semi-Polluted" case, demonstrating the impact of changes in the IN number concentration. $\Delta$ Precip. between the "IN-Polluted" and "Clean" cases is given in parentheses.

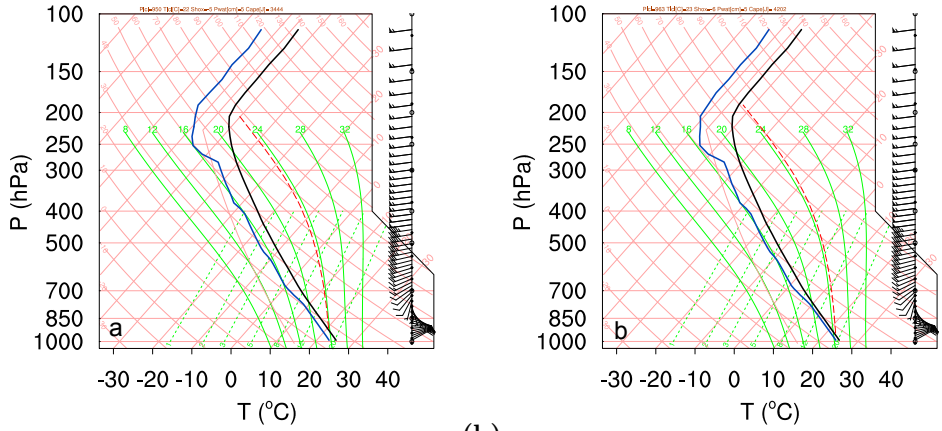


**(a)** **(b)**

**Figure 3.1:** Skew $T$-Log-$P$ diagrams of the initial temperature and moisture data for the **(a)** lowRH and **(b)** highRH simulations. The soundings are adopted from Khain and Lynn (2009) with modifications.

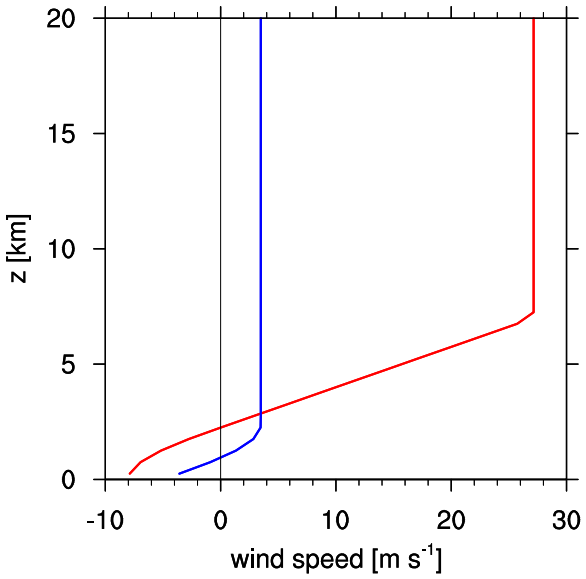


**Figure 3.2:** Quarter circle shear wind profile. The zonal wind ($u$) is in red and and the meridional wind ($v$) is in blue. The values are derived following Weisman and Klemp (1982) as modified for inclusion in WRF.

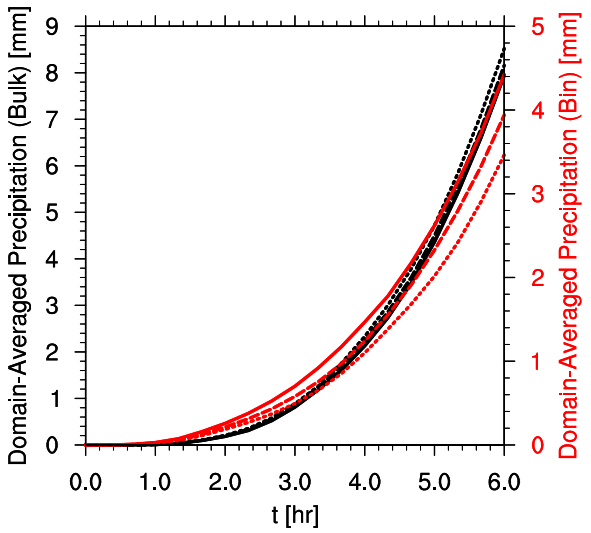


**Figure 3.3:** Domain-averaged cumulative precipitation for the highRH simulations using the bulk (black) and bin (red) microphysics models. CCN effects are shown for the "Clean" (solid), "Semi-Polluted" (dashed), and "Polluted" (dotted) scenarios.

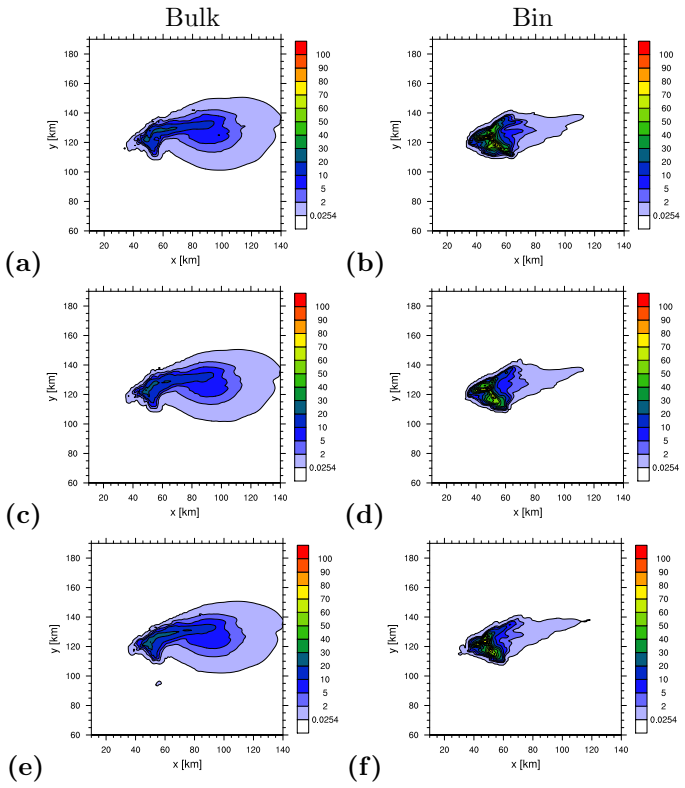


**Figure 3.4:** Cumulative precipitation after 2 h of simulation time for the (**a** and **b**) "Clean", (**c** and **d**) "Semi-Polluted", and (**e** and **f**) "Polluted" scenarios for high RH. Simulations performed with bulk microphysics are shown in **(a, c, and e)** and those with bin microphysics in **(b, d, and f)**. Note that the $x$- and $y$-axes represent the grid location index and that the portrayed region is a subset of the entire domain, chosen to elicit the largest differences amongst the set of simulations performed. The first contour level is chosen to be 0.0254 mm, which corresponds to 0.01 in. Any rainfall below this amount is considered to be a trace amount. Consequently, areas shown in white represent regions in which a trace or less of precipitation as fallen.

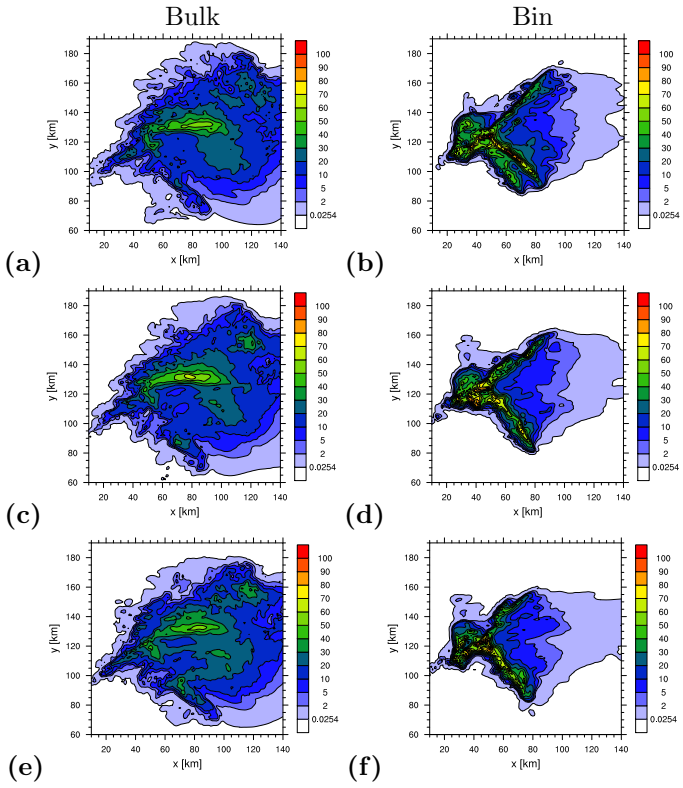


**Figure 3.5:** As in Fig. 3.4 except after 4 h of simulation time.

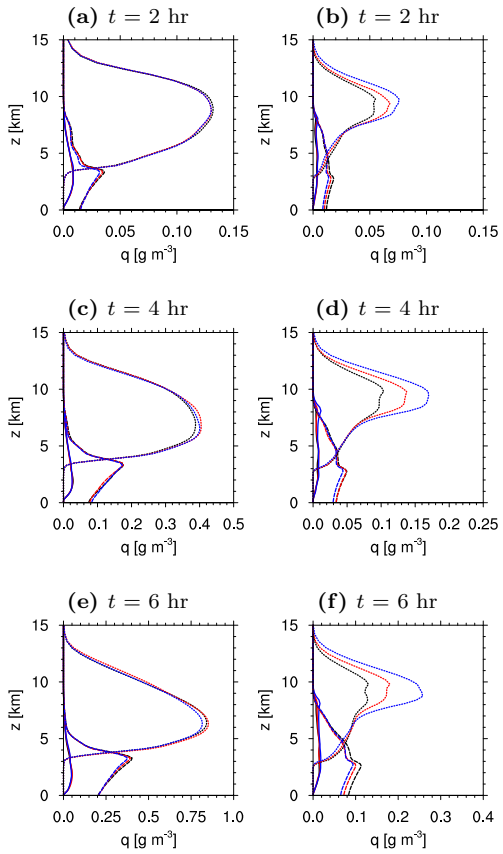


**Figure 3.6:** Hourly domain-averaged cloud (solid), rain (dashed), and ice (dotted) water contents for the bulk (left) and bin (right) simulations. The aerosol sensitivity is shown for the "Clean" (black), "Semi-Polluted" (red), and "Polluted" (blue) scenarios. Note that the $x$-axes are different in order to clearly demonstrate changes in the bulk cloud properties with time and increased aerosol loading. Simulation time is shown in the subcaptions.

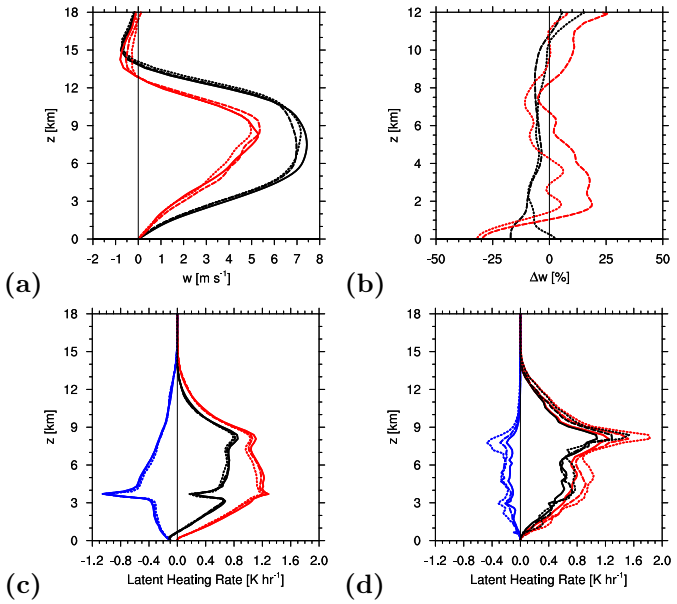


**Figure 3.7:** [Mean vertical velocity profiles within the convective core]**(a)** Average of the vertical velocity profile within the convective core and **(b)** the change in the mean vertical velocity due to changes in CCN number concentration. The convective core is defined to contain the columns in which the mean vertical velocity is more than $1\,\mathrm{m\,s^{-1}}$. Bulk (black) and bin (red) are displayed on the same graph. The differences are performed for the "Semi-Polluted" (dashed) and "Polluted" (dotted) cases relative to the "Clean" (solid) case. **(c)** and **(d)** show the latent heating rates for the bulk and bin model simulations, respectively. The net heating rate (black) is separated into warming (red) and cooling (blue). The vertical axes are different so as to highlight the differences within the cloud itself and because the relative differences at cloud top and above are much larger than those within the cloud. Simulation time is shown in the subcaptions.

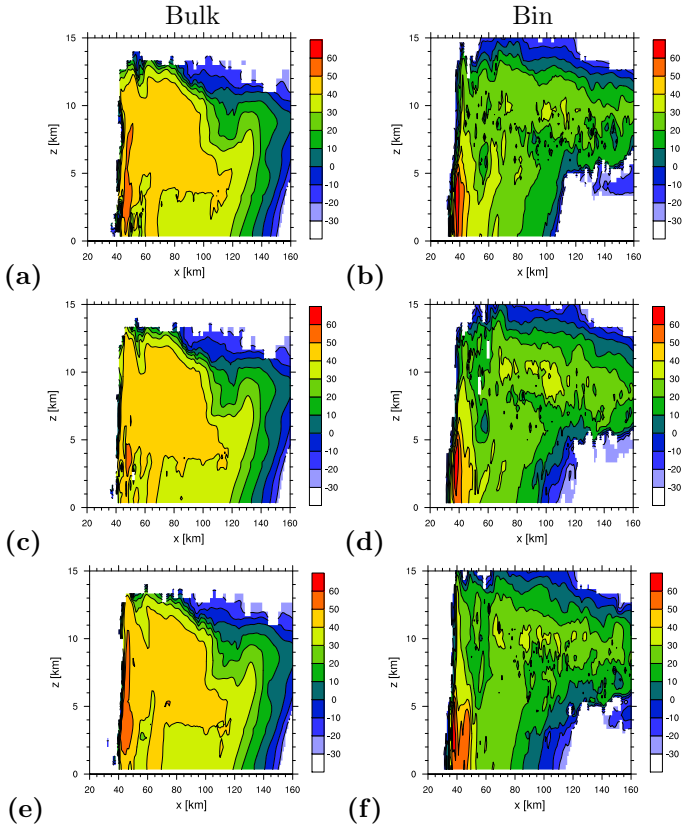


**Figure 3.8:** Zonal vertical transects of the radar reflectivity factor ($Z$) in dBZ. The transects are taken after 2 hours of simulation for $y = 125$ km. (**a**, **c**, and **e**) are for the simulations with bulk microphysics and (**b**, **d**, and **f**) are for the simulations with bin microphysics. The "Clean" (**a** and **b**), "Semi-Polluted" (**c** and **d**), and "Polluted" (**e** and **f**) cases are shown.

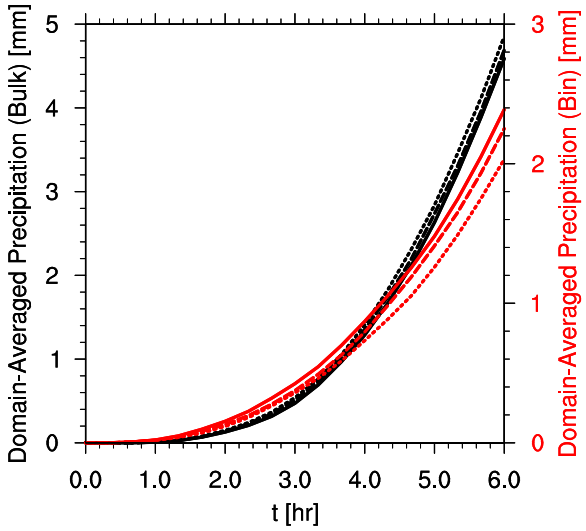


**Figure 3.9:** Same as in Fig. 3.3 except for the lowRH simulations.

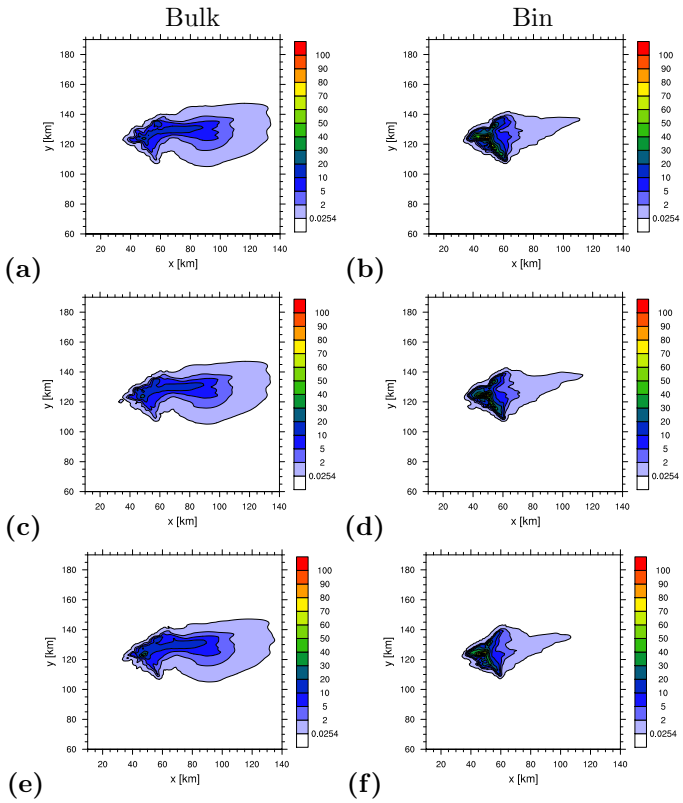


**Figure 3.10:** As in Fig. 3.4 except for the low relative humidity scenario.

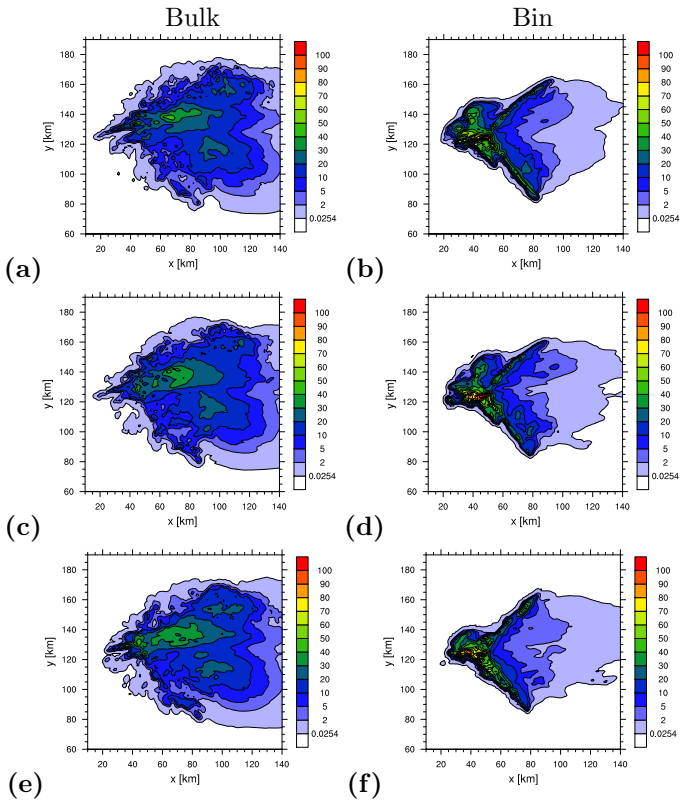


**Figure 3.11:** As in Fig. 3.10 except after 4 h of simulation time.

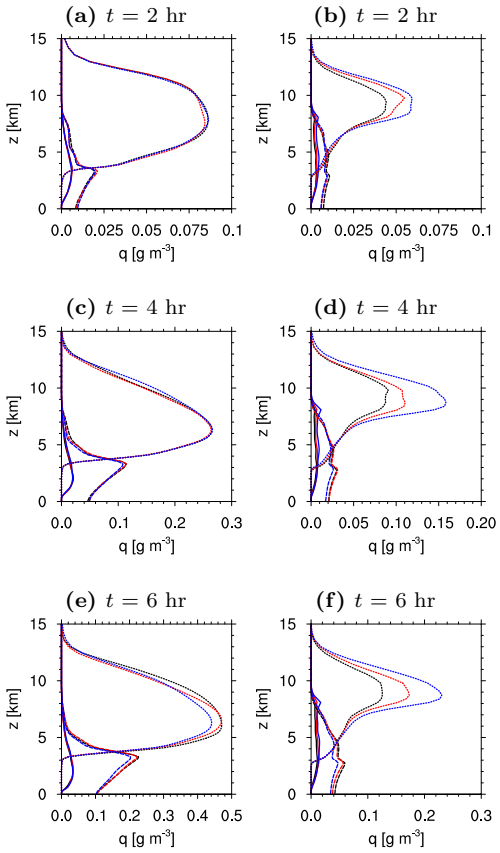


**Figure 3.12:** Same as Fig. 3.6 except for the lowRH simulations. Simulation time is shown in the subcaptions.

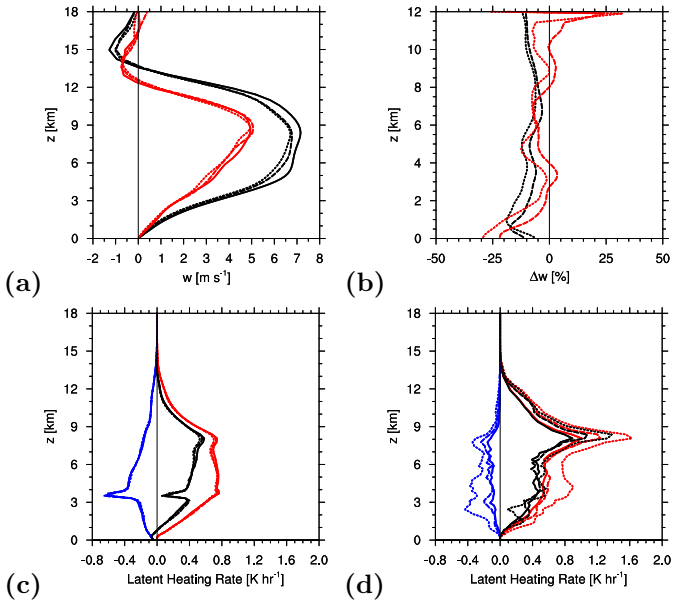


**Figure 3.13:** As in Fig. 3.7 except for the lowRH simulations.

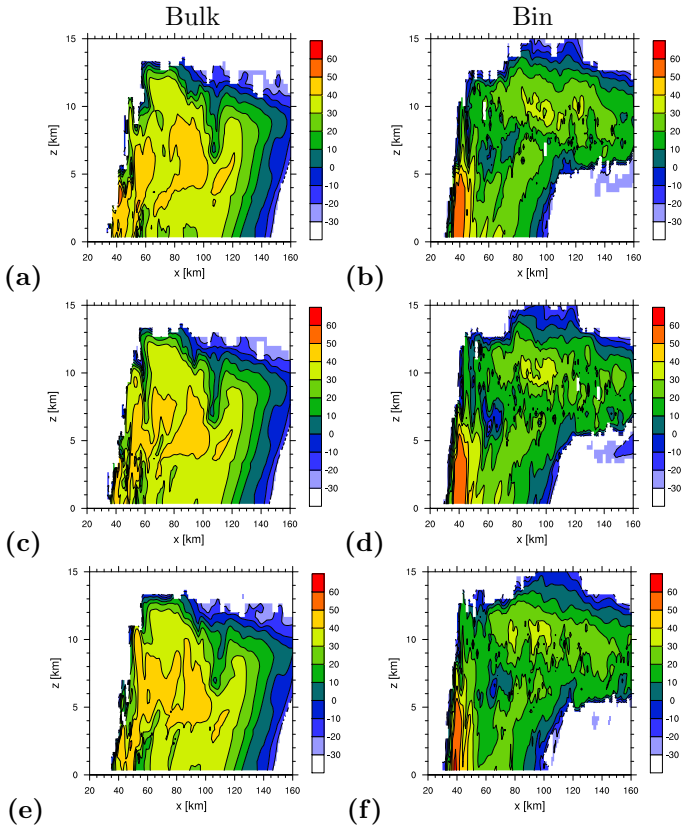


**Figure 3.14:** As in Fig. 3.8 except for the lowRH scenario

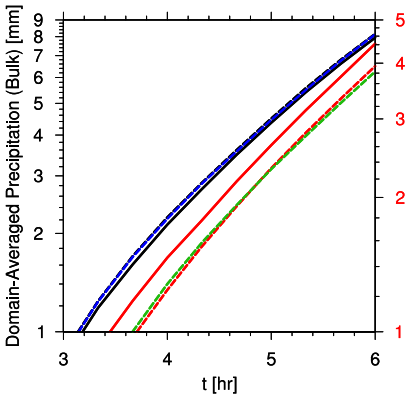


**Figure 3.15:** Domain-averaged cumulative precipitation for the highRH simulations using **(a)** bulk and **(b)** bin microphysics. CCN/IN effects are shown for the "Clean" (solid), "Semi-Polluted" (dashed), and "IN-Polluted" (dotted) scenarios. Note the difference in the $y$-axis scale between **(a)** and **(b)**. The bulk and bin results have been separated here for clarity.

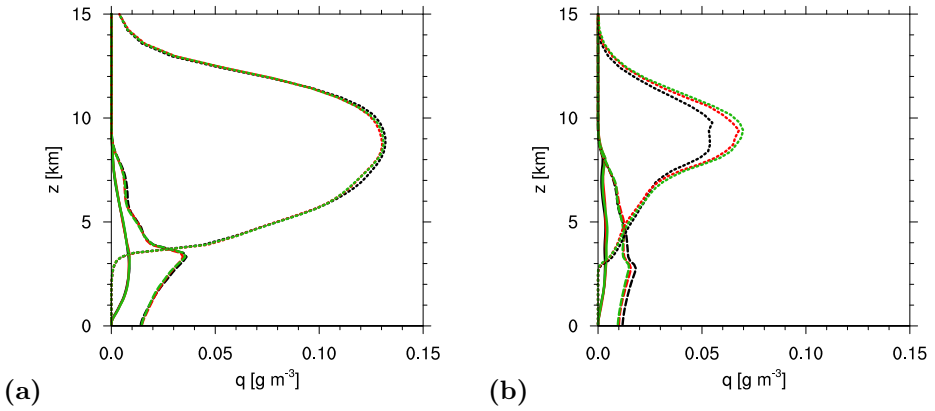


**Figure 3.16:** ]
Domain-averaged cloud (solid), rain (dashed), and ice (dotted) water contents for the bulk (left) and bin (right) simulations after 2 h of simulation time. The aerosol sensitivity is shown for the "Clean" (black), "Semi-Polluted" (red), and "IN-Polluted" (green) scenarios.

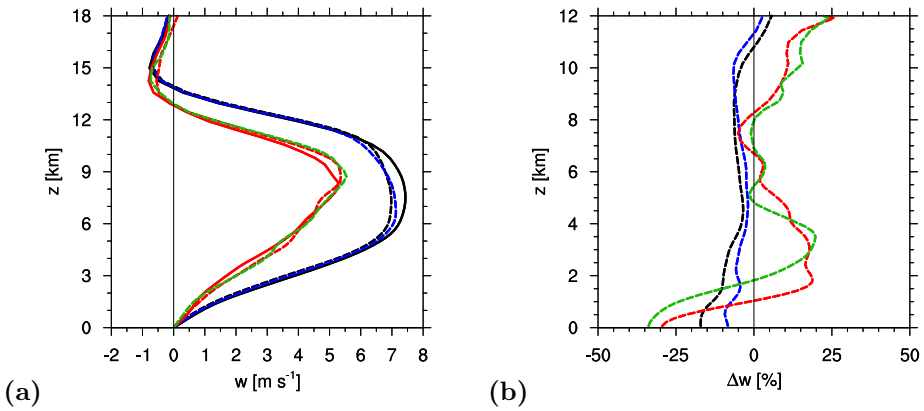


**Figure 3.17:** **(a)** Average of the vertical velocity profile within the convective core and **(b)** the change in the mean vertical velocity due to changes in CCN number concentration. The convective core is defined to contain the columns in which the mean vertical velocity is more than $1\,\mathrm{m\,s^{-1}}$. Bulk (black) and bin (red) are displayed on the same graph. The differences are performed for the "Semi-Polluted" (dashed) and "IN-Polluted" (dashed, green and blue for bin and bulk simulations, respectively) cases relative to the "Clean" (solid) case. The vertical axis is different so as to highlight the differences within the cloud itself and because the relative differences at cloud top and above are much larger than those within the cloud. Simulation time is shown in the subcaptions.

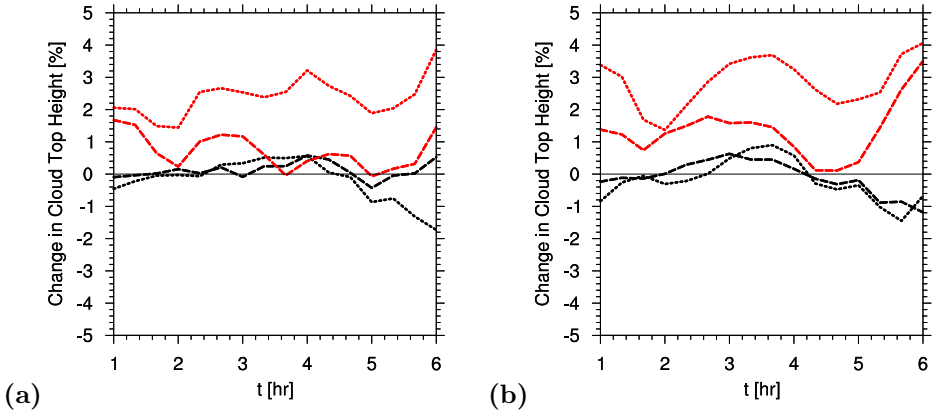


**Figure 3.18:** The change in mean cloud top height is depicted for the "Semi-Polluted" (dashed) and "Polluted" (dotted) scenarios relative to the "Clean" case using both the bulk (black) and bin (red) microphysics schemes for the **(a)** highRH and **(b)** lowRH scenarios.

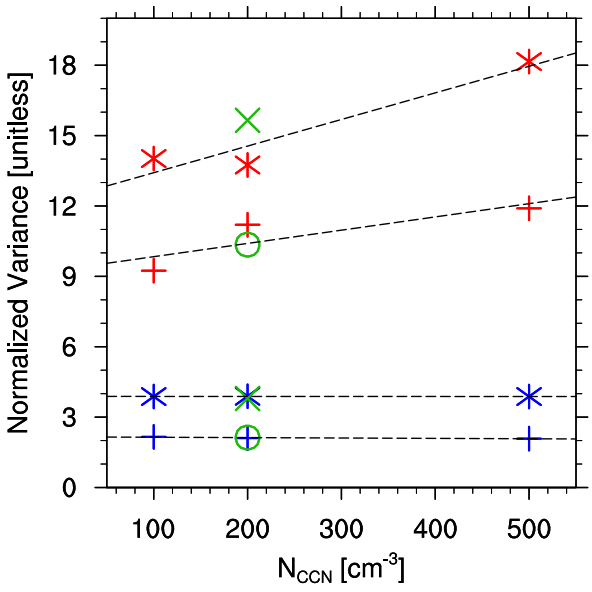


**Figure 3.19:** Variance in the normalized cumulative precipitation for all simulations shown as a function of $N_{\mathrm{CCN}}$. Both bin (red) and bulk (blue) simulations are shown. The IN sensitivity runs are also shown (green). The lowRH scenario (stars) and highRH scenarios are depicted (pluses). The dashed lines are drawn to show any potential trend in the variance with changes in aerosol loading.

## 3.9 Bibliography

Ackerman, A. S., Kirkpatrick, M. P., Stevens, D. E., and Toon, O. B.: The impact of humidity above stratiform clouds on indirect aerosol climate forcing, Nature, 432, 1014–1017, 2004.

Albrecht, B.: Aerosols, Cloud Microphysics, and Fractional Cloudiness, Science, 245, 1227–1230, doi:10.1126/science.245.4923.1227, 1989.

Andreae, M. O.: Correlation between cloud condensation nuclei concentration and aerosol optical thickness in remote and polluted regions, Atmos. Chem. Phys., 9, 543–556, 2009.

Andrejczuk, M. O., Rosenfeld, D., Artaxo, P., Costa, A. A., Frank, G. P., Longo, K. M., and Silva-Dias, M. A. F.: Smoking rain clouds over the Amazon, Science, 303, 1337–1342, 2004.

Barahona, D. and Nenes, A.: Parameterizing the competition between homogeneous and heterogeneous freezing in cirrus cloud formation - monodisperse ice nuclei, Atmos. Chem. Phys., 9, 1–13, 2009.

Bigg, E. K.: The formation of atmospheric ice crystals by the freezing of droplets, Quart. J. Roy. Meteor. Soc., 79, 510–519, 1953.

Chuang, P. Y., Charlson, R. J., and Seinfeld, J. H.: Kinetic limitations on droplet formation in clouds, Nature, 390, 94–96, 1997.

Clark, T. L.: A Study in Cloud Phase Parameterization Using The Gamma Function, J. Atmos. Sci., 31, 142–155, 1974.

Cooper, W. A.: Ice initiation in natural clouds, Meteor. Monograph, 21, 29–32, 1986.

DeMott, P. J., Sassen, K., Poellot, M. R., Baumgardner, D., Rogers, D. C., Brooks, S. D., Prenni, A. J., and Kreidenweis, S. M.: African dust aerosols as atmospheric ice nuclei, Geophys. Res. Let., 30, 1732–1735, doi:10.1029/2003GL017410, 2003.

DeMott, P. J., Prenni, A. J., Liu, X., Kreidenweis, S. M., Petters, M. D., Twohy, C. H., Richardson, M. S., Eidhammer, T., and Rogers, D. C.: Predicting Global Atmospheric Ice Nuclei

Distributions and their Impacts on Climate, Proc. Nat. Acad. Sci. USA, 107, 11 217–11 222, doi:10.1073/pnas.0910818107, 2010.

Fan, J., Yuan, T., Comstock, J. M., Ghan, S., Khain, A. ., Leung, L. R., Li, Z., Martins, V. J., and Ovchinnikov, M.: Dominant role by vertical wind shear in regulating aerosol effects on deep convective clouds, J. Geophys. Res., 114, doi:10.1029/2009JD012352, 2009.

Feingold, G., Tzivion, S., and Levin, Z.: Evolution of raindrop spectra. Part I: solution to the stochastic collection/breakup equation using the method of moments, J. Atmos. Sci., 45, 3387–3399, 1988.

Fletcher, N. H.: The Physics of Rainclouds, Cambridge University Press, 1962.

Freud, E., Rosenfeld, D., Andreae, M. O., Costa, A. A., and Artaxo, P.: Robust relations between CCN and the vertical evolution of cloud drop size distribution in deep convective clouds, Atmos. Chem. Phys., 8, 1661–1675, 2008.

Geresdi, I. and Rasmussen, R. M.: Freezing drizzle formation in stably stratified layer clouds. Part II: T role of giant nuclei and aerosol particle size distribution and solubility, J. Atmos. Sci., 62, 2037–2057, 2005.

Harrington, J. Y., Feingold, G., and Cotton, W. R.: Radiative Impacts on the Growth of a Population of Drops within Simulated Summertime Arctic Stratus, J. Atmos. Sci., 57, 766–785, 2000.

Heymsfield, A. J. and Kajikawa, M.: An Improved Approach to Calculating Terminal Velocities of Plate-like Crystals and Graupel, J. Atmos. Sci., 44, 1088–1099, 1987.

Hill, A. A., Dobbie, S., and Yin, Y.: The impact of aerosols on non-precipitating marine stratocumulus. Model description and prediction of the indirect effect, Quart. J. Roy. Meteor. Soc., 134, 1143–1154, doi:10.1002/qj.278, 2008.

Hill, A. A., Feingold, G., and Jiang, H.: The influence of entrainment and mixing assumption on aerosol-cloud interactions in marine stratocumulus, J. Atmos. Sci., 66, 1450–1464, 2009.

Houze, R. A.: Cloud Dynamics, vol. 53 of *International Geophysics Series*, Academic Press, Inc., San Diego, California, USA, 1993.

IPCC: Summary for Policymakers, in: Climate Change 2007: The Physical Science Basis. Contribution of Working Group I to the Fourth Assessment Report of the Intergovernmental Panel on Climate Change, edited by Solomon, S., Qin, D., Manning, M., Chen, Z., Marquis, M., Averyt, K. B., Tignor, M., and Miller, H. L., Cambridge University Press, 2007.

Khain, A. and Lynn, B.: Simulation of a supercell storm in clean and dirty atmosphere using weather research and forecasting model with spectral bin microphysics, J. Geophys. Res., 114, doi:10.1029/2009JD011827, 2009.

Khain, A. and Pokrovsky, A.: Simulation of effects of atmospheric aerosols on deep turbulent convective clouds using a spectral microphysics mixed-phase cumulus cloud model. Part II: sensitivity study, J. Atmos. Sci., 61, 2983–3001, 2004.

Khain, A., Ovtchinnikov, M., Pinsky, M., Pokrovsky, A., and Krugliak, H.: Notes on the state-of-the-art numerical modeling of cloud microphysics, Atmos. Res., 55, 159–224, 2000.

Khain, A., Pokrovsky, A., Pinsky, M., Seifert, A., and Phillips, V.: Simulation of effects of atmospheric aerosols on deep turbulent convective clouds using a spectral microphysics mixed-phase cumulus cloud model. Part I: Model description and possible applications, J. Atmos. Sci., 161, 2963–2982, 2004.

Khain, A., BenMoshe, N., and Pokrovsky, A.: Factors Determining the Impact of Aerosols on Surface Precipitation from Clouds: An Attempt at Classification, J. Atmos. Sci., 65, 1721–1748, 2008.

Khain, A., Rosenfeld, D., Pokrovsky, A., Blahak, U., and Ryzhkov, A.: The role of CCN in precipitation and hail in a mid-latitude storm as seen in simulation using a spectral (bin) microphysics model in a 2D dynamic frame, Atmos. Res., 99, 129–146, 2011.

Kogan, Y. L.: The simulation of a convective cloud in a 3D model with explicit microphysics. Part I: Model description and sensitivity experiments, J. Atmos. Sci., 48, 1160–1189, 1991.

Koren, I., Kaufman, Y. J., Rosenfeld, D., Remer, L. A., and Rudich, Y.: Aerosol invigoration and restructuring of Atlantic convective clouds, Geophys. Res. Let., 32, doi:10.1029/2005GL023187, 2005.

Koren, I., Remer, L. A., Altaratz, ., Martins, J. V., and Davidi, A.: Aerosol-induced changes of convective cloud anvils produce climate warming, Atmos. Chem. Phys., 10, 5001–5010, doi:10.5194/acp-10-5001-2010, 2010.

Lee, S. S.: Dependence of aerosol-precipitation interactions on humidity in a multiple-cloud system, Atmos. Chem. Phys., 11, 2179–2196, doi:10.5194/acp-11-2179-2011, 2011.

Lee, S. S. and Feingold, G.: Precipitating cloud-system response to aerosol perturbations, Geophys. Res. Let., 37, doi:10.1029/2010GL045596, 2010.

Locatelli, J. D. and Hobbs, P. V.: Fall Speeds and Masses of Solid Precipitation Particles, J. Geophys. Res., 79, 2185–2197, 1974.

Long, A. B.: Solutions to the droplet collection equation for polynomial kernels, J. Atmos. Sci., 31, 1040–1052, 1974.

Lu, M. and Seinfeld, J. H.: Effect of aerosol number concentration on cloud droplet dispersion: A large-eddy simulation study and implications for aerosol indirect forcing, J. Geophys. Res., 111, doi:10.1029/2005JD006419, 2006.

Meyers, M. P., DeMott, P. J., and Cotton, W. R.: New primary ice nucleation parameterization in an explicit model, J. Appl. Meteor., 31, 708–721, 1992.

Morales, R. and Nenes, A.: Characteristic Updrafts for Computing Distribution-Averaged Cloud Droplet Number and Stratocumulus Cloud Properties, Geophys. Res. Let., 115, doi:10.1029/2009JD013233, 2010.

Morrison, H. and Pinto, J. O.: Mesoscale Modeling of Springtime Arctic Mixed-Phase Stratiform Clouds Using a New Two-Moment Bulk Microphysics Scheme, J. Atmos. Sci., 62, 3683–3704, 2005.

Morrison, H., Curry, J. A., and Khvorostyanov, V. I.: A new double-moment microphysics parameterization for application in cloud and climate models. Part I: Description, J. Atmos. Sci., 62, 1665–1677, 2005.

Orville, H. D. and Kopp, F. J.: Numerical Simulation of the Life History of a Hailstorm, J. Atmos. Sci., 34, 1596–1618, 1977.

Phillips, V. T. J., Pokrovsky, A., and Khain, A.: The Influence of Time-Dependent Melting on the Dynamics and Precipitation Production in Maritime and Continental Storm Clouds, J. Atmos. Sci., 64, 338–359, 2007.

Pruppacher, H. R. and Klett, J. D.: Microphysics of Clouds and Precipitation, Kluwer Academic Publishers, Boston, 1997.

Reisin, T., Levin, Z., and Tzivion, S.: Rain production in convective clouds as simulated in an axisymmetric model with detailed microphysics. Part I: description of the model, J. Atmos. Sci., 53, 497–519, 1996.

Rosenfeld, D., Lohmann, U., Raga, G. B., O'Dowd, C. D., Kulmala, M., Fuzzi, S., Reissell, A., and Andreae, M. O.: Flood or Drought: How do aerosols affect precipitation?, Science, 321, 1309–1313, 2008a.

Rosenfeld, D., Woodley, W. L., Axisa, D., Freud, E., Hudson, J. G., and Givati, A.: Aircraft measurements of the impacts of pollution aerosols on clouds and precipitation over the Sierra Nevada, J. Geophys. Res., 113, doi:10.1029/2007JD009544, 2008b.

Sandu, I., Brenguier, J., Geoffroy, O., Thouron, O., and Masson, V.: Aerosol impacts on the diurnal cycle of marine stratocumulus, J. Atmos. Sci., 65, 2705–2718, 2008.

Sassen, K., DeMott, P. J., Prospero, J. M., and Poellot, M. R.: Saharan dust storms and indirect aerosol effects on clouds: CRYSTAL-FACE results, Geophys. Res. Let., 30, 1633–1736, doi:10.1029/2003GL017371, 2003.

Seifert, A., Khain, A., Pokrovsky, A., and Beheng, K.: A Comparison of Spectral Bin and Two-Moment Bulk Mixed-Phase Cloud Microphysics, Atmos. Res., 80, 146–66, 2006.

Seinfeld, J. H. and Pandis, S. N.: Atmospheric Chemistry and Physics, John Wiley and Sons, Inc., Hoboken, NJ, 2 edn., 2006.

Skamarock, W. C., Klemp, J. B., Dudhia, J., Gill, D. O., Barker, D. M., Duda, M. G., Huang, X.-Y., Wang, W., and Powers, J. G.: A description of the advanced research WRF Version 3, National Center for Atmospheric Research, Boulder, Colorado, USA, 2008.

Stevens, B. and Feingold, G.: Untangling aerosol effects on clouds and precipitation in a buffered system, Nature, 461, 607–613, doi:10.1038/nature08281, 2009.

Stevens, B., Feingold, G., Cotton, W. R., and Walko, R. L.: Elements of the Microphysical Structure of Numerically Simulated Nonprecipitating Stratocumulus, J. Atmos. Sci., 53, 980–1006, 1996.

Teller, A. and Levin, Z.: The effects of aerosols on precipitation and dimensions of subtropical clouds: a sensitivity study using a numerical cloud model, Atmos. Chem. Phys., 6, 67–80, 2006.

Twomey, S.: The nuclei of natural cloud formation Part 2: The supersaturation in natural clouds and the variation of cloud droplet concentration, P. Appl. Geo., 43, 243–249, 1959.

Twomey, S.: The Influence of Pollution on the Shortwave Albedo of Clouds, J. Atmos. Sci., 34, 1149–1152, 1977.

Tzivion, S., Feingold, G., and Levin, Z.: An Efficient Numerical Solution to the Stochastic Collection Equation, J. Atmos. Sci., 44, 3139–3149, 1987.

Tzivion, S., Feingold, G., and Levin, Z.: The Evolution of raindrop spectra. Part II: collisional collection/breakup and evaporation in a rainshaft, J. Atmos. Sci., 46, 3312–3327, 1989.

Vali, G.: Remarks on the mechanism of atmospheric ice nucleation, in: Proceedings of the Eighth International Conference on Nucleation, pp. 265–269, St. Petersburg, Russia, 1975.

Van den Heever, S. C. and Cotton, W. R.: Urban Aerosol Impacts on Downwind Convective Storms, J. Appl. Meteor. Clim., 46, 828–850, 2007.

Van den Heever, S. C., Carri, G. G., Cotton, W. R., DeMott, P. J., and Prenni, A. J.: Impacts of Nucleating Aerosol on Florida Storms. Part I: Mesoscale Simulations, J. Atmos. Sci., 63, 1752–1775, 2006.

vanZanten, M. C., Stevens, B., Vali, G., and Lenschow, D. H.: Observations of Drizzle in Nocturnal marine stratocumulus, J. Atmos. Sci., 62, 88–106, 2005.

Wang, H. and Feingold, G.: Modeling mesoscale cellular structures and drizzle in marine stratocumulus. Part I: Impact of drizzle on the formation and evolution of open cells, J. Atmos. Sci., 66, 3237–3256, 2009a.

Wang, H. and Feingold, G.: Modeling mesoscale cellular structures and drizzle in marine stratocumulus. Part II: The microphysics and dynamics of the boundary region between open and closed cells, J. Atmos. Sci., 66, 3257–3275, 2009b.

Wang, H., Feingold, G., Wood, R., and Kazil, J.: Modeling microphysical and meteorological controls on precipitation and cloud cellular structures in Southeast Pacific stratocumulus, Atmos. Chem. Phys., 10, 6347–6362, doi:10.5194/acp-10-6347-2010, 2010.

Weisman, M. L. and Klemp, J. B.: The dependence of numerically simulated convective storms on vertical wind shear and buoyancy, Mon. Wea. Rev., 110, 504–520, 1982.

Xue, H., Teller, A., Rasmussen, R., Geresdi, I., and Pan, Z.: Effects of aerosol solubility and regeneration on warm-phase orographic clouds and precipitation simulated by a detailed bin microphysics scheme, J. Atmos. Sci., 67, 3336–3354, 2010.

# Chapter 4

# Are Simulated Aerosol-Induced Effects on Deep Convective Clouds Strongly Dependent on Saturation Adjustment? *

*Submitted to *Atmos. Chem. Phys.*

## 4.1 Abstract

Three configurations of a bulk microphysics scheme in conjunction with a detailed bin scheme are implemented in the Weather Research and Forecasting (WRF) model to specifically address the role of the saturation adjustment assumption (i.e., condensing/evaporating the surplus/deficit water vapor relative to saturation in one time step) on aerosol-induced invigoration of deep convective clouds. The bulk model configurations are designed to treat cloud droplet condensation/evaporation using either saturation adjustment, as employed in most bulk models, or an explicit representation of supersaturation over a time step, as used in bin models. Results demonstrate that the use of saturation adjustment artificially enhances condensation and latent heating at low levels and limits the potential for an increase in aerosol concentration to increase buoyancy at mid to upper levels. This leads to a small weakening of the time- and domain-averaged convective mass flux (∼-3%) in polluted compared to clean conditions. In contrast, the bin model and bulk scheme with explicit prediction of supersaturation simulate an increase in latent heating aloft and the convective updraft mass flux is weakly invigorated (∼5%). The bin model also produces a large increase in domain-mean cumulative surface precipitation in polluted conditions (∼18%), while all of the bulk model configurations simulate little change in precipitation. Finally, it is shown that the cold pool weakens substantially with increased aerosol loading when saturation adjustment is applied, which acts to reduce the low-level convergence and weaken the convective dynamics. With an explicit treatment of supersaturation in the bulk and bin models there is little change in cold pool strength, so that the convective response to polluted conditions is influenced more by changes in latent heating aloft. It is concluded that the use of saturation adjustment can explain differences in the response of cold pool evolution and convective dynamics with aerosol loading simulated by the bulk and bin models, but cannot explain large differences in the response of surface precipitation between these models.

## 4.2 Introduction

Recent studies have investigated the effects of increased aerosol loading on the behavior and response of deep convective clouds (e.g., Khain et al., 2004; Khain and Pokrovsky, 2004; Khain et al., 2005; Wang, 2005; Koren et al., 2005; Grabowski, 2006; Seifert and Beheng, 2006; Teller and Levin, 2006; Van den Heever et al., 2006; Fan et al., 2007; Tao et al., 2007; Van den Heever and Cotton, 2007; Khain et al., 2008; Lee et al., 2008a,b; Rosenfeld et al., 2008; Fan et al., 2009; Khain and Lynn, 2009; Koren et al., 2010; Noppel et al., 2010; Ekman et al., 2011; Lee, 2011; Lebo and Seinfeld, 2011; Grabowski and Morrison, 2011; Seifert et al., 2012; Morrison, 2012). Changes in cloud properties resulting from aerosol loading can have potentially significant effects on the radiative forcing, precipitation patterns and amounts, and storm severity. The inherent complexity of untangling aerosol effects in a system with numerous, interacting dynamical and microphysical feedbacks is highly challenging. This is especially true in a mixed-phase convecting environment. Although the initial effect of an increase in aerosol loading may be to suppress the collision-coalescence process and thus mitigate the formation of precipitation within a warm cloud or the warm region of a mixed-phase cloud (i.e., Gunn and Phillips, 1956; Squires, 1958; Albrecht, 1989), feedbacks with the environment or changes in the microphysical process rates in other regions of the cloud may result in a negligible change in precipitation, or even potentially an increase.

Specific effects of aerosol perturbations on the strength of convection and cumulative precipitation through their impact on cloud microphysics (i.e., indirect aerosol effects) have been suggested recently from both satellite observational analyses and numerical modeling studies. Conceptually, we categorize the conclusions of these works as follows:

1. Increased Buoyancy — Rosenfeld et al. (2008) provided a conceptual model describing how an increase in aerosol number concentration can lead to a decrease in collision-coalescence and thus an increase in the mass of liquid hydrometeors that are lofted above the freezing level. There, the particles freeze and the resulting latent heating provides a positive buoyancy contribution (and hence an increase in vertical velocity). Note that an increase in condensate loading

aloft has offsetting effects on buoyancy, but under some conditions there is an invigoration, all else being equal (Rosenfeld et al., 2008). There may be either an increase or decrease in surface precipitation depending in part on factors such as environmental relative humidity (e.g., Rosenfeld et al., 2008; Khain and Lynn, 2009; Lebo and Seinfeld, 2011).

2. Cold Pool Strengthening — Lee et al. (2008a), and Lee (2011) found that an increase in aerosol loading leads to an increase in low-level convergence, resulting from an increase in evaporation and a stronger cold pool. Tao et al. (2007) showed that in polluted environments, evaporation may increase or decrease, producing a stronger or weaker cold pool depending upon the environmental conditions. On the other hand, Van den Heever and Cotton (2007) and Morrison (2012) showed that a weakening in cold pool strength arises from an increase in aerosol number concentration.

3. Cloud Deepening and Detrainment — Stevens and Feingold (2009) postulated that in polluted conditions, the cloud hydrometeors ought to be more numerous and smaller and consequently, more likely to evaporate or sublimate when detrained near cloud top. An increase in evaporation or sublimation at cloud top will moisten environmental air, allowing subsequent clouds to deepen by reducing entrainment of dry air. Changes in evaporative cooling at the lateral cloud edges associated with smaller droplets in polluted conditions can also impact cloud-scale vorticity and entrainment (e.g., Xue and Feingold, 2006). These effects have been studied primarily for shallow cumulus and cumulus congestus; their impact on deep convective clouds is potentially important but highly uncertain.

While it is convenient to categorize conceptually the different mechanisms by which an aerosol perturbation can alter the dynamics of moist deep convection, in reality, a combination of these effects is likely to occur and the importance of specific mechanisms is likely to vary from case to case (c.f., Morrison, 2012). Given this complexity, it is not surprising that simulations of the resulting changes in surface precipitation with aerosol loading are inconsistent among modeling studies (e.g., see Table 5 in Tao et al. (2007)). Van den Heever et al. (2006) demonstrated using a

three-dimensional (3-D) cloud resolving model (CRM) that an increase in cloud condensation nuclei (CCN), giant CCN (GCCN), and/or ice nuclei (IN) results in a decrease in precipitation. Similar results have been reported by Fan et al. (2009) using a 2-D CRM with bin microphysics in high wind shear environments, Lebo and Seinfeld (2011) using a 3-D CRM with bin microphysics, and Khain and Lynn (2009) using a 3-D CRM with bulk microphysics. However, these same studies, when using a different microphysics model, predicted that increased aerosol loading can lead to an increase in precipitation. For example, Lebo and Seinfeld (2011) compared the results of both bin and bulk microphysics models for an increase in aerosol number concentration and found that the bin model predicted a decrease in precipitation while the bulk model predicted the opposite. On the other hand, for increased aerosol loading, Khain and Lynn (2009) predicted an increase in precipitation using a bin microphysics scheme, and a decrease with a bulk microphysics scheme.

Previous studies have also disagreed on the potential for aerosol loading to invigorate convective dynamics. Some studies have predicted negligible changes in the strength of convection (e.g, Khain and Lynn, 2009), or a weakening, especially in high shear environments (e.g., Fan et al., 2009). Other studies have indicated a strengthening of convective drafts (e.g, Khain et al., 2005; Lebo and Seinfeld, 2011). A difficulty in comparing these studies is that different metrics were used to define changes in convective strength with aerosol loading. For example, Khain and Lynn (2009) and Fan et al. (2009) used the domain-maximum vertical velocity as a way to quantify changes in convective strength. Van den Heever et al. (2006) and Lebo and Seinfeld (2011) presented an alternative metric for invigoration, the mean updraft within the convective core, in which the convective core was defined as all columns in which the mean vertical velocity between two levels, one near cloud base and one near cloud top, exceeded 1 m $s^{-1}$. Recently, Morrison (2012) used yet another metric by analyzing changes in the domain-averaged convective mass flux. The convective mass flux was defined in this study as the mean mass flux for all grid points at a given level in which the updraft velocities exceeded 2 m $s^{-1}$, divided by the total area of the domain. Morrison (2012) showed that for a supercell storm, differences between pristine and polluted conditions in the domain-maximum vertical velocity and mean updraft within convective cores (as defined above) had considerably more

temporal variability and sensitivity to perturbed initial conditions compared to differences in the domain-averaged convective mass flux, and concluded that the convective mass flux was a more robust metric.

In terms of modification of cold pool dynamics resulting from an aerosol perturbation, Tao et al. (2007) and Lee et al. (2008a) found that low-level evaporation increased with aerosol loading and, consequently, more cooling within the cold pool was simulated. By generating a colder cold pool, the low-level convergence increased and drove stronger mesoscale convection. On the other hand, Van den Heever and Cotton (2007) and Morrison (2012) found the opposite. In these studies, the net evaporation at low levels decreased under polluted conditions, thus weakening the cold pool and reducing low-level convergence. Differences in the sign of the change in cold pool strength among these studies may be related to complex interactions between melting, raindrop mean size, sedimentation, evaporation, and environmental wind shear along cold pool boundaries. More generally, the impact of cold pool strength and low-level shear on storm dynamics is described by "RKW" theory Rotunno et al. (1988); Weisman and Rotunno (2004). According to this theory, overall storm strength can either increase or decrease depending upon the relative balance of vorticity between the cold pool circulation and the low-level environmental shear. This picture is qualitatively consistent with modeling studies that have shown changes in convective strength with aerosol loading are dependent upon relative humidity (which affects cold pool strength through rain evaporation) and environmental wind shear Khain et al. (2008); Fan et al. (2009). Nonetheless, the relationship between increased aerosol loading and cold pool strength is uncertain and more work in this area is needed.

It is also important to point out that most numerical modeling studies of aerosol-induced effects on deep convective clouds have examined the response of individual convective storms. However, Grabowski (2006), Grabowski and Morrison (2011), and Van den Heever et al. (2011) used a Convective-Radiative Quasi-Equilibrium Model to address aerosol effects on deep convection over larger spatiotemporal scales, in a system allowing feedback between numerous interacting clouds and their environment. In these studies, little to no change in domain-mean surface precipitation

occurred with increased aerosols because surface precipitation in equilibrium conditions is strongly constrained by the atmospheric radiative cooling, which was relatively unaffected by aerosols (with fixed surface conditions). Similarly, Seifert et al. (2012) found that while an increase in aerosol number concentration led to large instantaneous, local changes in precipitation, the impact was very small when averaged over larger spatiotemporal scales. They emphasized feedbacks between convection and mesoscale dynamics in explaining the much smaller response when averaged over time and space.

In short, the various numerical modeling studies cited above do not agree on the sign of the effect of an increase in aerosol number concentration on precipitation amount or convective strength. Different environmental conditions among these studies (e.g., shear, relative humidity) likely explain some of these differences (see Fig. 17 in Khain et al. (2008)). Other differences can be explained by analysis of the storm-scale response versus the larger system-wide response, as described above. Nonetheless, large differences in simulated aerosol effects have been shown using different microphysics schemes even when all other aspects of the model and case study were identical. In particular, bulk and bin microphysics schemes have produced a different sign of the response of convective dynamics and precipitation to aerosols in several studies (e.g., Li et al., 2009; Khain and Lynn, 2009; Lebo and Seinfeld, 2011; Fan et al., 2012). Thus, one must carefully examine differences between these schemes. Inherently, the algorithms and parameterizations of the various microphysical processes between bulk and bin microphysics models are different. Khain and Lynn (2009), Lebo and Seinfeld (2011) and Fan et al. (2012) suggested that a potential cause of these differences lies in the use of a saturation adjustment scheme to predict droplet condensation in bulk models, versus explicit supersaturation prediction in bin schemes. However, to our knowledge no study has systematically investigated this hypothesis. The purpose of the current study is therefore to rigorously test the idea that saturation adjustment has a large impact on the response of deep convection to aerosol loading relative to bin models that explicitly predict supersaturation.

In a saturation adjustment scheme, condensation/evaporation is predicted by simply condensing/evaporating all surplus/deficit in the water vapor mixing ratio relative to the saturation value,

i.e., the saturation ratio is adjusted to unity at the end of the time step, after all other microphysical and dynamical (e.g., mixing, advection and adiabatic warming/cooling) processes are calculated. For many applications, i.e., large grid spacing and long model time steps ($\Delta t$), the model results are not expected to be sensitive to the use of a saturation adjustment scheme for representing condensation/evaporation since for $\Delta t > \approx$1 min, the condensational timescale for cloud droplets is likely shorter than the model time step (e.g., Chuang et al., 1997). In other words, equilibrium conditions can be assumed. Thus, by the end of the time step the drops are able to take up most of the available water vapor surplus (or deficit in the case of evaporation). Moreover, large grid spacings cannot resolve convective dynamics and hence updraft speeds and ambient supersaturations are small. However, as one reduces the domain grid spacing to cloud-resolving scales, updrafts are better resolved and hence supersaturations may be relatively large, while the time step is not long enough for the droplets to take up all of the available water vapor surplus. This may be especially problematic for cloud-resolving simulations of moist deep convection, with large updraft speeds. Hence, forcing the saturation ratio to unity on short timescales can result in excess latent heating that may have potentially important effects on the simulated dynamics. Correspondingly, saturation adjustment in moist downdrafts may produce excessive evaporation and cooling. Previous studies have indicated the important role of evaporation timescale (assumed to be instantaneous using saturation adjustment) on buoyancy reversal and vorticity in shallow convective clouds (e.g., Xue and Feingold, 2006). Impacts of saturation adjustment on downdraft dynamics for moist deep convection have not yet been explored.

The saturation adjustment method also assumes that the bulk condensation/evaporation rates are independent of the droplet microphysical characteristics, whereas, physically, these rates are roughly proportional to the droplet number concentration times the mean droplet size (Pruppacher and Klett, 1997). Hence, in polluted conditions with a relative high droplet concentration in updrafts, the condensation rate for a given total droplet mass mixing ratio will be larger than that in pristine conditions with a lower droplet concentration, all else being equal. This implies differences in condensation rate and hence latent heating can occur between pristine and polluted conditions,

subsequently leading to differences in buoyancy and updraft strength. While differences in condensation between pristine and polluted conditions may be initially rather small, the positive feedback between condensation rate, latent heating, and updraft strength can enhance this effect. In other words, an initially small enhancement of latent heating in polluted relative to pristine conditions can increase buoyancy and updraft strength, leading to further increases in latent heating, buoyancy, updraft strength, and so on. This effect cannot be represented by saturation adjustment schemes.

In light of recent studies showing large differences in aerosol-cloud-precipitation interactions and invigoration of moist deep convection, specifically for supercell storms, using either bulk or bin microphysics schemes (e.g. Khain and Lynn, 2009; Lebo and Seinfeld, 2011), we examine the hypothesis that differences in the sign of aerosol effects on precipitation and convective strength between bulk and bin schemes are sensitive to the use of a saturation adjustment scheme versus explicit treatment of supersaturation. Supercells present an interesting testbed for determining the effect of aerosol perturbations on mesoscale convection for a few reasons. First, this represents a natural continuation of previous studies of aerosol effects on idealized supercell storms (e.g., Khain and Lynn, 2009; Lebo and Seinfeld, 2011; Morrison, 2012). Second, supercells are the most intense type of deep convective system in the atmosphere and are often responsible for producing large hail and spawning dangerous tornadoes (e.g., Houze, 1993). We note that the mesoscale updrafts in supercells are driven by stretching and titling of environmental vorticity in addition to buoyancy effects (Klemp, 1987), and hence may be expected to be relatively less sensitive to aerosols than other types of deep convection occurring under weaker environmental shear. Nonetheless, previous modeling studies have shown large effects of aerosols on these storms (e.g., Khain and Lynn, 2009; Lebo and Seinfeld, 2011). It is therefore important to understand this behavior and how it differs among models.

In Sect. 2 we describe the bin and bulk models utilized and the necessary modifications to the bulk model to address the potential impact of saturation adjustment on the response of a supercell to aerosol loading. Section 3 discusses the modeling framework, environmental conditions, and sensitivity configurations of test cases. The simulated results are presented in Sect. 4. A brief

discussion regarding the potential impact of the results on other cloud types and ambient conditions appears in Sect. 5 and Sect. 6 reviews the key results of the study.

## 4.3 Methods

In order to analyze potential dependencies of simulated aerosol-induced effects on deep convective clouds on model formulation we utilize, as a benchmark, a detailed bin microphysics scheme (Lebo and Seinfeld, 2011) in conjunction with a two-moment bulk microphysics model (Morrison et al., 2009) that has been modified specifically for the study. We present here the essential modifications and details required to rigorously assess the impact of saturation adjustment on the simulations.

### 4.3.1 Bin Microphysics Model

We employ the bin microphysics scheme of Lebo and Seinfeld (2011). This scheme predicts droplet activation following Köhler theory from a predefined aerosol distribution. Aerosol particles are regenerated in a one-to-one manner (in other words, for each drop that evaporates during a time step, one aerosol particle is regenerated) and added to the aerosol size bins corresponding to preset distribution parameters. For the purpose of this study, we exclude Brownian Diffusion, thermophoresis, and gravitational collection of aerosol particles, as these are not essential to the good of the work. Thus, the regenerated aerosol size distribution parameters are equivalent to those used to initially populate the domain with aerosol particles.

The new configuration of the bin microphysics scheme includes the treatment of the Hallet-Mossop rime-splintering mechanism (Hallett and Mossop, 1974). The spectral treatment of the cloud particle distributions permits the use of the following relation to predict the rate of production of splinters caused by the riming process ($P_c$) as (Pruppacher and Klett, 1997):

$$P_c = \sum_{k=1}^{36} \sum_{j=4}^{36} \frac{1}{250} \pi r_{i,k}^2 V_{i,k} K(r_{i,k}, r_{c,j}) N_{c,j} f(T_p) \tag{4.1}$$

where the subscripts $i$ and $c$ correspond to ice (here, we include snow and graupel to account for all

riming) and cloud drops, subscripts $k$ and $j$ correspond to the ice and cloud droplet bins, respectively (bin 4 of the liquid drop distribution corresponds to drops with a radius of 12.5 $\mu$m and thus only drops of this size or larger are included in the splintering calculations), $r$ is the spherical-equivalent radius of an ice particle or cloud drop, $K(r_{i,k}, r_{c,j})$ is the gravitational collection kernel for collisions between ice particles and cloud droplets, $N$ is number concentration in a given bin, and $f(T_p)$ is defined as a function of particle temperature ($T_p$) as

$$f(T_p) = \begin{cases} 0 & T_p > 270.16 \text{ K} \\ (270.16 - T_p)/2 & 270.16 \geq T_p \geq 268.16 \text{ K} \\ (T_p - 265.16)/3 & 268.16 > T_p \geq 265.16 \text{ K} \\ 0 & T_p < 265.16 \text{ K} \end{cases} \tag{4.2}$$

Equation 4.1 accounts for the observed fact that 1 splinter is produced per 250 collisions of ice particles with drops with a radius larger than 12 $\mu$m.

The representation of sedimentation within the bin model for frozen hydrometeors has been updated using the method of Mitchel (1996), in which power-law relationships are established between the Reynolds number of a falling hydrometeor and its Best (or Davies) number. This is used to determine the flow regime and the appropriate relationship between the maximum dimension of a particle and its projected area. Thus, the parameters used in computing the fall speed of frozen hydrometeors are also a function of particle size. Note that this differs from the sedimentation algorithm utilized in the bulk scheme described below since here, the parameters used in the power-law relationships are a function of particle size whereas the parameters are fixed in the bulk model (as in nearly all bulk schemes). The increased complexity of the bin microphysics model requires a more physically consistent algorithm for representing the sedimentation process.

### 4.3.2 Bulk Microphysics Model

We utilize the Morrison et al. (2009) two-moment bulk microphysics scheme in the present study with modifications to explicitly analyze the effects of the saturation adjustment scheme. In order

to include the effect of aerosols on droplet number concentration during the activation process, a binned aerosol size distribution is included in the model. The method for calculating the activation of aerosol particles and regenerating aerosols upon the evaporation of cloud drops is the same as that in the bin scheme (Lebo and Seinfeld, 2011). By representing the aerosol distribution, as well as the activation/regeneration processes, in a consistent manner between the bin and bulk schemes, we reduce the number of degrees of freedom when analyzing and comparing the results for the models. Here, we discuss the three configurations of the bulk scheme:

1. *Standard Model (bulk-original)* - In this configuration, the bulk microphysics scheme is employed as in Morrison et al. (2009) and thus includes the calculation of saturation adjustment for condensation and evaporation of cloud drops with the addition of the aforementioned activation/regeneration scheme for a binned aerosol size distribution. This is similar to the approach for activation used for the bulk microphysics scheme tested by Lebo and Seinfeld (2011). In this approach, activation of cloud droplets is predicted using the ambient supersaturation *after* advection, adiabatic expansion/cooling, and subgrid-scale mixing, but *before* saturation adjustment (following the bulk scheme of Seifert and Beheng, 2006). Note that all of the bulk schemes including bulk-original include an explicit representation of ice supersaturation and vapor deposition/sublimation. Hence, for bulk-original the saturation adjustment is only applied to condensation/evaporation of liquid cloud droplets.

2. *Supersaturation Forced Condensation/Evaporation & Activation (bulk-explicit)* - Here, the bulk model is configured *without* saturation adjustment for condensation/evaporation *and* the activation of aerosol particles. Instead, following, e.g., Clark (1973); Reisin et al. (1996); Stevens et al. (1996); Harrington et al. (2000); Morrison and Grabowski (2008); Lebo and Seinfeld (2011), we express the rate of change of the water vapor surplus ($\eta = q_v - q_{v,s}$, $q_v$ is the water vapor mixing ratio and $q_{v,s}$ is the saturation water vapor mixing ratio) as a function of time ($t$) as:

$$\frac{d\eta(t)}{dt} = D - G\eta(t) \tag{4.3}$$

where $G$ is a function of temperature ($T$), pressure ($P$), droplet mass, and number concentration, i.e., the loss (gain) of water vapor due to condensation (evaporation), and $D$ represents the dynamical forcing,

$$D = -\frac{1}{\rho}\nabla \cdot (\rho\eta) + \frac{dq_s}{dT}\frac{g}{c_p}w - q_{v,s}\frac{\rho g w}{P - e} \tag{4.4}$$

where $\frac{dq_s}{dT}$ is the psychrometric term, $g$ is the acceleration due to gravity, $c_p$ is the specific heat of air, $w$ is vertical velocity, and $e$ is the saturation vapor pressure. In Eq. 4.4, the first term on the right hand side represents the advected tendency in the water vapor surplus, the second term corresponds to changes in the water vapor surplus due to adiabatic compression/expansion, and the third term represents the effect of changes in pressure on $\eta$. As in the bin microphysics scheme (Reisin et al., 1996; Harrington et al., 2000; Lebo and Seinfeld, 2011), Eq. 4.3 is integrated analytically over the time step, and the integrated water vapor surplus is, in turn, used to explicitly calculate condensation/evaporation. Moreover, the average water vapor surplus ($\eta_a$) is used to compute droplet activation following the method used in the bin model (Lebo and Seinfeld, 2011).

3. *Supersaturation Forced Condensation/Evaporation Only (bulk-cond)* - In order to distinguish between the influence of the saturation adjustment scheme on aerosol effects caused by condensation/evaporation and activation separately, we include an additional configuration of the bulk model in which condensation/evaporation is computed following the algorithm described above using the predicted supersaturation over the course of the model time step, while activation is treated as in bulk-original by predicting the temperature and water vapor mixing ratio as if the saturation adjustment was used at the end of the previous time step. Thus, instead of using $\eta_a$ to predict the activation of aerosol particles, saturation adjustment is performed at the end of a time step, and the subsequent $T$ and $q_v$ are reserved for calculating the supersaturation following advection at the next time for the purposes of computing activation only. Thus, in this model configuration, activation is treated as in the bulk-original

model while condensation/evaporation is treated following the method used in the bulk-explicit model configuration.

## 4.4 Model Setup and Description of Test Cases

The bin and bulk microphysics models described in Sect. 4.3 are coupled to the Weather Research and Forecasting (WRF) model Version 3.3 (Skamarock et al., 2008) as a 3-dimensional CRM. The model is compressible and nonhydrostatic. The domain extends to 200 $\times$ 200 km$^2$ in the horizontal and 24 km in the vertical. The grid spacing is 1 km in the horizontal and 343 m in the vertical (i.e., 70 levels). The model time step is chosen to be 5 s to ensure numerical stability, and the duration of the simulations is 2 h. Rayleigh dampening is applied in the top 5 km of the grid, and open lateral boundary conditions are employed. For the purposes of this idealized study, we exclude radiation, surface fluxes, and Coriolis force. All scalars are advected in the horizontal and vertical using 5th and 3rd order positive-definite advection schemes, respectively.

The WRF model is initialized with a thermodynamic profile conducive to convective development, following Weisman and Klemp (1982, 1984), containing a convective available potential energy (CAPE) of 2160 J kg$^{-1}$ (Fig. 4.1). We use the quarter-circle shear wind profile of Morrison and Milbrandt (2011) and Morrison (2012). Convection is initiated using a thermal perturbation ($\theta'$) of 3 K with a height of 1.5 km and a radius of 10 km that varies as a function of the cosine of the distance from the center of the bubble. This method for initializing convection is analogous to that used in many recent studies (e.g., Fan et al., 2009; Khain and Lynn, 2009; Lebo and Seinfeld, 2011).

In order to assess the effects of an increase in aerosol loading with the bin and bulk models, we perform simulations with CCN number concentrations ($N_a$) of 100, 250, and 750 cm$^{-3}$, representing 'Clean', 'Semi-Polluted', and 'Polluted' environments. Aerosols are assumed to be ammonium sulfate and completely soluble. While the latter may be an oversimplification of the ambient aerosol chemistry, it is important to remember that the focus of this study is the effect of a physical change in the number concentration and not the effect of aerosol chemistry. The aerosols are distributed following a lognormal distribution with a geometric mean diameter ($D_g$) of 0.1 $\mu$m and a standard

deviation ($\sigma_g$) of 1.8 (Lebo and Seinfeld, 2011).

We assess the robustness of the simulated results by performing an additional set of 6 simulations by both increasing and decreasing the perturbation in the potential temperature ($\theta'$) within the bubble ($\pm 0.5\ K$), wind shear ($\pm 5\%$), and the ambient relative humidity (RH, $\pm 2\%$). The variables are only perturbed individually. It is important to note that the additional simulations serve as a test for robustness to small perturbations (following Morrison, 2012) and are not intended to study aerosol-effects on deep convective clouds occurring under significantly different environmental conditions. Details of the suite of simulations performed are summarized in Table 4.1. Owing to the extreme computational expense required to perform bin microphysics simulations with the chosen domain size and grid spacing, the perturbed simulations with the bin model are restricted to only perturbing the strength of the initial thermal bubble. Thus, we present the results from a set of 72 simulations.

## 4.5 Results and Discussion

Results of the suite of model simulations described in Table 4.1 are discussed here, focusing on various aspects of the storm response to an increase in aerosol loading. Namely, we discuss sensitivity of aerosol impacts on the cumulative precipitation, convective dynamics, and cold pool strength to use of saturation adjustment.

### 4.5.1 Precipitation Response to Increased Aerosol Loading

Figure 4.2 demonstrates the different responses to an increase in aerosol loading for each model configuration. Detailed statistics for *all* 'Clean' and 'Polluted' simulations are presented in Table 4.2. The data are shown only for these two cases since the qualitative changes between 'Clean' and 'Semi-Polluted' are similar to those between 'Clean' and 'Polluted' scenarios. On the whole, the bulk-original model predicts the least domain-average precipitation, regardless of the aerosol number concentration. All but the bulk-cond model configuration predict an increase in the domain-averaged precipitation at 120 min in polluted compared to clean conditions, although the magnitude of the

increase is much larger using the bin model compared to any of the bulk configurations. It should be noted, from Table 4.2, that the sign of the change in precipitation for the bulk-cond model configuration is not robust to the sensitivity perturbations.

From Fig. 4.2, we see that there is little difference in domain-average cumulative precipitation between the bulk-explicit and bulk-cond simulations. In other words, for this case, Fig. 4.2 suggests that the surface precipitation is insensitive to the method used to compute the supersaturation for droplet activation. This is understandable, since within the convective core the supersaturation is relatively high, such that most, if not all, aerosol particles will activate regardless of the integrated supersaturation (bulk-explicit) or the pseudo-saturation adjusted temperature and water vapor mixing ratio (bulk-cond). Changes in other quantities (convective mass flux, cold pool perturbation $\theta$) are also similar between bulk-explicit and bulk-cond, as described later.

Fig. 4.2 and Table 4.2 suggest that the precipitation response to an increase in aerosol loading is much larger using the bin microphysics model than in any of the bulk configurations. In Fig. 4.3, contour plots of the difference in cumulative precipitation ($\Delta P$, 'Polluted' minus 'Clean') show that for all bulk model configurations, there is an enhancement in precipitation in the left (north) moving storm and a shift in precipitation toward the south in the center of the storm as it splits. While the precipitation pattern does change in the right-moving storm, the differences are smaller compared to the changes in the left-moving storm. Moreover, Fig. 4.3d shows that the increase in precipitation with increased aerosol loading for the bin model (Fig. 4.2) is the result of a large increase in precipitation in the left-moving storm. The large increase, caused by more intense rainfall in this area, is reduced for the domain-wide average because the precipitation decreases in the right-moving cell. The following question then arises: Why is the precipitation much more sensitive to an aerosol perturbation in the bin model compared with the bulk model configurations?

In Fig. 4.4, evolution of the domain-averaged vertical profile of the total water mixing ratio ($q_{\mathrm{tot}}$) within the convective core is depicted for the bin (green), bulk-explicit (black), and bulk-original (red) model configurations (note that the $x$-axes are different). Here, the conditional averaging comes from dividing the sum of $q_{\mathrm{tot}}$ for all points at a given level in which $z \geq 2$ m s$^{-1}$ by the horizontal

domain area. It is important to note that by averaging in this manner, we include both the effect of an increase in the magnitude of $q_{\text{tot}}$ within the core, as well as the effect of increasing the size of the convective core on $q_{\text{tot}}$ due to an increase in aerosol loading. Changes in amount of condensate aloft are further illustrated by timeseries of the difference ('Polluted' minus 'Pristine') in domain-mean total condensed water path (vertically-integrated) in Fig. 4.5. After 30 min, both the bin and bulk-explicit models predict an increase in $q_{\text{tot}}$ for 'Polluted' compared to 'Clean' throughout most of the column while the bulk-original model predicts a decrease (Fig. 4.4). However, the increase in $q_{\text{tot}}$ using the bin model is much larger than that predicted by the bulk-explicit model. The increased condensate then precipitates out of the column and total condensed water path decreases after about 70 min for the bin model while the bulk-explicit model demonstrates a steady increase in the total water path for 'Polluted' relative to 'Clean' (Fig. 4.5). This suggests that differences in the representation of ice growth processes and sedimentation can lead to potentially significant differences in the response of surface precipitation to aerosol loading in the bulk and bin model configurations. Large differences in graupel/hail growth between the bulk and bin models are suggested by Fig. 4.6, which shows the relative change in mean graupel diameter for 'Polluted' relative to 'Clean' using the bulk-explicit, bulk-original, and bin models. Throughout most of the troposphere, a clear increase in graupel size (due to an increase in riming) is predicted, regardless of the model configuration. However, the increase, especially in the mid to upper levels of the cloud, is much larger for the simulations using bin microphysics compared with the bulk model configurations. The large increase in graupel mean size leads to an increase in graupel sedimentation, melting, and surface precipitation for the bin model, consistent with the decrease in total condensed water path in 'Polluted' relative to 'Clean' after about 40 min (Fig. 4.5). This decrease in total water path with the bin model is primarily associated with ice condensate (mainly graupel) above $\sim$6 km (Fig. 4.4). The large increase in condensate aloft in 'Polluted' compared to 'Clean' before 40 min simulated by the bin model is ultimately removed by sedimentation, explaining the increase in surface precipitation. Thus, large differences in the response of surface precipitation between the bin and bulk models appear to be related to the treatment of graupel growth and sedimentation. In contrast, the use of

saturation adjustment instead of explicit supersaturation evolution and condensation calculations has little impact on the surface precipitation response. However, as shown below, other differences in the simulated storms between the bulk and bin models are reduced by including the explicit representation of the supersaturation evolution in the bulk-explicit model configuration.

### 4.5.2 Sensitivity of Aerosol Effects on Convective Dynamics to Saturation Adjustment

Convective mass flux is analyzed for the suite of bin and bulk simulations. As mentioned above, the changes shown for 'Clean' to 'Polluted' conditions are qualitatively similar to that for 'Clean' to Semi-Polluted' conditions for all model configurations and as a result are not shown for brevity in Table 4.2 . Here, as in Morrison (2012), the horizontally-averaged convective updraft mass flux (MF($z$)) is computed as the product vertical velocity ($w$) and air density ($\rho$) for all locations in which $w \geq 2$ m s$^1$ at a given level, divided by the area of the domain. For this analysis, MF($z$) is averaged between $z = 2.1$ and 9.1 km and is shown in Fig. 4.7. In all the model configurations (bulk and bin), the magnitude of the overall change in time-averaged MF between 'Polluted' and 'Clean' is small (less than $\sim$6%). In Fig. 4.7 and Table 4.2, we see that MF increases by 5.09% and 3.50% for the bulk-explicit and bulk-cond model configurations, respectively, when averaged from 30 to 120 min. With this in mind, we restrict the discussion to only the bulk-explicit, bulk-original, and bin model configurations (qualitatively, there are only small differences for all metrics between the bulk-explicit and bulk-cond model configurations as discussed earlier). On the other hand, the change is of opposite sign for the bulk-original configuration (in which the saturation adjustment scheme is employed). Namely, the bulk-original model configuration predicts a small decrease in the vertically- and temporally-averaged MF by -3.50%. Fig. 4.7b shows that at all instances from 30 to 120 min, the bulk-original model configuration predicts a decrease in vertically-averaged MF.

Differences in MF predicted by the bulk-explicit and bulk-original model configurations are further illustrated by vertical profiles of the horizontally-averaged MF in Fig. 4.8a. Here we see that the bulk-explicit model predicts an increase of MF in 'Polluted' compared to 'Clean' throughout the

troposphere up until the end of the simulation, when there is a slight decrease at lower levels. On the other hand, Fig. 4.8c shows that the bulk-original model predicts a decrease throughout most of the column, especially at the end of the simulation when the decrease between 3 and 6 km is much larger than that predicted by the bulk-explicit model. Overall, differences in MF between 'Polluted' and 'Clean' with bulk-explicit are much closer to those simulated by the bin model, compared to bulk-original. Thus, while there are still quantitative differences between the bulk-explicit and bin simulations in terms of the response of MF to increased aerosol loading, bulk-explicit narrows most of the gap between the bulk-original and bin models, especially over the first 90 min of the simulations.

To understand why the change in MF with increased aerosol loading is different between the bulk-explicit and bulk-original model configurations, we turn our attention to buoyancy. The buoyancy ($B$) equation can be defined as (Houze, 1993):

$$B = g\left[\frac{T^\star}{T_\mathrm{a}} - \frac{p^\star}{p_\circ} + 0.61q_\mathrm{v}^\star - q_\mathrm{tot}\right] \tag{4.5}$$

where $T^\star$ is the perturbation temperature, $p^\star$ is the pressure perturbation, $q_\mathrm{v}^\star$ is the perturbation water vapor mixing ratio, and $q_\mathrm{tot}$ is the total condensed water mass mixing ratio (here 'perturbation' refers to differences in quantities from the base state). From Eq. 4.5, we see that changes in aerosol loading can be linked to changes in buoyancy (and hence updraft velocity and convective mass flux), since changing the aerosol number concentration can potentially lead to changes in the total condensate (i.e., $q_\mathrm{tot}$) and latent heating ($T^\star/T_\mathrm{a}$). As described in the Introduction, these effects counteract since, for example, an increase in condensation will act to increase the latent heating and thus increase $B$, while the corresponding increase in $q_\mathrm{tot}$ will decrease $B$. This balance within deep convective systems can potentially affect the sign of the change in MF due to increased aerosol loading.

In Figs. 4.9a-i, latent heating rates at 60, 90, and 120 min are shown (first, second, and third columns, respectively). Remarkably, many of the signatures from the bin model in Figs. 4.9a-c are also present in the bulk-explicit simulations (Figs. 4.9d-f). In contrast, we see from Figs. 4.9g-i that

there are differences in the latent heating rates at all times predicted by the bulk-explicit and bulk-original models. These changes are depicted in Fig. 4.11, in which the differences in the heating rates (bulk-explicit minus bulk-original) are shown. Independent of the chosen time, Figs. 4.9g-i demonstrates that the bulk-original model predicts a higher latent heating rate relative to the bulk-explicit model simulations between about 3 and 9 km above the surface (as seen by the increase in latent heating relative to the bulk-explicit simulations, or a negative value for the changes shown). According to Eq. 4.5, this implies that the buoyancy, and consequently updraft mass flux, should be higher in the bulk-original model compared to the other model configurations. Consistent with this picture, MF is generally higher using the bulk-original model compared to bulk-explicit, for a given aerosol loading (Fig. 4.7).

If we focus our attention on the region between about 3 and 9 km in Figs. 4.9b,e, and h, we see that the bulk-explicit and bin models predict slight increases in latent heating for 'Polluted' relative to 'Clean' (positive buoyancy contribution, see Eq. 4.5). This is further demonstrated in Fig. 4.10 as an average over the time period from 30 to 120 min. On the other hand, the bulk-original model predicts a decrease in heating (negative buoyancy contribution). At lower cloud altitudes, the saturation adjustment scheme produces the largest differences in the heating response between 'Polluted' and 'Clean' compared to that simulated by bulk-explicit (Figs. 4.10a and b), i.e., the sign of the change in latent heating between 'Polluted' and 'Clean' is different between the two models. The increase in heating aloft in 'Polluted' predicted by the bulk-explicit and bin models is consistent with the increase in buoyancy and invigorated convection. However, it is important to note that there is an inherent challenge in untangling the cause and effect relationship between updraft strength (i.e., buoyancy) and latent heating. In other words, an increase in latent heating and hence buoyancy can increase updraft strength, but an increase in updraft strength can in turn increase condensation rate and latent heating. Despite this uncertainty, the bulk-original and bulk-explicit configurations allow us to unambiguously attribute changes in the response of heating and convective mass flux to the use of saturation adjustment versus explicit treatment of supersaturation.

Next, we examine differences in the latent heating and cooling rates predicted between the

models in more detail (Fig. 4.11). A positive (negative) value for heating (red) implies that the bulk-explicit model predicts more (less) condensation/deposition/freezing/riming than the bulk-original model. For cooling (blue), a negative (positive) value implies that the bulk-explicit model predicts more (less) evaporation/sublimation/melting than the bulk-original model configuration. The difference in latent heating and cooling rates between the bulk model configurations for a given aerosol concentration is *larger* than the sensitivity to aerosols for a given model (compare Fig. 4.11 with Fig. 4.10). In order for the aerosol effect to be identical between the model configurations, differences between the predicted latent heating rates of each model need to be the same for all aerosol number concentrations. In other words, in Fig. 4.11, the dashed and solid curves should coincide. However, Fig. 4.11 reveals that the bulk-original model predicts more heating and cooling due to latent heating throughout most of the column and over the duration of the simulation compared to bulk-explicit, but the differences are much larger for 'Clean' relative to 'Polluted' (compare the red solid and dashed curves).

We analyze next the change in horizontally-average $q_{\rm tot}$ (including only points within convective updrafts) in the context of impacts on convective dynamics. In Fig. 4.4, we see that for most of the column below 9 km, bulk-original and bulk-explicit predict a decrease in $q_{\rm tot}$ with increased aerosol loading (positive buoyancy contribution). The bin model predicts a larger decrease aloft and an increase at lower levels compared with the bulk model configurations, likely due to differences in ice growth and sedimentation as discussed earlier. However, there is not a clear relationship between changes in condensate between 'Polluted' and 'Clean' (fig:vproftot) and changes in MF (Fig. 4.8). Thus, differences in condensate loading do not appear to be a primary driver of changes in convective strength between 'Polluted' and 'Clean' in these simulations.

With the addition of an explicit representation of supersaturation in the bulk-explicit model configuration, we are able to directly compare the predicted supersaturation fields between the bulk-explicit and bin models. Since the bulk-original model adjusts the supersaturation to 0% at the end of every time step, no points in the domain have supersaturation (with respect to liquid water) following calculation of the microphysical process rates. Thus, in Fig. 4.12 both the probability

distribution function (PDF) and mean supersaturation as a function of $t$ are plotted for only the bulk-explicit and bin model configuration. Note that only positive values are shown and that all points between $z = 2.1$ and 9.1 km and $t$ =30 and 120 min are used in computing the PDFs. The large supersaturations seen in Fig. 4.12 are a result of large updraft velocities; these values are physical and confirmed by parcel model simulations (not shown). The PDFs portrayed in Fig. 4.12a show that for both the bulk-explicit and bin models, except at small supersaturations (i.e., $< 2\%$), there is a consistent reduction in the PDF from 'Clean' (solid) to 'Polluted' (dashed) conditions. Fig. 4.12 is consistent with previously discussed results regarding latent heating and invigoration since the decrease in the supersaturation PDF in 'Polluted' compared to 'Pristine' corresponds to an increase in condensation and consequently an increase in latent heating aloft (Fig. 4.9). Fig. 4.12b shows that the magnitude of the mean supersaturation differs between the bin and bulk-explicit model configurations, but the magnitude of the change from an increase in aerosol number concentration is quite similar. The bulk-original model cannot represent these changes in the supersaturation field resulting from increased aerosol loading, which limits its ability to predict the small invigoration simulated by the bulk-explicit and bin models (Fig. 4.7).

### 4.5.3 Cold Pool Characteristics

Much of the discussion in the literature on the potential for increased aerosol loading to result in convective invigoration has focused on changes in latent heating aloft (for a detailed conceptual overview, see Rosenfeld et al., 2008; Lebo and Seinfeld, 2011). However, increased aerosol number concentration can also lead to changes in the melting and evaporation below cloud, and thus cold pool strength. Interactions between cold pools and dynamics for supercell storms related to changes in microphysical process rates have been described in numerous recent studies (e.g., Van den Heever and Cotton, 2004; Milbrandt and Yau, 2006; Dawson II et al., 2010; James and Markowski, 2010; Morrison and Milbrandt, 2011). Tao et al. (2007) and Morrison (2012) discussed how changes in droplet number concentration caused by an increase in aerosol number concentration can lead to changes in the strength of cold pools and thus alter the convective dynamics. Morrison (2012) noted

that when the change in the simulated mean cold pool perturbation temperature ($\Delta\theta'$, 'Polluted' minus 'Clean') was at least 0.2 K (meaning a stronger cold pool in the 'Clean' aerosol scenario) there was a decrease in the convective mass flux with an increase in aerosol loading. However, when $\Delta\theta'$ was less than 0.2 K, the convective mass flux either increased or had a small decrease. Here, as in Morrison (2012), $\Delta\theta'$ is defined as the difference in the conditionally-averaged surface $\theta'$ ('Polluted' minus 'Clean"). The averaging is performed only within the cold pool, i.e., within the region confined by the -2 K perturbation in the potential temperature field at the lowest model level. Results here are similar to Morrison (2012) as seen in Table 4.2. For the bulk-original model configuration, a small weakening (-3.5%) of the average convective mass flux occurs in 'Polluted' relative to 'Clean' in conjunction with a substantial weakening in the strength of the cold pool ($\Delta\theta' = 0.467$ K), for the baseline initial conditions. On the other hand, the bulk-explicit and bin model configurations predict a much smaller weakening of the cold pool strength (0.175 and 0.068K, respectively) and a small increase in the convective mass flux (5.09 and 4.73%, respectively).

In Fig. 4.13, interactions near the cold pool edge of the left-moving storm at 90 min are shown. Here, the extent of the cold pool is shown by the dashed line (demarcated by the area in which $\theta' <$ -2 K), streamlines show the flow pattern and areas of convergence/divergence at the surface, dotted contours represent the updraft velocity at 1.5 km (starting at 2 m s$^{-1}$ and increasing by 2 m s$^{-1}$), and the shaded contours depict the vertical velocity at 9.1 km. For the bulk-original model configuration, Fig. 4.13 shows that the area of low-level convergence is elongated and the resulting low-level vertical velocities are higher in the 'Clean' scenario compared to 'Polluted', consistent with Morrison (2012). A stronger cold pool in the 'Clean' case, driving greater low-level convergence and flow of high equivalent potential temperature air into the storm along outflow boundaries, is consistent with weak invigoration of the convective mass flux at mid- and upper-levels compared to 'Polluted'. On the other hand, the explicit-bulk and bin model configurations depict a different situation in which there is little change in the extent of the low-level convergence zone near the cold pool boundary owing to limited change in cold pool strength (Table 4.2). Consequently, in the 'Polluted' scenario compared to 'Clean' for the bulk-explicit and bin model configurations (Figs. 4.13a, b, e, f), the

change in the low-level vertical velocity is quite small and it is the change in latent heat release aloft that helps drive the weak invigoration of convection (see discussion in Section 4.2).

Overall, these results suggest that there is more than a single pathway by which increasing the aerosol number concentration changes the overall convective dynamics, consistent with the discussion in Morrison (2012). It was suggested earlier that the bulk-explicit and bin microphysics models predict an increase in latent heating due to more deposition, condensation, freezing, and riming aloft when the aerosol number concentration is elevated. All else being equal, this leads to an increase in buoyancy and invigoration of the system. On the other hand, an increase in aerosol loading acts to weaken the cold pool (Table 4.2) which results in less low-level convergence and supply of high equivalent potential temperature air into the storm at the cold pool boundary, and hence a weakening of the convective mass flux. However, in the simulations using the bulk-explicit and bin model configurations, the small weakening in the cold pool strength appears to be more than offset by the increase in heating and buoyancy aloft. These results illustrate the importance of analyzing the system as a whole and not focusing on a single pathway by which the strength of the system can be altered in a polluted environment.

### 4.5.4 Robustness of Simulated Aerosol Effects

In order to investigate the robustness of the simulated results presented herein, we performed a suite of sensitivity experiments in which the initial perturbation in the potential temperature ($\theta'$) within the bubble ($\pm 0.5\ K$), environmental wind shear ($\pm 5\%$), and the ambient relative humidity (RH, $\pm 2\%$) are systematically increased or decreased. The combination of initial perturbations, chosen one at a time, provide a set of 6 sensitivity simulations for each aerosol scenario and model configuration. While previous works have focused on the sensitivity of aerosol effects on deep convective storms to changes in wind shear and relative humidity (Fan et al., 2009; Khain and Lynn, 2009; Lebo and Seinfeld, 2011), the purpose here is to address the robustness of the models' results to small perturbations and not to discern the effect of aerosol in different environmental conditions. For a complete review of such scenarios, see Khain et al. (2008). Data for the suite of simulations

performed are presented in Table 4.2. For the sensitivity scenarios, the data are presented such that the top value corresponds to the low perturbation (i.e., lower maximum $\theta'$, lower shear, and lower RH) and the bottom value corresponds to the high perturbation (i.e., higher maximum $\theta'$, higher shear, and higher RH).

While there are quantitative differences with perturbed initial conditions in the response of cumulative surface precipitation, average convective mass flux, and cold pool strength to an increase in aerosol loading for a given model configuration, the broader conclusions are robust. In particular, key differences among the model configurations are similar with perturbed initial conditions, namely, greater weakening of cold pool strength in bulk-original compared to bulk-explicit and bin, and a weakening of average convective mass flux in bulk-original but an invigoration in bulk-explicit and bin. Furthermore, the much larger surface precipitation response to aerosols simulated by the bin model compared to all of the bulk model configurations is robust.

Nonetheless, in some cases there is a change in the sign of the storm response to aerosols when the magnitude of the response is small. For example, the bulk-explicit and bulk-cond model configurations shift between small increases and decreases in precipitation for the suite of initial perturbation simulations performed (Table 4.2). Interestingly, although the sign of the change in precipitation, $\Delta P$, differs between some of the sensitivity experiments, the spread is comparable for all model configurations (4.19%, 3.55%, 3.58%, and 6.1% for the bulk-explicit, bulk-cond, bulk-original, and bin models, respectively). For the average convective mass flux, the bulk-explicit and bulk-cond model configurations predict a change from 'Clean' to 'Polluted' of between 1.61% and 5.09% across all sensitivity simulations. Similarly, the bin model predicts an increase between 4.73% and 6.43%, while the bulk-original model simulates a decrease that ranges from -1.75% to -3.64%. We note that the spread of results with perturbed initial conditions for a given model configuration is roughly comparable to previous studies investigating sensitivity aerosol effects on deep convection to model formulations (e.g., Ekman et al., 2011), and therefore may obscure analysis of such sensitivity. Thus, similar to Morrison (2012), we emphasize the importance of ensemble analysis when quantifying and generalizing aerosol effects on deep convection.

## 4.6 Saturation Adjustment Applicability

We have demonstrated the sensitivity of simulated aerosol effects on a supercell storm to the use of a saturation adjustment scheme. It was shown that saturation adjustment in the bulk-original model leads to a small weakening of the average convective mass flux. In contrast, using an explicit calculation of the supersaturation evolution in the bulk-explicit, bulk-cond, and bin models leads to a small invigoration. To further illustrate errors that occur from the use of saturation adjustment, we refer to Fig. 4.14. This diagram qualitatively depicts the supersaturation evolution in a steadily-rising parcel using a relatively short time step and either saturation adjustment (red curve) or explicit treatment of supersaturation (black curve). In Fig. 4.14, the vertical dashed lines correspond to the start and end of each time step. Following ascent of the parcel from left to right in the diagram, the supersaturation initially rises as a result of adiabatic expansion and thus cooling. As droplets activate and grow, the supersaturation continues to increase until enough droplets activate and/or grow large enough that the condensation rate exceeds the rate of supersaturation production due to upward motion. Then, the supersaturation decreases and eventually moves toward an equilibrium state, which occurs when the loss of supersaturation from condensation is balanced by the rate of supersaturation production from upward motion.

In contrast to the explicit supersaturation (black curve), supersaturation is reduced to zero at the first time step using saturation adjustment (red curve), thus condensing all of the water vapor surplus. Because the supersaturation relaxation timescale is longer than the model time step at this stage, condensation (and consequently latent heating) is overpredicted. As the parcel moves upward from cloud base (i.e., moving from left to right in Fig. 4.14), the supersaturation begins to decrease and hence saturation adjustment leads to an underprediction of condensation, until equilibrium is achieved. In general, if the explicit supersaturation increases during the time step, saturation adjustment leads to overprediction of the condensation rate. If the explicit supersaturation decreases during the time step, saturation adjustment leads to an underprediction. In exact equilibrium (i.e., no change in explicit supersaturation during the time step), there is no error in the condensation rate produced by saturation adjustment.

Whether or not there is a net overprediction of condensation and latent heating over the depth of the cloud using saturation adjustment depends upon the equilibrium value of the explicit supersaturation. The net error increases with larger values of equilibrium supersaturation; if the equilibrium supersaturation is zero then there is no net error in the condensation rate using saturation adjustment, although there may still be errors in the vertical distributions of condensation and heating. All else being equal, equilibrium supersaturation will be higher for stronger updrafts and lower droplet concentrations. Thus, net error will be greatest using saturation adjustment applied to strong updrafts in clean conditions, and smaller in weak updrafts or polluted conditions. This dependence on aerosol loading implies a different magnitude of error in the response of the condensation rate and hence latent heating to polluted and pristine conditions using saturation adjustment. This is consistent with differences in the response of the average convective mass flux using the bulk-original model with saturation adjustment compared to bulk-explicit or bin.

Note that there are complications to this general picture. In updrafts that substantially increase in intensity with height, as is generally the case for moist deep convection, supersaturation may increase with height even in the cloud interior well above cloud base. This effect will exacerbate the net overprediction of condensation rate and latent heating using saturation adjustment. Moreover, droplet concentration can decrease with height in the cloud due to collision-coalescence, increasing the supersaturation relaxation timescale. In the absence of additional droplet activation, this can lead to large values of supersaturation inside the cloud (Clark (1973)), which again increases errors in the net condensation rate and heating over the depth of the cloud using saturation adjustment.

We note that a similar situation occurs for moist downdrafts. If the supersaturation (evaporation) timescale is short compared to the model time step, conditions are near equilibrium and saturation adjustment is a good approximation. However, in non-equilibrium conditions, such as in an accelerating downdraft, saturation adjustment may produce noticeable error in the evaporation rates and hence latent cooling.

To briefly summarize, saturation adjustment produces errors in strongly non-equilibrium conditions, when the supersaturation relaxation timescale is much longer than the model time step. This

occurs near cloud base, especially in strong updrafts, and in the cloud interior when convective updrafts increase in intensity with height or when droplet number concentration is reduced as a result of collision-coalescence. On the other hand, saturation adjustment is a good approximation in other circumstances. In models with a relatively large grid spacing and long time step or in environments with weak vertical motion, supersaturation will be closer to equilibrium through most of the depth of the cloud and hence errors in the vertical distribution of condensation/evaporation rate using saturation adjustment will be small. Moreover, equilibrium supersaturation will be close to zero in weak updrafts, implying little error in net condensation over the depth of the cloud. To depict this scenario, we replicate Fig. 4.14 in Fig. 4.15, except for a much longer time step. Even though the condensational growth process is nonlinear (Fig. 4.15, solid black), the resulting saturation ratios at the end of the time step for both the saturation adjustment scheme and explicit prediction of supersaturation are nearly the same. Hence, there is little error in the condensation rate over the time step using saturation adjustment in this instance. However, we note that even though there may limited error in the condensation rate using saturation adjustment in this situation, large errors can occur in the peak supersaturation (near cloud base) and hence droplet number concentration in models that explicitly predict droplet activation as a function of supersaturation. Without performing detailed simulations using the microphysics models presented herein applied to other cases, this discussion serves to provide a conceptual view of the applicability of saturation adjustment in models. Detailed analysis of situations for which saturation adjustment is expected to produce little error is beyond the scope of this paper.

## 4.7 Conclusions

Previous studies of aerosol effects on convective development and cumulative precipitation have hypothesized that results using bin and bulk microphysics models do not agree because of the use of a saturation adjustment scheme, which is commonly employed in bulk microphysics models (e.g., Khain and Lynn, 2009; Lebo and Seinfeld, 2011; Fan et al., 2012). To quantitatively address this issue, we employ a high-resolution CRM to study the effects of increased aerosol loading on a

supercell storm using four microphysics model configurations:

1. Bin Model — All hydrometeors are represented using binned distributions following Lebo and Seinfeld (2011). Supersaturation is predicted explicitly over the course of a time step by accounting for dynamical tendencies, adiabatic cooling, and condensational growth.

2. Bulk-explicit Model — The two-moment bulk microphysics scheme of Morrison et al. (2009) is used without a saturation adjustment scheme. An algorithm, analogous to that used in the bin model, is used to more accurately predict the supersaturation over a time step for both droplet condensational growth and activation.

3. Bulk-Cond Model — The two-moment bulk microphysics scheme of Morrison et al. (2009) is used without a saturation adjustment scheme and droplet condensation is calculated from the explicit supersaturation as in the bulk-explicit and bin models. A pseudo-saturation adjustment scheme is employed, in which at the end of the microphysics routine, dummy variables for temperature and water vapor mixing ratio are saved and used to predict the supersaturation on the subsequent time step, after advection, for activation only.

4. Bulk-original Model — The two-moment bulk microphysics scheme of Morrison et al. (2009) is used with a saturation adjustment scheme applied to both droplet condensational growth and activation.

The results presented herein demonstrate, as suggested previously (e.g., Rosenfeld et al., 2008; Khain et al., 2008; Lebo and Seinfeld, 2011), the ability of an increase in the ambient aerosol number concentration to invigorate (or weaken) convection. The key results are summarized as follows:

1. The cumulative precipitation predicted using the bin model had the largest sensitivity to an increase in aerosol loading (17.5%) while the change predicted by the bulk model configurations was quite small ($\sim \pm 2.5\%$). It was shown that the bin model predicts a larger increase in ice growth and hence graupel mean size in polluted compared to pristine conditions relative to the bulk model configurations, ultimately leading to a greater increase in rain water production and surface precipitation.

2. Simulations with the bulk-explicit and bulk-cond model configurations exhibited little difference in the convective mass flux, precipitation, and cold pool strength, owing to the fact that for deep convective clouds with strong updrafts and high supersaturations, the activation of new droplets is insensitive to the method by which the supersaturation is calculated (i.e., nearly all of the aerosol population activates regardless of the method used to calculate supersaturation).

3. The bulk-explicit and bin models predicted a small but robust invigoration, as shown by an increase in the time- and domain-averaged convective mass flux of 2.52 to 5.09 and 4.73 to 6.43%, respectively, while the bulk-original model configuration predicted a small decrease of -1.75 to -3.65%. The invigoration predicted by the bulk-explicit and bin models was related to an increase in latent heating aloft with an increase in aerosol loading. The bulk-original model did not predict such an increase, and instead predicted more latent heating for the 'Clean' aerosol scenario.

4. Simulated cold pool strength (as measured by the average lowest level perturbation $\theta$ within the cold pool) was shown to weaken under higher aerosol loading. The weakening was greatest for the original-bulk model configuration (6.52 to 13.1%). The bulk-explicit and bin models predicted a much smaller weakening (0.87 to 9.35% and -2.36 to 3.90%, respectively), and so the response of the convective dynamics to increased aerosol loading was associated more with increased latent heating and buoyancy aloft than changes in the cold pool.

Figures 4.11 and 4.14 show qualitatively and quantitatively, respectively, the effect of saturation adjustment on the supersaturation evolution and thus condensation rate and latent heating. Model simulations (Fig. 4.11) show that the bulk-original model predicts more latent heating relative to the bulk-explicit model, especially below about 9 km. In order for the aerosol effect on convective strength to be the same between the two model configurations, the differences in latent heating between the models for each aerosol scenario ought to be the same. However, the differences are shown to be quite large (much more heating in the bulk-original model in the 'Clean' case compared

to 'Polluted'). This is consistent with differences in the response of the convective dynamics between bulk-original and bulk-explicit, bulk-cond, or bin. The bulk-original model overpredicts condensation (and hence latent heating) by forcing the saturation ratio to unity at the end of each time step in non-equilibrium conditions when the supersaturation should be increasing (as shown schematically in Fig. 4.14). Here, the model time step is shorter than the condensation time scale such that the grid box remains supersaturated at the end of the time step using the explicit treatment of supersaturation, unlike that which is predicted using the saturation adjustment scheme. This overprediction is consistent with large differences in the heating rates predicted by the bulk-original and bulk-explicit model configurations. Moreover, saturation adjustment schemes cannot capture changes in supersaturation, condensation, and latent heating resulting directly from differences in droplet concentration and size and hence the efficiency of vapor uptake between polluted and clean conditions. Overall, these differences in the models' physics explain much of the difference in the response of the convective dynamics between the bulk-original and bin models. However, the use of a saturation adjustment scheme cannot explain large differences in the response of surface precipitation to aerosol loading between the bin and bulk schemes. Results suggest that differing treatments of sedimentation, ice particle growth, or other microphysical factors contributed to these differences. A more detailed analysis of possible reasons for differences in the response of surface precipitation between the bulk and bin models is left for future work.

## 4.8 Acknowledgements

This work was supported by the Office of Naval Research grant N00014-10-1-0200. Computations were carried out on the CITerra cluster of the Geological and Planetary Sciences Division at Caltech. HM acknowledges partial support from NOAA grant NA08OAR4310543, U.S. DOE ARM DE-FG02-08ER64574, and the NSF Science and Technology Center for Multiscale Modeling of Atmospheric Processes (CMMAP), managed by Colorado State University under cooperative agreement ATM-0425247.

**Table 4.1:** Simulation descriptions.

| Category | Name | Description |
|---|---|---|
| Microphysics Scheme | Explicit | Bulk microphysics model incorporating an explicit representation of the supersaturation evolution within a time step, including effects on both condensation/evaporation and activation |
| | Cond | Bulk microphysics model incorporating an explicit representation of the evolution of the supersaturation within a time step, including effects on only condensation/evaporation. Activation is computed using the saturation adjusted temperature and water vapor mixing ratios. |
| | Original | Bulk microphysics model with saturation adjustment |
| | Bin | Bin microphysics model |
| Sensitivities | Base | Control case (i.e., no perturbations) |
| | delT25 | Maximum $\theta'$ in the thermal bubble reduced to 2.5 K |
| | delT35 | Maximum $\theta'$ in the thermal bubble increased to 3.5 K |
| | lowshear | Vertical wind shear increased by 5% in the lowest 7.5 km |
| | highshear | Vertical wind shear decreased by 5% in the lowest 7.5 km |
| | lowRH | RH reduced by 2% |
| | highRH | RH increased by 2% |
| Pollution | Clean | $N_a = 100$ cm$^{-3}$ |
| | Semi-Polluted | $N_a = 250$ cm$^{-3}$ |
| | Polluted | $N_a = 750$ cm$^{-3}$ |

**Table 4.2:** Summary of results for the suite of model configurations described in Table 4.1. The change in precipitation ($\Delta P$), convective mass flux ($\Delta MF$), and average potential temperature within the cold pool ($\Delta\theta'$) are shown for 'Polluted' minus 'Clean' conditions. Statistics for $\Delta MF$ are computed by averaging between $t = 30$ and 120 min and between $z = 2.1$ and 9.1 km. For $\Delta\theta'$ and $\Delta P$ the results are shown only for $t = 120$ min. The percent change relative to the 'Clean' case is shown in parentheses. Within each column, the top values correspond to the low perturbation sensitivity simulations while the bottom values correspond to the high perturbation simulations (i.e., the delT25 run is above the delT35 run, etc.).

| Model Configuration | $\Delta P$ [0.01 mm] | | | | $\Delta MF$ [0.001 kg m$^{-2}$ s$^{-1}$] | | | | $\Delta\theta'$ [0.1 K] | | | |
|---|---|---|---|---|---|---|---|---|---|---|---|---|
| | Base | delT | shear | RH | Base | delT | shear | RH | Base | delT | shear | RH |
| Bulk-Explicit | 1.21 (0.93) | 2.44 (1.17)<br>-1.62 (-1.18) | -1.86 (-1.50)<br>2.51 (1.85) | 1.40 (1.20)<br>-3.56 (-2.34) | 6.31 (5.09) | 3.75 (3.18)<br>4.96 (3.80) | 3.05 (2.52)<br>6.13 (4.74) | 4.47 (4.06)<br>4.79 (3.40) | 1.75 (5.20) | 0.82 (2.44)<br>2.71 (8.16) | 3.17 (9.35)<br>0.29 (0.87) | 2.05 (6.35)<br>1.39 (4.02) |
| Bulk-Cond | -0.53 (-0.41) | 1.63 (1.34)<br>-1.46 (-1.06) | -2.42 (-1.95)<br>0.51 (0.38) | -1.14 (-1.00)<br>-3.33 (-2.21) | 4.50 (3.50) | 3.55 (2.99)<br>3.56 (2.70) | 2.69 (2.22)<br>6.42 (4.94) | 3.50 (3.14)<br>2.30 (1.61) | 2.76 (8.25) | -0.71 (-2.16)<br>2.23 (6.70) | 3.62 (10.8)<br>1.07 (3.26) | 3.61 (11.1)<br>2.21 (6.35) |
| Bulk-Original | 2.77 (2.50) | 1.59 (1.52)<br>3.25 (2.81) | 1.74 (1.65)<br>2.25 (1.92) | 3.67 (3.71)<br>0.17 (0.13) | -4.93 (-3.50) | -4.25 (-3.17)<br>-3.93 (-2.73) | -4.86 (-3.62)<br>-2.60 (-1.75) | -2.40 (-1.90)<br>-5.72 (-3.64) | 4.67 (12.0) | 2.46 (6.54)<br>4.28 (10.9) | 4.30 (10.0)<br>2.43 (6.52) | 3.33 (9.13)<br>5.38 (13.1) |
| Bin | 22.2 (17.5) | 28.9 (23.6)<br>22.5 (16.8) | -<br>- | -<br>- | 5.50 (4.73) | 7.04 (6.43)<br>6.51 (5.40) | -<br>- | -<br>- | 0.68 (1.98) | -0.79 (-2.36)<br>1.2 (3.90) | -<br>- | -<br>- |

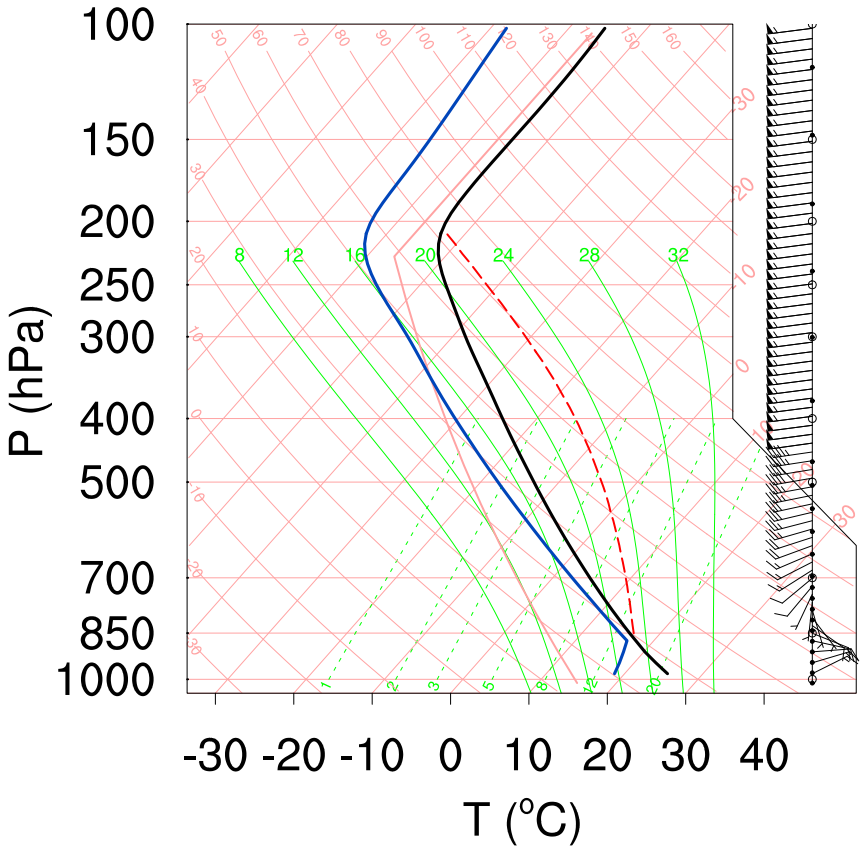


**Figure 4.1:** Skew-T log-P diagram for the simulations with baseline initial conditions. Temperature ($T$, black) and dew point temperature ($T_d$, blue) are shown.

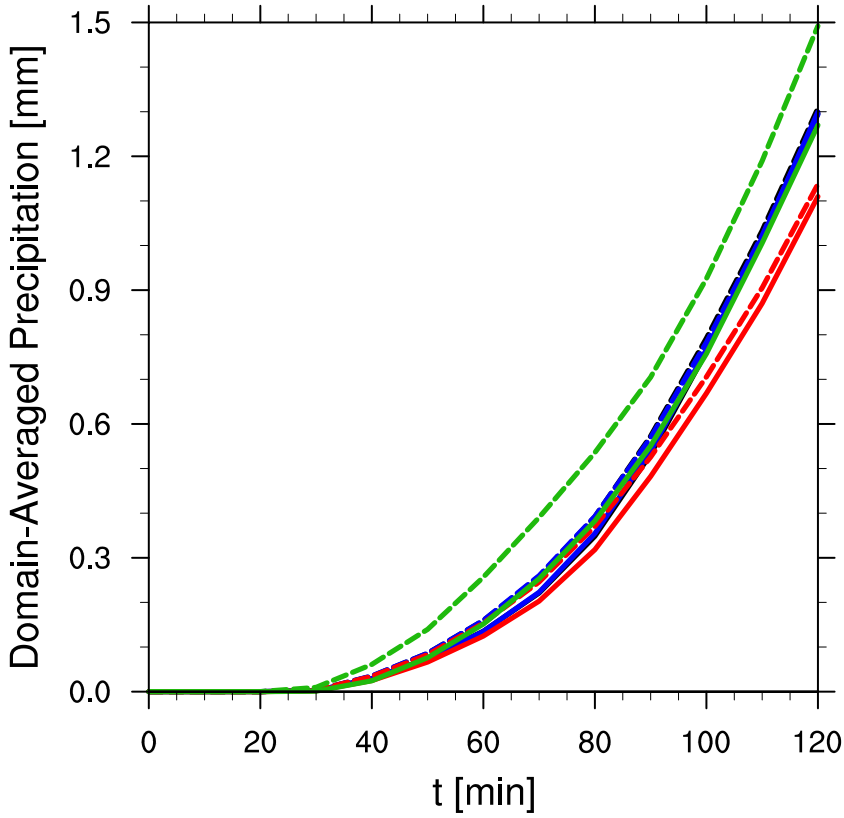


**Figure 4.2:** Domain-average cumulative precipitation. Depicted here are the 'Clean' (solid) and 'Polluted' (dashed) aerosol scenarios for simulations using the baseline initial conditions. All four model configurations are presented, i.e., bin (green), bulk-explicit (black), bulk-cond (blue), and bulk-original (red).

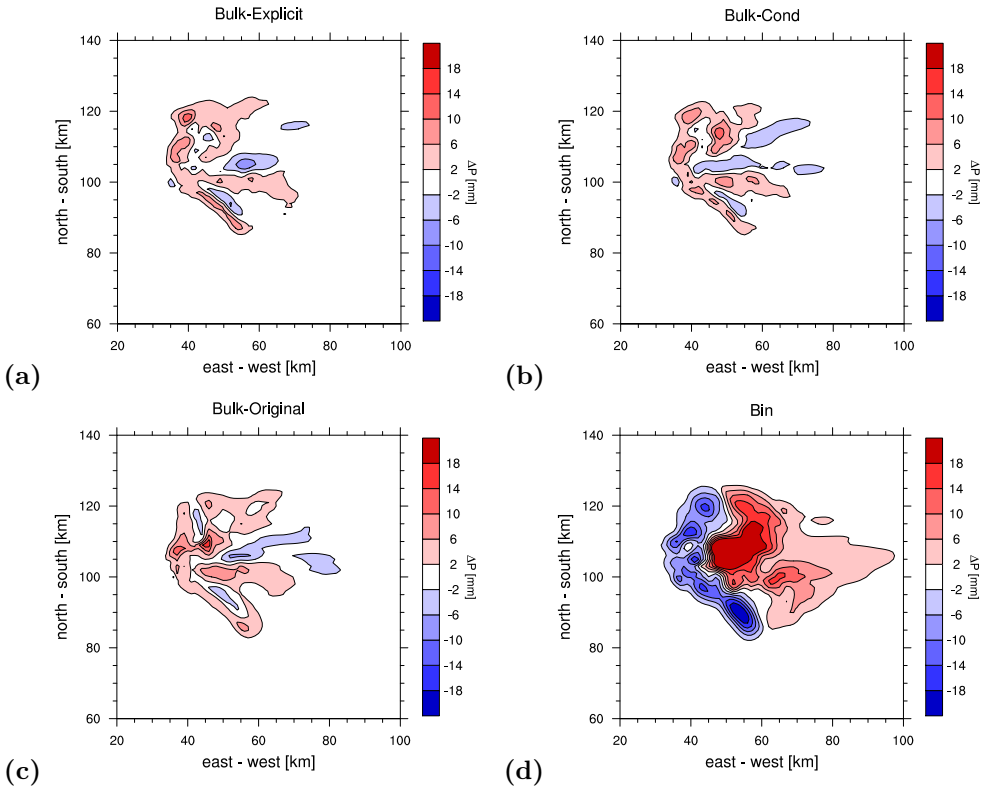


**Figure 4.3:** Contour plots of the change in cumulative precipitation ($\Delta P$, 'Polluted' minus 'Clean') at 90 min for all model configurations and baseline initial conditions. Precipitation is given in mm. Note that only the portion of the domain in which precipitation has accumulated is shown. Here, red implies an increase in precipitation with increased aerosol loading and blue a decrease.

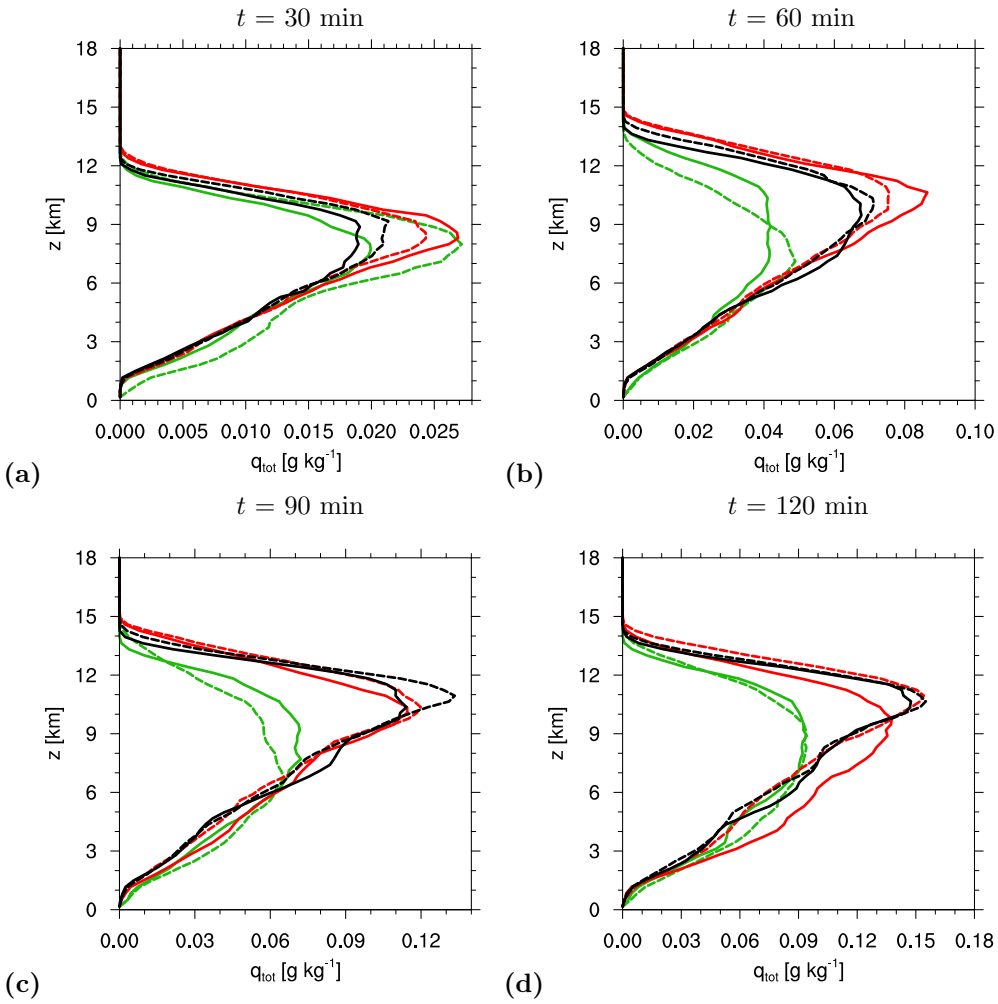


**Figure 4.4:** Conditionally-averaged total condensate mixing ratios ($q_{\rm tot}$) at 30 min (a), 60 min (b), 90 min (c), and 120 min (d) are depicted for the bin (green), bulk-explicit (black), and bulk-original (red) model configurations. Here, the sum of $q_{\rm tot}$ at each level for all points in which $w \geq 2$ m s$^{-1}$ is computed and divided by the horizontal domain size to calculate the conditional average. Shown here are the 'Clean' (solid) and 'Polluted' (dashed) aerosol scenarios. Note that the $x$-axes are different so as to clearly represent the change in $q_{\rm tot}$ between aerosol scenarios and not to distinguish between the changes in $q_{\rm tot}$ between different times.

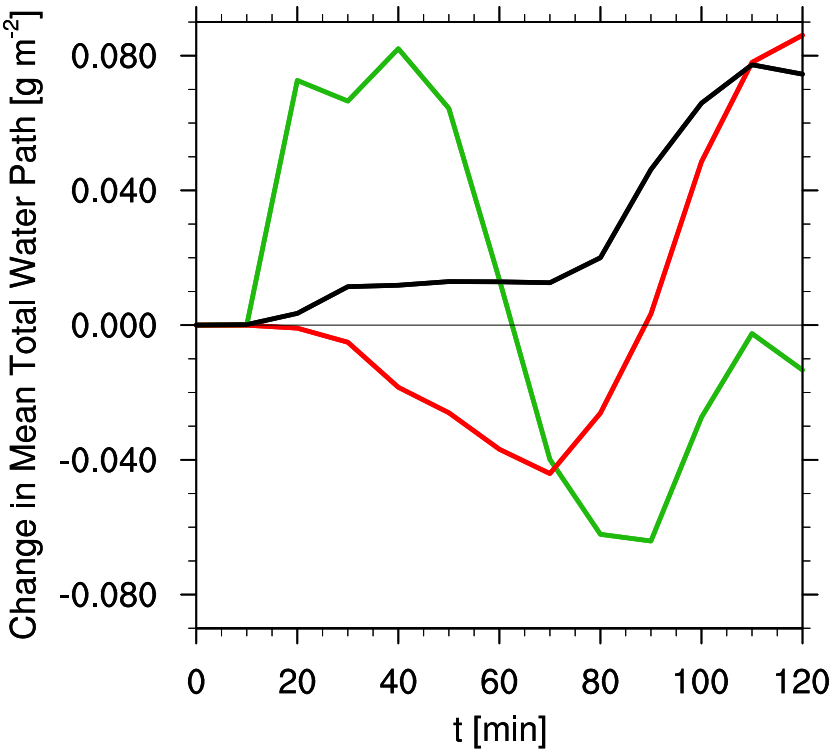


**Figure 4.5:** Change in the domain-averaged total condensed water path ('Polluted' minus 'Clean') as a function of time ($t$) for the bin (green), bulk-explicit (black), and bulk-original (red) model configurations.

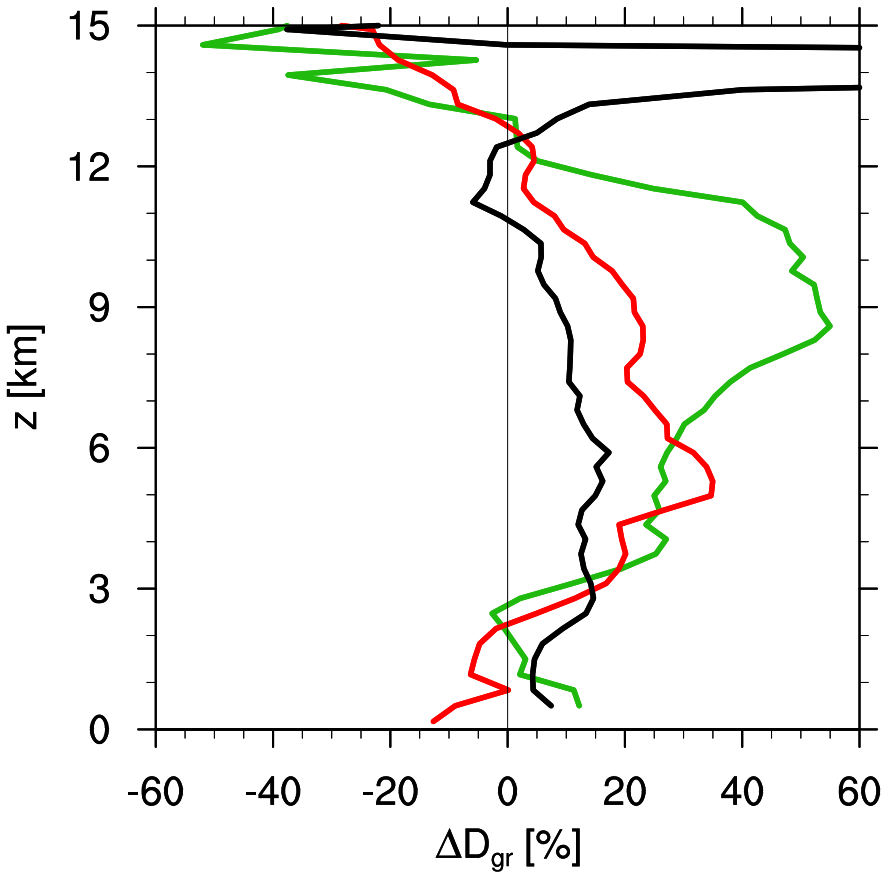


**Figure 4.6:** Relative change in the mean graupel diameter ($D_{\mathrm{gr}}$) due to an increase in aerosol loading ('Polluted' minus 'Clean') averaged between 60 and 120 min. Curves correspond to the bin (green), bulk-explicit (black), and bulk-original (red) model configurations.

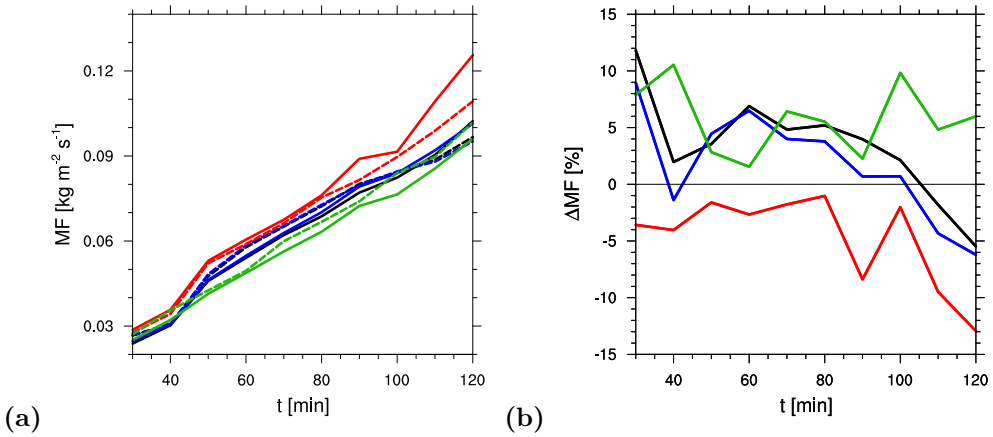


**Figure 4.7:** (a) Vertical- and domain-average convective mass flux (MF) between 2.1 and 9.1 km and (b) the relative change in MF for an increase in aerosol loading. Depicted here are only the 'Clean' (solid) and 'Polluted' (dashed) aerosol scenarios for the base simulation setup. All four model configurations are presented, i.e., bin (green), bulk-explicit (black), bulk-cond (blue), bulk-original (red).

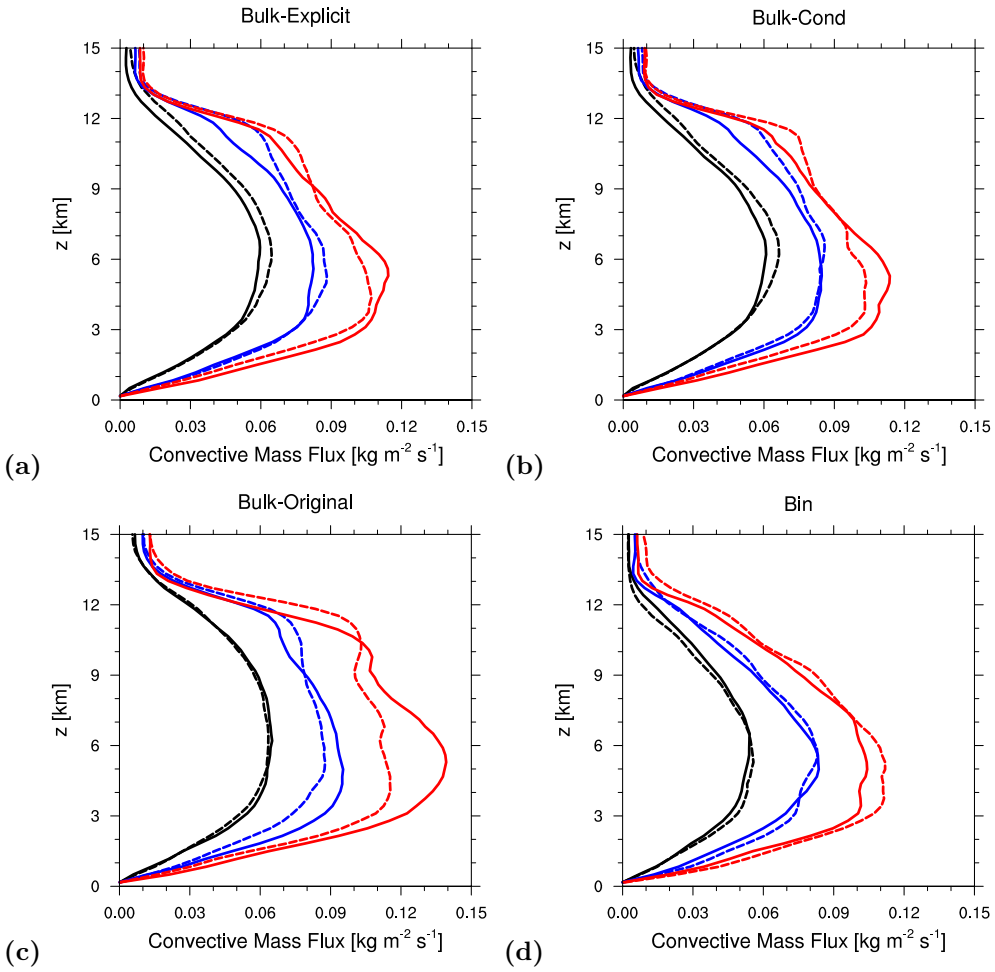


**Figure 4.8:** Domain-average convective mass flux profiles for all four model configurations at 60 min (black), 90 min (blue), and 120 min (red). Depicted here are the 'Clean' (solid) and 'Polluted' (dashed) aerosol scenarios for the baseline initial conditions.

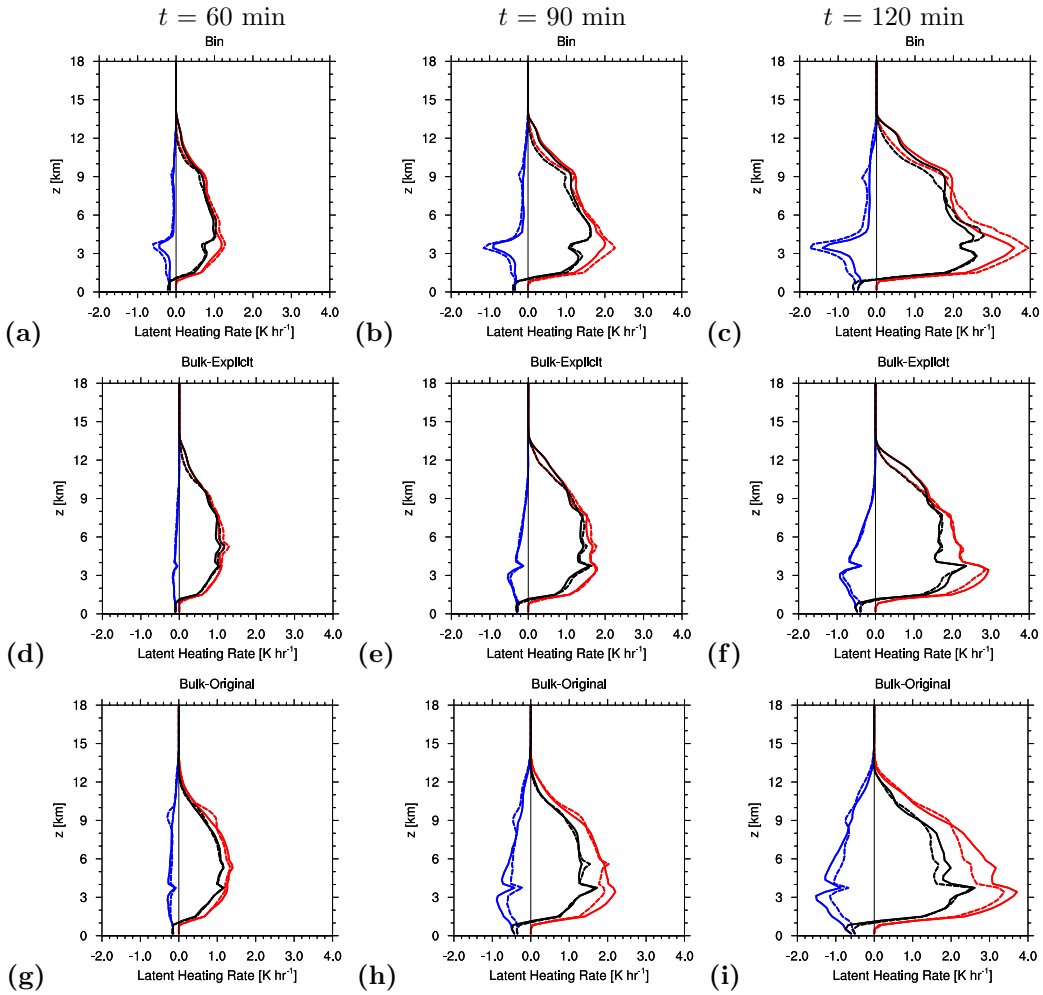


**Figure 4.9:** Simulated latent heating rates for the bin (a-c), bulk-explicit (d-f), bulk-original (g-i) model configurations at 60 min (a, d, g), 90 min (b, e, h), and 120 min (c, f, i). The net heating rate (black) is decomposed into the heating (red) caused by condensation, deposition, freezing, and riming and cooling (blue) caused by evaporation, sublimation, and melting. Results are shown for the 'Clean' (solid) and 'Polluted' (dashed) aerosol scenarios and baseline initial conditions.

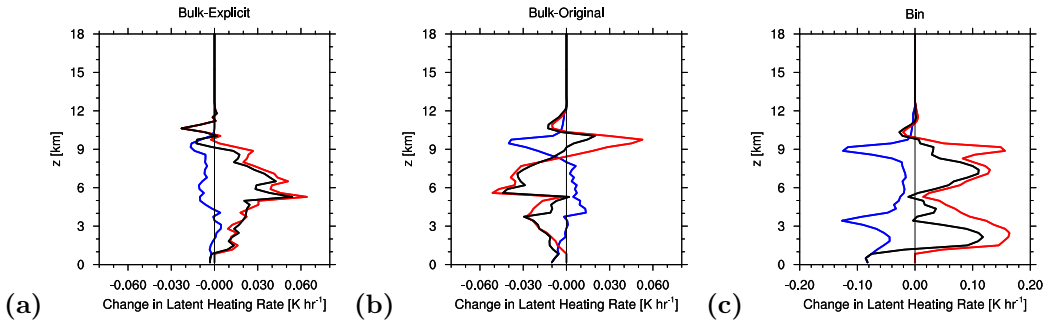


**Figure 4.10:** Change in the latent heating rates ('Polluted' minus 'Clean') for the bulk-explicit (a), bulk-original (b), and bin (c) model configurations. Shown are the changes in heating (red), cooling (blue), and net (black) heating rates for an increase in aerosol loading. Here, positive values correspond to an increase in heating (or decrease in cooling) from the 'Clean' to 'Polluted' scenarios.

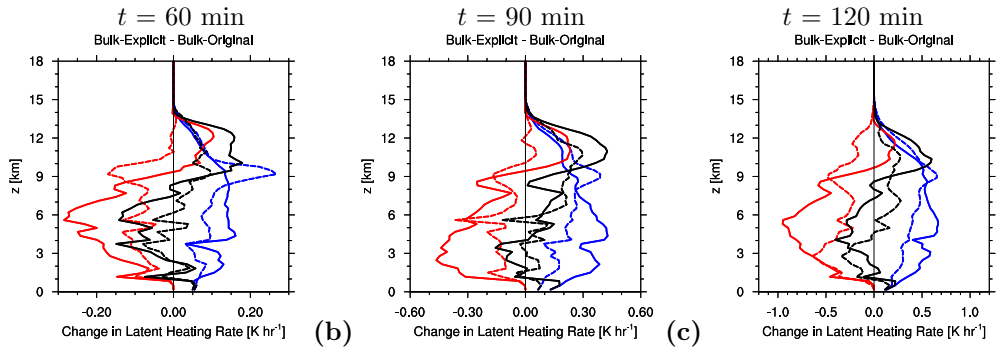


**Figure 4.11:** Differences in the simulated latent heating rates for the bulk-explicit minus the bulk-original model configurations. Colors correspond to those used in Fig. 4.9. Here, a negative value for heating (positive value for cooling) corresponds to more heating (cooling) predicted by the bulk-original model than bulk-explicit.

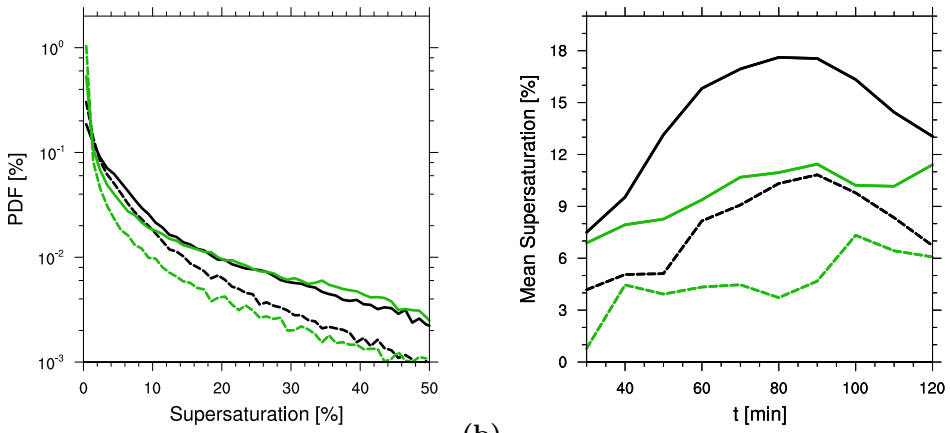


**Figure 4.12:** (a) Probability distribution function (PDF) of the supersaturation and (b) conditionally-averaged supersaturation as a function of time. Shown are results for the bulk-explicit (black) and bin (green) model configurations for the 'Clean' (solid) and 'Polluted' (dash) aerosol scenarios. The PDFs are generated by analyzing all points for which 2.1 km $\leq z \leq$ 9.1 km and 30 min $\leq t \leq$ 120 min. In (b), only points in which the supersaturation is positive are considered when computing the mean.

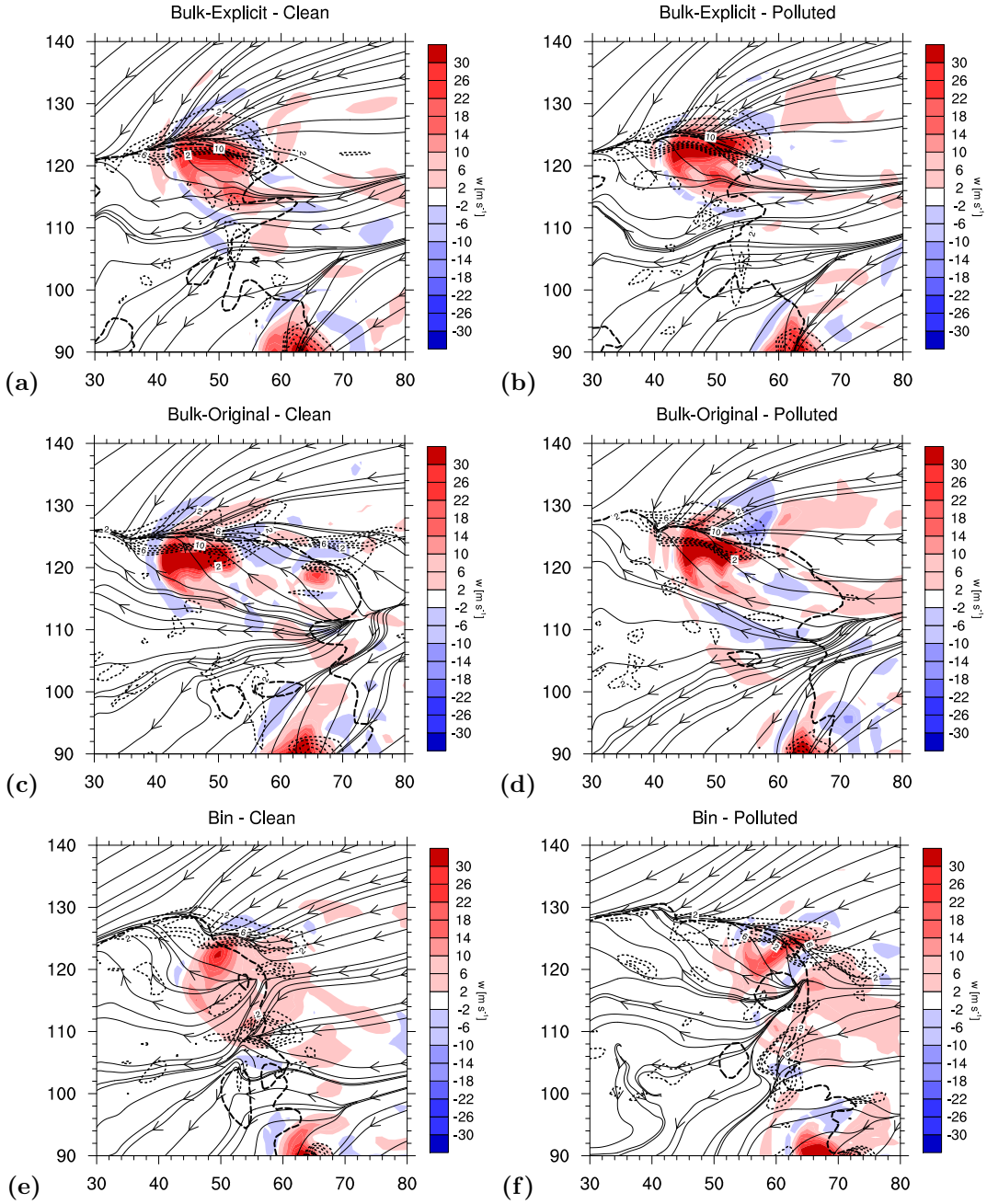


**Figure 4.13:** Interaction between cold pool strength and convergence is shown. The cold pool boundary is demarcated by the dashed curve ($\theta'$ < -2K). Streamlines represent the flow at the lowest model level. Dotted contours depict the vertical velocity at 1.5 km starting at 2 m s$^{-1}$ and stepping by 2 m s$^{-1}$, while the filled contours (color bar) show the vertical velocity at 9.1 km. The 'Polluted' (b, d, f) and 'Clean' (a, c, e) scenarios are shown for the bulk-explicit (a, b), bulk-original (c, d), and bin (e, f) model configurations at 90 min.

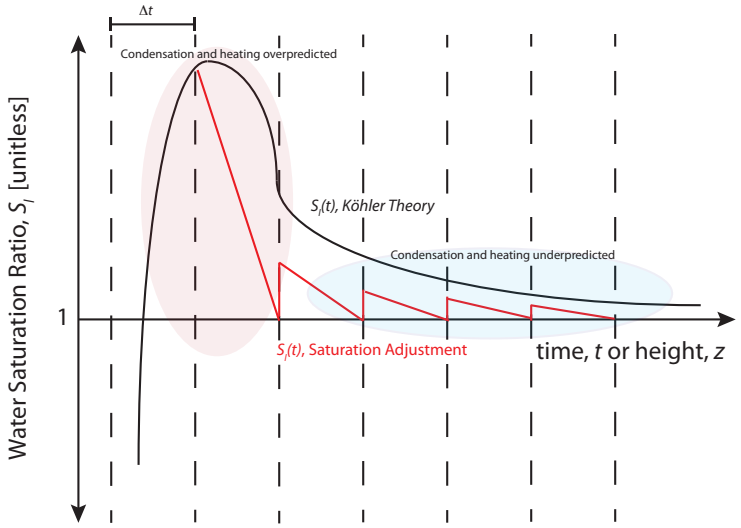


**Figure 4.14:** Schematic of the evolution of supersaturation using saturation adjustment (red) compared to an explicit treatment following Köhler Theory (black) for a steadily-rising parcel. The time step ($\Delta t$) is relatively short and comparable to that used by a cloud-resolving model.

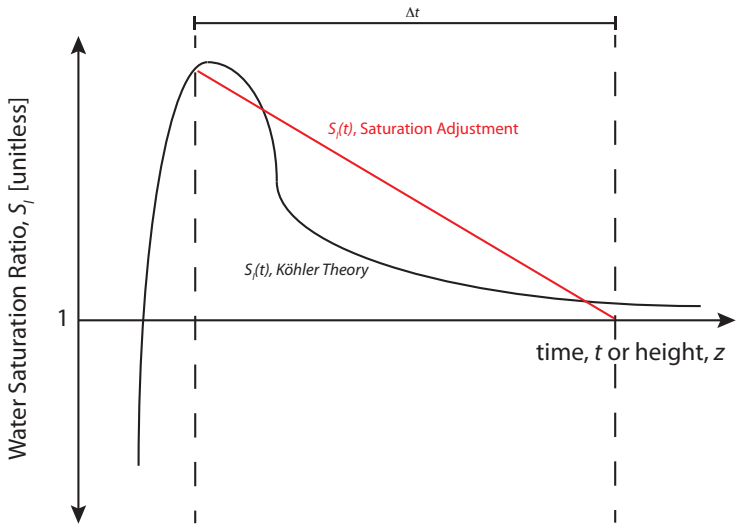


**Figure 4.15:** As in Fig. 4.14 but for a longer time step.

## 4.9 Bibliography

Albrecht, B.: Aerosols, cloud microphysics, and fractional cloudiness, Science, 245, 1227–1230, doi:10.1126/science.245.4923.1227, 1989.

Chuang, P. Y., Charlson, R. J., and Seinfeld, J. H.: Kinetic limitations on droplet formation in clouds, Nature, 390, 94–96, 1997.

Clark, T. L.: Numerical Modeling of the Dynamics and Microphysics of Warm Cumulus Convection, J. Atmos. Sci., 30, 857–878, 1973.

Dawson II, D. T., Xue, M., Milbrandt, J. A., and Yau, M. K.: Comparison of evaporation and cold pool development between single-moment and multi-moment bulk microphysics schemes in idealized simulations of tornadic thunderstorms, Mon. Wea. Rev., 138, 1152–1171, 2010.

Ekman, A. M. L., Engstrom, A., and Soderberg, A.: Impact of two-way aerosol-cloud interaction and changes in aerosol size distribution on simulated aerosol-induced deep convective cloud sensitivity, J. Atmos. Sci., 68, 685–697, 2011.

Fan, J., Zhang, R., Li, G., and Tao, W.-K.: Effects of aerosols and relative humidity on cumulus clouds, J. Geophys. Res., 112, doi:10.1029/2006JD008136, 2007.

Fan, J., Yuan, T., Comstock, J. M., Ghan, S., Khain, A., Leung, L. R., Li, Z., Martins, V. J., and Ovchinnikov, M.: Dominant role by vertical wind shear in regulating aerosol effects on deep convective clouds, J. Geophys. Res., 114, doi:10.1029/2009JD012352, 2009.

Fan, J., Leung, L. R., Li, Z., Morrison, H., Chen, H., Zhou, Y., Qian, Y., and Wang, Y.: Aerosol impacts on clouds and precipitation in easter China: Results form bin and bulk microphysics, J. Geophys. Res., 117, doi:10.1029/2011JD016537, 2012.

Grabowski, W. W.: Indirect Impact of Atmospheric Aerosol in Idealized Simulations of Convective-Radiative Quasi Equilibrium., J. Climate, 19, 4664–4682, 2006.

Grabowski, W. W. and Morrison, H.: Indirect Impact of Atmospheric Aerosol in Idealized Simulations of Convective-Radiative Quasi Equilibrium. Part II: Double-moment microphysics, J. Climate, 24, 1897–1912, 2011.

Gunn, R. and Phillips, B. B.: An experiment investigation of the effect of air pollution on the initiation of rain, J. Meteor., 14, 272–280, 1956.

Hallett, J. and Mossop, S. C.: Production of secondary ice particles during the riming process, Nature, 249, 26–28, doi:10.1038/249026a0, 1974.

Harrington, J. Y., Feingold, G., and Cotton, W. R.: Radiative impacts on the growth of a population of drops within simulated summertime Arctic stratus, J. Atmos. Sci., 57, 766–785, 2000.

Houze, R. A.: Cloud Dynamics, vol. 53 of *International Geophysics Series*, Academic Press, Inc., San Diego, California, USA, 1993.

James, R. P. and Markowski, P. M.: A numerical investigation of the effects of dry air aloft on deep convection, Mon. Wea. Rev., 138, 140–161, 2010.

Khain, A. and Lynn, B.: Simulation of a supercell storm in clean and dirty atmosphere using weather research and forecasting model with spectral bin microphysics, J. Geophys. Res., 114, doi:10.1029/2009JD011827, 2009.

Khain, A. and Pokrovsky, A.: Simulation of effects of atmospheric aerosols on deep turbulent convective clouds using a spectral microphysics mixed-phase cumulus cloud model. Part II: Sensitivity study, J. Atmos. Sci., 61, 2983–3001, 2004.

Khain, A., Pokrovsky, A., Pinsky, M., Seifert, A., and Phillips, V.: Simulation of effects of atmospheric aerosols on deep turbulent convective clouds using a spectral microphysics mixed-phase cumulus cloud model. Part I: Model description and possible applications, J. Atmos. Sci., 161, 2963–2982, 2004.

Khain, A., Rosenfeld, D., and Pokrovsky, A.: Aerosol impact on the dynamics and microphysics of deep convective clouds, Quart. J. Roy. Meteor. Soc., 131, 2639–2663, doi:10.1256//qj.04.62, 2005.

Khain, A., BenMoshe, N., and Pokrovsky, A.: Factors Determining the Impact of Aerosols on Surface Precipitation from Clouds: An Attempt at Classification, J. Atmos. Sci., 65, 1721–1748, 2008.

Klemp, J. B.: Dynamics of tornadic thunderstorms, Am. Rev. Fluid Mech., 19, 369–402, 1987.

Koren, I., Kaufman, Y. J., Rosenfeld, D., Remer, L. A., and Rudich, Y.: Aerosol invigoration and restructuring of Atlantic convective clouds, Geophys. Res. Let., 32, doi:10.1029/2005GL023187, 2005.

Koren, I., Remer, L. A., Altaratz, ., Martins, J. V., and Davidi, A.: Aerosol-induced changes of convective cloud anvils produce climate warming, Atmos. Chem. Phys., 10, 5001–5010, doi:10.5194/acp-10-5001-2010, 2010.

Lebo, Z. J. and Seinfeld, J. H.: Theoretical basis for convective invigoration due to increased aerosol concentration, Atmos. Chem. Phys., 11, 5407–5429, doi:10.5194/acp-11-5407-2011, 2011.

Lee, S. S.: Dependence of aerosol-precipitation interactions on humidity in a multiple-cloud system, Atmos. Chem. Phys., 11, 2179–2196, doi:10.5194/acp-11-2179-2011, 2011.

Lee, S. S., Donner, L. J., Phillips, V. T. J., and Ming, Y.: Examination of aerosol effects on precipitation in deep convective clouds during the 1997 ARM summer experiment, Quart. J. Roy. Meteor. Soc., 134, 1201–1220, doi:10.1002/qj.287, 2008a.

Lee, S. S., Donner, L. J., Phillips, V. T. J., and Ming, Y.: The dependence of aerosol effects on clouds and precipitation on cloud-system organization, shear and stability, J. Geophys. Res., 113, doi:10.1029/2007JD009224, 2008b.

Li, G., Wang, Y., Lee, K.-H., Diao, Y., and Zhang, R.: Impacts of aerosols on the development and precipitation of a mesoscale squall line, J. Geophys. Res., 114, doi:10.1029/2008JD011581, 2009.

Milbrandt, J. A. and Yau, M. K.: A multi-moment bulk micriphysics parameterization. Part IV: Sensitivity experiments, J. Atmos. Sci., 63, 3137–3159, 2006.

Mitchel, D. L.: Use of Mass- and area-dimensional power laws for determining precipitation particle terminal velocities, J. Atmos. Sci., 53, 1710–1713, 1996.

Morrison, H.: On the robustness of aerosol effects on an idealized supercell storm simulated with a cloud system-resolving model, Atmos. Chem. Phys. Disc., 12, *submitted*, 2012.

Morrison, H. and Grabowski, W. W.: Modeling supersaturation and sub-grid scale mixing with two-moment warm bulk microphysics, J. Atmos. Sci., 65, 792–812, 2008.

Morrison, H. and Milbrandt, J. A.: Comparison of two-moment bulk microphysics schemes in idealized supercell thunderstorm simulations, Mon. Wea. Rev., 139, 1103–1130, 2011.

Morrison, H., Thompson, G., and Tatarskii, V.: Impact of Cloud Microphysics on the Development of Trailing Stratiform Precipitation in a Simulated Squall Line: Comparison of One- and Two-Moment Schemes, Mon. Wea. Rev., 137, 991–1007, 2009.

Noppel, H., Blahak, U., Seifert, A., and Beheng, K. D.: Simulations of a hailstorm and the impact of CCN using an advanced two-moment cloud microphysics scheme, Atmos. Res., 96, 286–301, 2010.

Pruppacher, H. R. and Klett, J. D.: Microphysics of Clouds and Precipitation, Kluwer Academic Publishers, Boston, 1997.

Reisin, T., Levin, Z., and Tzivion, S.: Rain production in convective clouds as simulated in an axisymmetric model with detailed microphysics. Part I: Description of the model, J. Atmos. Sci., 53, 497–519, 1996.

Rosenfeld, D., Lohmann, U., Raga, G. B., O'Dowd, C. D., Kulmala, M., Fuzzi, S., Reissell, A., and Andreae, M. O.: Flood or Drought: How do aerosols affect precipitation?, Science, 321, 1309–1313, 2008.

Rotunno, R., Klemp, J. B., and Weisman, M. L.: A theory for strong, long-lived squall lines, J. Atmos. Sci., 45, 463–485, 1988.

Seifert, A. and Beheng, K. D.: A two-moment cloud microphysics parameterization for mixed-phase clouds. Part 2: Maritime vs. continental deep convective storms, Meteor. Atmos. Phys., 92, 45–66, 2006.

Seifert, A., Köhler, C., and Beheng, K. D.: Aerosol-cloud-precipitation effects over Germany as simulated by a convective-scale numerical weather prediction model, Atmos. Chem. Phys., 12, 709–725, doi:10.5194/acp-12-709-2012, 2012.

Skamarock, W. C., Klemp, J. B., Dudhia, J., Gill, D. O., Barker, D. M., Duda, M. G., Huang, X.-Y., Wang, W., and Powers, J. G.: A description of the advanced research WRF Version 3, National Center for Atmospheric Research, Boulder, Colorado, USA, 2008.

Squires, P.: The microstructure and Colloidal Stability of Warm Clouds: Part I - The Relation between Structure and Stability, Tellus, 10, 256–261, 1958.

Stevens, B. and Feingold, G.: Untangling aerosol effects on clouds and precipitation in a buffered system, Nature, 461, 607–613, doi:10.1038/nature08281, 2009.

Stevens, B., Feingold, G., Cotton, W. R., and Walko, R. L.: Elements of the microphysical structure of numerically simulated nonprecipitating stratocumulus, J. Atmos. Sci., 53, 980–1006, 1996.

Tao, W.-K., Li, X., Khain, A., Matsui, T., Lang, S., and Simpson, J.: Role of atmospheric aerosol concentration on deep convective precipitation: Cloud-resolving model simulations, J. Geophys. Res., 112, doi:10.1029/2007JD008728, 2007.

Teller, A. and Levin, Z.: The effects of aerosols on precipitation and dimensions of subtropical clouds: a sensitivity study using a numerical cloud model, Atmos. Chem. Phys., 6, 67–80, 2006.

Van den Heever, S. C. and Cotton, W. R.: The impact of hail size on simulated supercell storms, J. Atmos. Sci., 61, 1596–1609, 2004.

Van den Heever, S. C. and Cotton, W. R.: Urban Aerosol Impacts on Downwind Convective Storms, J. Appl. Meteor. Clim., 46, 828–850, 2007.

Van den Heever, S. C., Carri, G. G., Cotton, W. R., DeMott, P. J., and Prenni, A. J.: Impacts of Nucleating Aerosol on Florida Storms. Part I: Mesoscale Simulations, J. Atmos. Sci., 63, 1752–1775, 2006.

Van den Heever, S. C., Stephens, G. L., and Wood, N. B.: Aerosol indirect effects on tropical convection characteristics under conditions of radiative-convective equilibrium, J. Atmos. Sci., 68, 699–718, 2011.

Wang, C.: A modeling study of the response of tropical deep convection to the increase of cloud condensation nuclei concentration: 1. Dynamics and microphysics, J. Geophys. Res., 110, doi:10.1029/2004JD005720, 2005.

Weisman, M. L. and Klemp, J. B.: The dependence of numerically simulated convective storms on vertical wind shear and buoyancy, Mon. Wea. Rev., 110, 504–520, 1982.

Weisman, M. L. and Klemp, J. B.: The structure and classification of numerically simulations convective storms in directionally varying wind shears, Mon. Wea. Rev., 112, 2479–2498, 1984.

Weisman, M. L. and Rotunno, R.: "A theory for strong long-lived squall lines" revisited, J. Atmos. Sci., 61, 361–382, 2004.

Xue, H. and Feingold, G.: Large-eddy simulations of trade wind cumulus: Investigation of aerosol indirect effects, J. Atmos. Sci., 63, 1605–1622, 2006.

# Chapter 5

# Conclusions and Future Work

## 5.1 Conclusions

The work presented herein has demonstrated the use and capability of both an explicit 1-D bin microphysics model, including size resolved aerosol activation and regeneration explicitly designed for studying mixed-phase clouds and cloud systems, as well as a complete 2-D continuous spectral aerosol-droplet microphysics model. The key results from employing these models are summarized hereafter.

### 5.1.1 Continuous Aerosol-Droplet Microphysics Model

Surprisingly, even the most detailed current bin microphysics schemes do not accurately represent aerosol regeneration. When a cloud droplet evaporates, the solute remains and a CCN is reformed. However, information regarding aerosol size (and composition) is lost when the aerosol activates. It is often assumed that regenerated aerosol particles conform to a predefined distribution. However, the solute mass within a droplet will change due to collision-coalescence and aerosol scavenging. A continuous spectral aerosol-cloud microphysics scheme containing all of the pertinent microphysics was developed by Lebo and Seinfeld (2011b) to study this problem, the first of its kind to be employed in a three-dimensional dynamical model. Condensation/evaporation for all bins is computed simultaneously, including curvature, solute, and kinetic effects. The calculations are performed in a self-consistent manner so that activation, condensation, evaporation, and regeneration are all calculated in one routine. In other words, there is computationally no distinction between wet aerosol, haze particles, and cloud droplets. Moreover, a detailed collection scheme predicts the evolution of the droplet and solute mass spectra for all binary bin pairs. It was found that the number concentration of large CCN can increase by nearly a factor of 10 within just 2 hours in a marine stratocumulus cloud. Hence, upon evaporation, one would expect a shift in the regenerated CCN distribution toward larger sizes when compared to the initial size distribution. This shift could have important effects for subsequent activation of cloud-processed aerosol.

### 5.1.2 Aerosol Induced Invigoration of Deep Convective Clouds

The aerosol-cloud-precipitation problem in deep convective clouds was brought to the forefront in recent years with studies attempting to understand the issue by using everything from 1-D bulk thermodynamic models to detailed bin microphysics schemes. In Lebo and Seinfeld (2011a) a detailed mixed-phase bin microphysics scheme with explicit treatment of aerosol activation and regeneration was designed to directly study this problem. This work focused on the effect of aerosol perturbations on the strength of convection, cumulative precipitation, and precipitation intensity. It was previously hypothesized (e.g., Rosenfeld et al., 2008; Stevens and Feingold, 2009), that an increase in aerosol number concentration could invigorate deep convective clouds, due to suppressed collision-coalescence and enhanced latent heat release aloft, due to more riming, freezing, and deposition. Our work demonstrated that the subsequent increase in cloud water aloft does not necessarily imply an increase in precipitation, since an increase in aerosol number concentration will increase the number of cloud particles and thus decrease their sizes. Ultimately, this acts to increase the sedimentation timescale and decrease the evaporation timescale. Thus, under particular environments, an aerosol perturbation acts to reduce precipitation and moisten the mid- to upper-troposphere.

### 5.1.3 Dependency of Aerosol Effects on Deep Convective Clouds to Saturation Adjustment

The sensitivity of the simulated invigoration in deep convective clouds to the saturation adjustment scheme in a bulk microphysics model was addressed using a configuration of the bulk model with an explicit representation of supersaturation over the time step. It was shown that when the model incorporates saturation adjustment, the model predicts a decrease in the convective mass flux for an increase in aerosol loading, whereas when the model explicitly determines the supersaturation an invigoration in convection occurs, analogous to that which is predicted by the bin model. Moreover, numerous perturbations to the initial sounding are performed to demonstrate the robustness of the simulated results. The simulations confirm the hypothesis that the saturation adjustment scheme erroneously overpredicts condensation at lower levels in the 'Clean' scenario, such that when the

aerosol concentration is increased, the latent heat release decreases (and thus provides a negative buoyancy contribution). Moreover, it was shown that the change in the strength of the cold pool is relatively small for the simulations using bin and the bulk model without supersaturation. However, the bulk model with saturation adjustment predicts a significantly weaker cold pool in polluted conditions and thus a reduction in low-level convergence. This ultimately contributes to the predicted weakening in convection. The study demonstrates that the representation of supersaturation in a physically consistent manner is necessary for studying aerosol-cloud-precipitation interactions and the potential for an increase in aerosol loading to lead to convective invigoration. However, differences between the bin and bulk model without saturation adjustment do still exist and more work is needed to close this gap.

## 5.2 Future Work

### 5.2.1 Persistence of Arctic Mixed-Phase Stratus

The concomitant existence of liquid droplets and ice crystals is thought to be an unstable state. Due to the difference in the equilibrium vapor pressure over liquid and ice, it is expected that liquid droplets will evaporate, supplying water vapor for subsequent growth of ice crystals, ultimately leading to the mixed-phase cloud glaciating — commonly referred to as the Bergeron process. Observations suggest otherwise (e.g., Curry et al., 1996; Intrieri et al., 2002). Previous works have looked at low ice nuclei (IN) concentrations acting to reduce the mass of condensed water that freezes (e.g., Harrington et al., 1999; Morrison et al., 2005; Prenni et al., 2007), the effect of small crystals (e.g., Rauber and Tokay, 1991), and updraft strength (e.g., Korolev and Isaac, 2003) on the longevity of mixed-phase stratiform clouds. However, no overarching theory has yet been established that explains the long lifetime of these clouds. Observations suggest that large droplets can exist with ice crystals in the absence of small droplets (Hobbs and Rangno, 1998).

Lebo et al. (2008) noted that large droplets were observed up until the mixed-phase cloud glaciated in a Lagrangian parcel model study. It was suggested that the loss of small droplets

due to evaporation supplies water vapor to allow the large droplets and ice crystals to coexist in a quasi-stable equilibrium. It seems plausible that this phenomenon may exist for broader ambient conditions and may provide a physical basis for the unusually long lifetime of low- and mid-level mixed-phase stratiform clouds. From a climate perspective, a theory that fully explains the persistence of mixed-phase Arctic stratiform clouds is needed to constrain the cloud radiative forcing, especially in the Arctic.

It has been hypothesized by Lebo et al. (2008) and Lance et al. (2011) that the formation of large droplets is necessary for the persistence of cloud ice in the presence of liquid water. Physically, the generation of large cloud droplets comes from the fact that the solute effect forces the small droplets to readily evaporate, while collision-coalescence allows for the rapid formation of large droplets that are subsequently less likely to evaporate and can even exist in subsaturated environments. Detailed calculations need to be performed for a wide range of input parameters that include detailed treatments of aerosol activation, condensation/evaporation, deposition/sublimation, and collision-coalescence in order to evaluate this hypothesis.

### 5.2.2 Anvil Dynamics

How do aerosol perturbations affect the anvil of deep convective clouds and ultimately top of the atmosphere (TOA) radiative forcing? Koren et al. (2010) suggested that an increase in aerosol loading (or an increase in aerosol optical depth) leads to deeper clouds, an increase in anvil area (relative to the tower), and a decrease in the anvil cloud optical depth (due to the particles spreading out, i.e., decreasing the number density). Both an increase in cloud top height and a decrease in anvil optical depth ought to increase the TOA radiative forcing. However, an increase in aerosol loading results in an increase in the number of cloud droplets, ice particles, etc. All else being equal, the cloud particles ought to be smaller and more numerous under polluted conditions and, consequently, *increase* the cloud optical depth of the anvil. This hypothesis needs to be critically evaluated. Moreover, secondary questions include: Is the aerosol-induced change in anvil height and optical depth affected by changes in vertical wind shear? Or in mid- to upper-troposphere

water vapor mixing ratio? Combining fundamental modeling with satellite observations and climate predictions, we seek to obtain a comprehensive and conclusive analysis of this problem.

### 5.2.3 Hybrid Bin-Bulk Model Development

An additional area of interest is grounded in the area of collection of various cloud particles, specifically within the mixed-phase and cold regions of clouds. Unlike liquid droplets, i.e., spherical particles, ice often takes on non-spherical shapes, and thus it is challenging to accurately represent aggregation, riming, and self-collection, even in detailed bin microphysics schemes. Given the large uncertainty in the mixed- and cold-phase collection processes, a potential avenue to improve such models would be to develop a new hybrid bulk-bin model. In this scheme, warm-phase processes would be explicitly represented by binned microphysics. (Binned liquid droplet calculations would be prudent to accurately predict the rain droplet formation, and our knowledge of this process is extensive.) On the other hand, the ice phase would be represented by bulk calculationsm both for efficiency and because our knowledge of these processes is limited. Calculations with such a model would permit a wide range of sensitivity simulations to be performed to determine the robustness of the invigoration in deep convective clouds caused by increased aerosol loading (e.g. Rosenfeld et al., 2008; Fan et al., 2009; Lebo and Seinfeld, 2011a) without requiring a computationally expensive full bin microphysics scheme. A model of this kind could be implemented into the Weather Research and Forecasting (WRF) model for use by the community.

### 5.2.4 Improving Cloud Representation in GCMs

One of the largest uncertainties in climate predictions lies in the representation of clouds in current GCMs (IPCC, 2007). There is an extensive range of scales involved in representing detailed cloud processes in a model that is designed to predict the mean climate over the course of a century. Moreover, the low resolution required for such simulations (compared to high-resolution cloud resolving models (CRMs) or large eddy simulations (LES)) further complicates the situation, since many cloud processes and inherent feedbacks are at the sub-grid scale. Understandably, the use of

detailed spectral microphysics in a GCM is currently not practical. However, a combination of the present microphysical representation in GCMs with more detailed bulk microphysics calculations or parameterizations developed using CRMs or LES could serve to improve the prediction of clouds in GCMs. In other words, as we move toward simulations with higher resolution, an increase in "microphysical resolution" should occur simultaneously. Unfortunately, such improvements come with limitations, due to the sub-grid scale variability. Recent work in this area, e.g., Morales and Nenes (2010), provides a method for numerically including such variability in large-scale models. Significant strides can potentially be made toward developing an improved, more physically accurate representation of clouds in GCMs. Large advances in the representation of clouds in GCMs are essential in order to accurately depict climate response to aerosol perturbations via both direct and indirect effects.

## 5.3 Bibliography

Curry, J. A., Rossow, W. B., Randall, D., and Schramm, J. L.: Overview of Arctic cloud and radiation characteristics, J. Climate, 9, 1731–1764, 1996.

Fan, J., Yuan, T., Comstock, J. M., Ghan, S., Khain, A., Leung, L. R., Li, Z., Martins, V. J., and Ovchinnikov, M.: Dominant role by vertical wind shear in regulating aerosol effects on deep convective clouds, J. Geophys. Res., 114, doi:10.1029/2009JD012352, 2009.

Harrington, J. Y., Reisin, T., Cotton, W. R., and Kreidenweis, S. M.: Cloud resolving simulations of Arctic stratus. Part II: Transition season clouds, Atmos. Res., 51, 45–75, 1999.

Hobbs, P. V. and Rangno, A. L.: Microstructure of low and middle-level clouds over the Beaufort Sea, Quart. J. Roy. Meteor. Soc., 124, 2035–2071, 1998.

Intrieri, J., Fairall, C., Shupe, M., Persson, P., Andreas, E., Guest, P., and Morritz, R.: An annual cycle of Arctic surface cloud forcing at SHEBA, J. Geophys. Res., 107, doi:10.1129/2000JC000439, 2002.

IPCC: Summary for Policymakers, in: Climate Change 2007: The Physical Science Basis. Contribution of Working Group I to the Fourth Assessment Report of the Intergovernmental Panel on Climate Change, edited by Solomon, S., Qin, D., Manning, M., Chen, Z., Marquis, M., Averyt, K. B., Tignor, M., and Miller, H. L., Cambridge University Press, 2007.

Koren, I., Remer, L. A., Altaratz, ., Martins, J. V., and Davidi, A.: Aerosol-induced changes of convective cloud anvils produce climate warming, Atmos. Chem. Phys., 10, 5001–5010, doi:10.5194/acp-10-5001-2010, 2010.

Korolev, A. and Isaac, G.: Phase transformation of mixed-phase clouds, Quart. J. Roy. Meteor. Soc., 129, 19–38, doi:10.1029/qj.01.203, 2003.

Lance, S., Shupe, M. D., Feingold, G., Brock, C. A., Cozic, J., Holloway, J. S., Moore, R. H., Nenes, A., Schwarz, J. P., Spackman, J. R., Froyd, K. D., Murphy, D. M., Brioude, J., Cooper, O. R.,

Stohl, A., and Burkhart, J. F.: Cloud condensation nuclei as a modulator of ice processes in arctic mixed-phase clouds, Atmos. Chem. Phys., 11, 8003–8015, doi:10.1594/acp-11-8003-2011, 2011.

Lebo, Z. J. and Seinfeld, J. H.: Theoretical basis for convective invigoration due to increased aerosol concentration, Atmos. Chem. Phys., 11, 5407–5429, doi:10.5194/acp-11-5407-2011, 2011a.

Lebo, Z. J. and Seinfeld, J. H.: A continuous spectral aerosol-droplet microphysics model, Atmos. Chem. Phys. Disc., 11, 23 655–23 705, doi:10.5194/acp-11-23655-2011, 2011b.

Lebo, Z. J., Johnson, N. C., and Harrington, J. Y.: Radiative influences on ice crystal and droplet growth within mixed-phase stratus clouds, J. Geophys. Res., 113, doi:10.1029/2007JD009262, 2008.

Morales, R. and Nenes, A.: Characteristic Updrafts for Computing Distribution-Averaged Cloud Droplet Number and Stratocumulus Cloud Properties, Geophys. Res. Let., 115, doi:10.1029/2009JD013233, 2010.

Morrison, H., Curry, J. A., and Khvorostyanov, V. I.: A new double-moment microphysics parameterization for application in cloud and climate models. Part I: Description, J. Atmos. Sci., 62, 1665–1677, 2005.

Prenni, A. J., Harrington, J. Y., Tjernstrom, M., DeMott, P. J., Avramov, A., Long, C. N., Kreidenweis, S. M., Olsson, P. Q., and Verlinde, J.: Can ice nucleating aerosols affect Arctic seasonal climate?, Bull. Amer. Meteorol. Soc., 88, 541–550, 2007.

Rauber, R. C. and Tokay, A.: An explanation for the existence of supercooled liquid at the tops of cold clouds, J. Atmos. Sci., 48, 1005–1023, 1991.

Rosenfeld, D., Lohmann, U., Raga, G. B., O'Dowd, C. D., Kulmala, M., Fuzzi, S., Reissell, A., and Andreae, M. O.: Flood or Drought: How do aerosols affect precipitation?, Science, 321, 1309–1313, 2008.

Stevens, B. and Feingold, G.: Untangling aerosol effects on clouds and precipitation in a buffered system, Nature, 461, 607–613, doi:10.1038/nature08281, 2009.